A Search for Squarks and Gluinos with the Multijet and Missing Energy Signature in Run 1b

Adam L. Lyon

University of Maryland, College Park, MD

Marc Paterno

University of Rochester, Rochester, NY

DØ Note Draft

May 16, 1997

Abstract

This DØ note details the search for supersymmetric partners of the quarks (squarks) and gluons (gluinos) of minimal low energy Supergravity with the traditional jets and missing transverse energy channel. Results are given for 79.2 pb^{-1} of data collected during Tevatron Run 1b.

Contents

List of Figures

List of Tables

1 Introduction

The Standard Model has been extremely successful in predicting and describing the physics of what are so far believed to be the fundamental units of matter. It seems clear, however, that the SM is not a final theory, since it cannot explain why things are the way they are. For example, there are no predictions of the lepton and quark masses, and the Higgs mechanism that yields electroweak symmetry breaking must be added in an ad hoc manner. There are additional difficulties. The masses of fundamental scalar particles, the Higgs for instance, will be infinite due to self-energy corrections that contribute quadratic divergences (the fine tuning problem). Furthermore, there is no explanation as to why the weak scale is so far below where the coupling constants appear to converge at the GUT scale (the hierarchy problem). Theories that go “Beyond the Standard Model” have attempted to rectify the fine tuning problem and usually contain electroweak symmetry breaking, alleviating the hierarchy problem. Supersymmetry (SUSY) is one such theory, and the search for two types of the many particles it predicts is the subject of this analysis.

1.1 Supersymmetry models: MSSM and SUGRA

Supersymmetry [1–4] solves the fine tuning problem by introducing a new symmetry that relates fermions to bosons and vice versa. An immediate consequence is that there is a supersymmetric partner particle for every degree of freedom of a Standard Model particle. Since SUSY is a space-time symmetry, these new particles, or *sparticles*, have the same internal quantum numbers as their SM counterparts (eg. charge, lepton number, baryon number, etc.) except they differ in spin by $\pm 1/2$. These sparticles introduce their own

PARTICLE	SPARTICLE	
gluon (g)		gluino ($\tilde{g}$)
charged Higgs ($H^{\pm}$)	Higgsino ($\tilde{H}^{\pm}$)	chargino $\tilde{\chi}^{\pm}_{1,2}$
charged weak boson ($W^{\pm}$)	wino ($\tilde{W}^{\pm}$)	
light Higgs (h)	Higgsino ($\tilde{h}$)	neutralino $\tilde{\chi}^{0}_{1,2,3,4}$
heavy Higgs (H)	Higgsino ($\tilde{H}$)	
pseudoscalar Higgs (A)	Higgsino ($\tilde{A}$)	
neutral weak boson (Z)	zino ($\tilde{Z}$)	
photon (γ)	photino ($\tilde{\gamma}$)	
quark (q)		squark ($\tilde{q}_{R,L}$)
lepton (ℓ)		slepton ($\tilde{\ell}_{R,L}$)
top (t)	scalar top ($\tilde{t}_{R,L}$)	scalar top ($\tilde{t}_{1,2}$)
graviton (G)		gravitino ($\tilde{G}$)

Table 1: MSSM Particle Spectrum

loop diagrams that cancel out the quadratic divergences causing the infinite Higgs mass. SUSY can also naturally produce electroweak symmetry breaking and thus provides an understanding of the hierarchy problem.

Much of the SUSY literature describes the Minimal Supersymmetric Standard Model (MSSM), which is a scheme for adding the fewest sparticles to the Standard Model. The SM particles and their MSSM partners are shown in Table 1. Each SM particle receives one sparticle per "degree of freedom". For example, each SM lepton has two degrees of freedom, one for each helicity state. A scalar *slepton* has only one helicity degree of freedom (spin zero), and therefore there must be two of them for each SM lepton. One is labeled left handed and the other right handed. Similarly, the quarks are associated with scalar supersymmetric quarks or *squarks*. The massless spin 1 gluon has 16 degrees of freedom (2 helicity $\times$ 8 color) and receives the massive spin 1/2 *gluino*, also with 16 degrees of freedom.

The partners of the gauge and Higgs bosons are more complicated. First, there must exist two Higgs doublets in order to provide mass for the up type quarks and the down type quarks (in the SM, the Higgs field and its conjugate are enough to give mass to u and d type quarks, but in SUSY two doublets are needed so that infinite masses cancel). Consequently, five Higgs particles exist: two charged scalars ($H^{\pm}$), two neutral scalars (h, H), and one neutral pseudoscalar (A). The MSSM partners of the Z, photon, and the neutral Higgses (8 degrees of freedom total) mix to form the four spin 1/2 *neutralinos* (also 8 total degrees of freedom). The partners of the W and the charged Higgses (8 d.o.f.) are the two charged fermion *charginos* (8 d.o.f. total). Charginos and neutralinos are collectively labeled *gauginos*.

SUSY also introduces a new multiplicative quantum number named R–Parity which is defined to be

$$R = (-1)^{3(B-L)+2S} \tag{1}$$

where B is the particle's baryon number, L is the lepton number, and S is the spin. According to this definition, R–Parity is $+1$ for SM particles and -1 for their SUSY counterparts. In this analysis, it is assumed that R–Parity is conserved. Although R–parity conservation is not required by the model, violation of R–parity implies that lepton and baryon number are violated as well. DØ has a search for R–parity violating SUSY not covered here.

For R–parity conserving SUSY, sparticles must be produced in pairs, and the lightest supersymmetric particle (LSP) must be stable. The LSP must also be neutral, since charged LSPs would have been seen in atomic physics. From cosmological considerations, the LSP is assumed to be the lightest neutralino ($\tilde{\chi}_1^0$) and is weakly interacting, thus producing missing energy in a detector. Without R–parity conservation, the missing energy signature would not be present.

Although the MSSM allows one to add the minimum number of new particles to to the Standard Model, it unfortunately leads to an enormous number of new parameters. For example, the MSSM gives no predictions for the masses and mixing angles of the sparticles. The usual method for reducing the number of independent parameters is to work within the framework of a Grand Unified Theory (GUT). A GUT inspired MSSM relies on some symmetry at a high energy scale, such as *SU(5)*, flipped *SU(5)*, *SO(10)* or string theories, to give relations between some of the sparticle masses.

Recently, theorists have started to employ the Minimal Supergravity model (SUGRA) as another GUT framework for the MSSM. In the SUGRA model, the three gauge couplings of *SU(3)*, *SU(2)*, and *U(1)* are unified at some huge energy scale M_X where gravitational interactions become important (perhaps at the Planck scale). At this M_X scale, the gauginos are mass degenerate (true for any GUT model), and in the simplest SUGRA model the scalar sparticles also share a common mass as seen in Figure 1. Thus, the only parameters needed are as follows:

- M_0, the common mass for all scalar sparticles at the M_X scale.
- $M_{1/2}$, the common mass for all gauginos at the M_X scale.
- $\tan\beta$, the ratio of vacuum expectation values of the two Higgs doublets.
- sign(μ), the sign of the Higgsino mixing parameter.
- A_0, a common trilinear term in the lagrangian at the M_X scale.

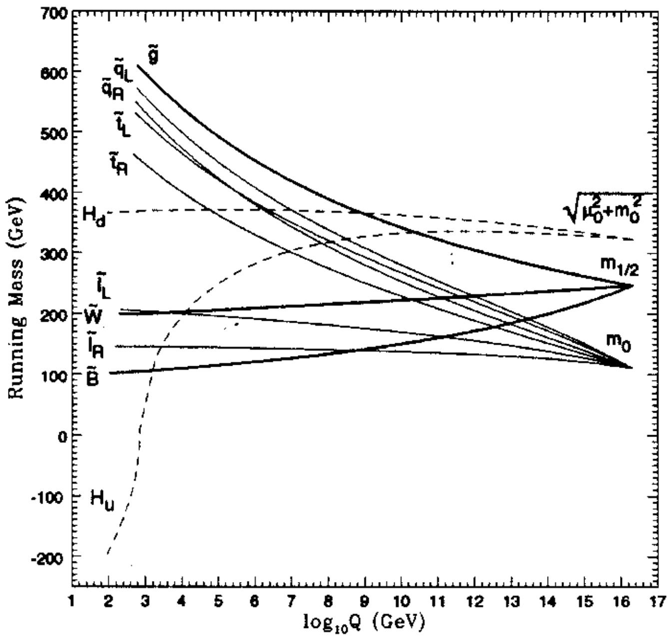

Figure 1: Evolution of sparticle masses in Supergravity. This plot [?] shows masses of various sparticles vs. energy scale (Q). Note how the masses converge to $M_{1/2}$ for the gluinos and gauginos (here displayed before electroweak symmetry breaking as $\tilde{W}$ and $\tilde{B}$) and to M_0 for the scalars. The Higgs mass running negative is the originator of electroweak symmetry breaking.

Note that there is also a bilinear coupling constant, B_0, but it is recast into $\tan\beta$ and μ. Only the sign of μ is needed, because the magnitude is constrained to yield the correct Z mass by electroweak symmetry breaking. Figure 27 on page 78 shows the correspondence of gluino and squark mass to M_0 and $M_{1/2}$.

Given the SUGRA parameters and masses of the Standard Model particles, masses and mixing angles for the sparticles can be determined at the weak scale by solving the Renormalization Group Equations (RGEs) of the model. The SUGRA framework will be used for this analysis, since it is favored by most phenomenologists. Of course one would like to test the validity of all SUSY models, but one must be able to produce Monte Carlo simulations for each; a prohibitive task.

1.2 The Squark and Gluino Signature

Squark and Gluino production occurs in $p\bar{p}$ collisions through the strong interactions of quark anti-quark annihilation, gluon fusion, and gluon – quark interactions. From conservation of R–Parity, squarks and gluinos must be produced in pairs, thus one may have squark – squark, gluino – gluino, or associated squark – gluino production. Another consequence of R–Parity conservation is that each squark or gluino must ultimately decay to the lightest supersymmetric particle (LSP). The LSP is stable and only interacts weakly, thus escaping detection and creating missing energy in the event. If squarks and gluinos are light, each will decay directly into jets and an LSP. If they are heavier than the gauginos, then *cascade* decays are allowed. In cascade decays, the squarks and gluinos decay through charginos and neutralinos eventually down to the LSP, releasing leptons and jets along the way. If the squark is heavier than the gluino, it is most likely that the squark will decay into a soft jet and a gluino as the first step. The cascade decay scheme yields more jets and a softer missing transverse energy ($\not{E}_T$) spectrum compared to direct decays. An example cascade decay is shown in Figure 2.

For this analysis, squarks and gluinos are searched for by their direct or cascade hadronic decays. Hadronic decays are advantageous due to large branching fractions. Since squarks and gluinos are produced in pairs, the signature for this analysis is multijet events with large missing transverse energy from the two LSPs and no leptons. Leptonic decays are the subject of other analyses [5], not covered here.

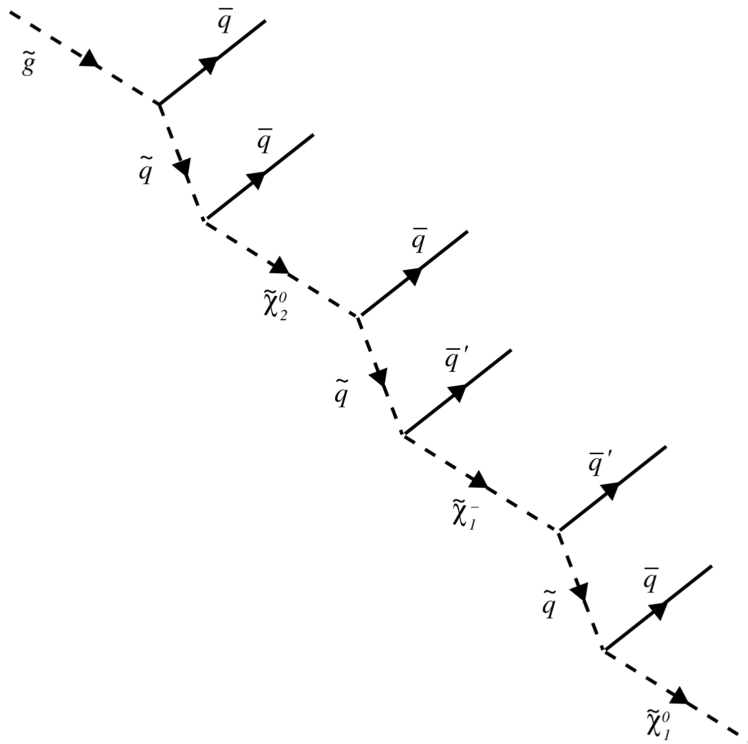

Figure 2: A cascade decay. Here a gluino decays through the second lightest neutralino and the lightest chargino to many jets and an LSP. Note that the quarks may be replaced by leptons for leptonic decays.

1.3 Backgrounds

While hadronic cascade decays of squarks and gluinos have the largest branching fractions, there are also very large backgrounds to contend with. Background sources that generate events with many jets and missing transverse energy fall under two categories: those with $\not{E}_T$ due to physics processes and those where detector effects are solely responsible for the $\not{E}_T$ in the event.

Backgrounds due to physics sources of $\not{E}_T$ include $W \to \ell\nu$ + jets, $Z \to \nu\nu$ + jets, and $t\bar{t} \to \ell(\ell)$ + jets. Each of these examples involve at least one neutrino in the final state generating $\not{E}_T$. For those final states with leptons, the leptons must be lost or misidentified for such events to be collected by this analysis. Such detector effects may also act to enhance the $\not{E}_T$. The invisible decays of the Z and events with the Z and W involving hadronic tau decays also mimic the desired signal.

There are also many types of backgrounds that arise from pure instrumental effects. Balanced QCD multijet and $t\bar{t} \to$ all jets events with mismeasured jets may acquire large $\not{E}_T$. Energy in the calorimeter may be very unbalanced in events with main ring activity, large number of interactions pasting the inner calorimeter, and negative energy (due to preamps saturated by the previous collision). Balanced jet events where the primary vertex is misplaced far from the hard scattering position may have $\not{E}_T$ grossly mismeasured. Finally, balanced Z decays where a lepton is lost or mismeasured may also be a source of background events. The requirements on events for this analysis are designed to retain as much of the signal as possible while reducing the background from the above sources.

1.4 The Run 1b Analysis

The Run 1b analysis is an extension of a similar analysis [6, 7] from Run 1a. The primary differences between these analyses are below and are described in more detail throughout this note.

- The run 1b data set corresponds to approximately ten times the integrated luminosity of the run 1a sample.
- Signal samples are produced using the SUGRA parameters.
- The misreconstruction of vertices has been addressed and a single interaction requirement is no longer needed.
- An H_T requirement is used to significantly reduce vector boson backgrounds.
- The limit is obtained within the Bayesian probability framework described in Reference 8.
- $\not\!\!E_T$ and H_T requirements are optimized for each (M_0, $M_{1/2}$) point.

2 Event Selection Criteria

The criteria used to select the squark and gluino candidate events and reduce background contamination are described in this section. A summary of the event requirements is shown below.

Total Scalar Energy (Clean up) Removes events with main ring activity, beam halo activity, negative energy, electronics failures, and cosmic rays.

Vertex Position (Clean up) Assures a well centered event.

Removed Cells from Jets (Clean up) Events are rejected if a jet had a cell removed by the hot cell killer.

Bad Jets (Clean up) Remove events with jets that fail good quality requirements. Also removes events with electrons.

Jet – Missing Energy Correlations Reduces mismeasured QCD multijet background.

Muon Veto Defines signal and reduces background with muons.

Missing Transverse Energy Defines signal and reduces all backgrounds.

Three Good Jets Defines signal and reduces all backgrounds.

Leading Jet $\mathbf{E_T}$ Allows use of `jet85` multijet background model.

$\mathbf{H_T}$ Removes vector boson backgrounds.

Confirmation of Primary Vertex (Clean up) Removes events that are misvertexed.

2.1 Total Scalar Transverse Energy

In order to eliminate events due to high energy cosmic rays showering in the calorimeter and calorimeter electronics failures (*eg.* bad BLS cards), events are required to have less than 1.8 TeV of scalar transverse energy deposited in the calorimeter.

The top two plots of Figure 3 are histograms of total scalar E_T for a signal sample and a $t\bar{t}$ Monte Carlo sample. The bottom plot is scalar E_T for data QCD multijet events collected by the `jet85` trigger where at least three good jets are required (events where `aida` removed

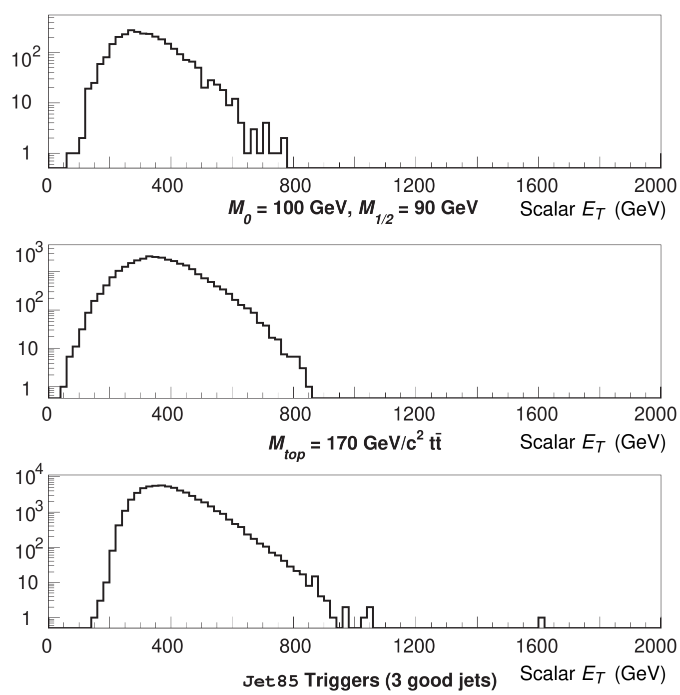

Figure 3: Total calorimeter scalar E_T. The top plot is a signal MC sample. The middle histogram is from $t\bar{t}$ MC. The bottom plot is collider data QCD multijet events with at least three good jets. Events where the hot cell killer removed a cell from a jet are rejected.

a cell from within a jet are also rejected; see Section 2.3). Not seen on that plot are 10 overflow events, with one event at scalar E_T of 2.5 TeV and the rest over 80 TeV. Note that this total scalar E_T condition is used instead of a *total energy* requirement. Requiring total $E < 1.8$ TeV may inadvertently remove events with multiple interactions.

Figure 4 is a plot of $\not\!\!E_T$ vs. scalar E_T for events passing the analysis trigger (requiring only $\not\!\!E_T > 40$ GeV). Several events in the three distinct regions of the plot (denoted by roman numerals) were scanned in order to determine the type of backgrounds that are present. Note that the plot is misleading; 99% of events lie in the "good" region with $\not\!\!E_T < 300$ GeV and scalar $E_T < 800$ GeV.

Region I contains events used by this analysis. Anomalous events with small $\not\!\!E_T$ and very large scalar E_T seem to be due to beam halo where one side of the detector has large

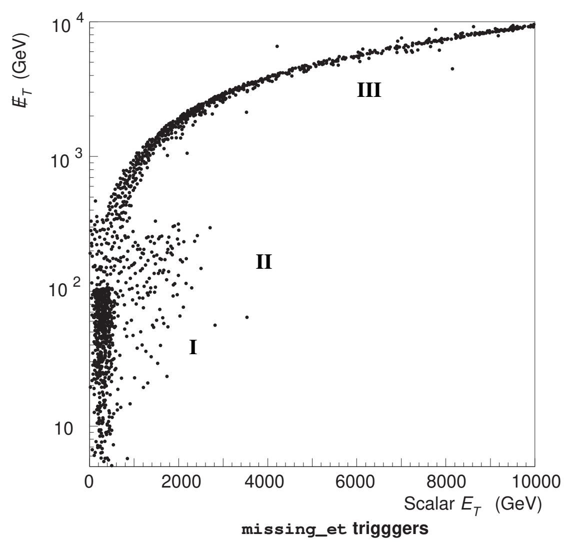

Figure 4: $\not\!\!E_T$ vs. total scalar E_T for collider data passing the `missing_et` trigger. The regions denoted by roman numerals are described in the text.

energy deposits and many hits in muon and central tracking chambers. Events in region II have $\not\!\!E_T$ much larger than expected for a good event. A scan of events there found several clear cosmic ray events (where a muon showered in the calorimeter), a beam halo event, and an event with large energy deposits from the main ring. In region III events have huge $\not\!\!E_T$ and scalar E_T and appear to be caused by enormous main ring losses.

Events are also required to have scalar $E_T > 0$ GeV. This requirement eliminates events with large amounts of negative energy in the calorimeter. Negative energy arises when a previous event saturated some calorimeter preamps, and the current event was taken before those preamps returned to baseline levels. The `missing_et` trigger will not fire on negative energy (see Section 3.1), but may still collect such an event if it is accompanied by large amounts of noise due to the unsettled preamps. This condition is not applied to the Monte Carlo samples and is assumed to be 100% efficient.

2.2 Vertex Position

To assure that events are well centered in the detector, the z position of the primary vertex is required to be within ± 60 cm of the center of the detector. A sample vertex position distribution is shown for $Z \to ee$ events in Figure 5. This requirement is applied to the `isajet` vertex position for the Monte Carlo samples.

2.3 Removed Cells from Jets

Hot cells are anomalous isolated energy deposits in the calorimeter, possibly caused by intermittent shorts or sparks in calorimeter modules due to contaminants in the liquid argon

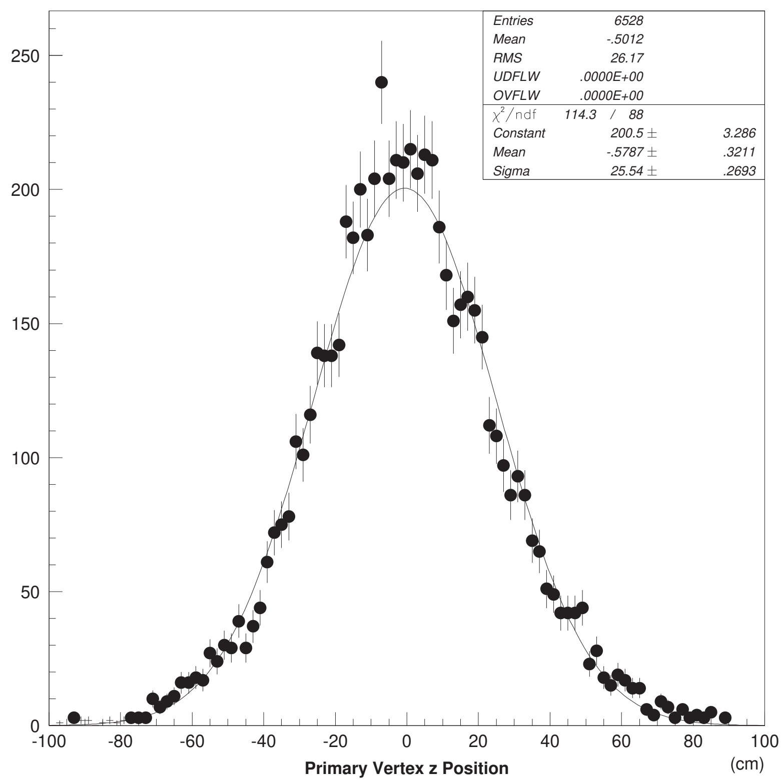

Figure 5: Primary vertex distribution for Z events. The fit is to a Gaussian.

or inside the modules themselves. A hot cell can generate $\not\!\!E_T$ and spurious jets. Since events with hot cells will quickly drive up trigger rates and swamp high $\not\!\!E_T$ data samples, a "hot cell killer" run at level 2 for some triggers and in the reconstruction program removes isolated high energy cells from events.

The hot cell killer, called `aida` [9], removes hot cells by looking for large energy deposits that are isolated *longitudinally*. For a cell to removed, it must meet the following criteria,

- The suspect cell must have $E_T > 10$ GeV.

- $E_{T_{\text{neighboring cell}}} < 0.05 E_{T_{\text{suspect cell}}}$ is true for each cell neighboring the suspect cell in depth.

The hot cell killer in Level 2 can only remove one hot cell from the $\not\!\!E_T$ and total scalar E_T calculations and was only run on events taken by the `missing_et` and `scalar_et` triggers. `aida` in `reco` will remove as many hot cells as it finds. Those removed cells will not be included in $\not\!\!E_T$ and scalar E_T calculations and will not make up any jets.

Generally, when a hot cell is removed from an event the $\not\!\!E_T$ will decrease, since most events are balanced QCD multijet events and will no longer have the anomalous cell to drive up the $\not\!\!E_T$. Rarely, it has been observed that a jet will have a longitudinal shower profile such that a cell within a jet cone will meet the removal criteria, although the cell's energy is probably not be anomalous. Since `aida` only looks in the longitudinal direction to determine if a cell is anomalously larger than its neighbors, such cells within jets will be removed, possibly *raising* the $\not\!\!E_T$ of the event.

QCD jet [?] and Top quark [?] analyses "recover" these removed cells by adding them back into the jet and correcting the $\not\!\!E_T$ accordingly. When they perform a $\not\!\!E_T$ requirement, they use the minimum of the hot cell corrected and uncorrected $\not\!\!E_T$. That procedure works to recover events if the expected signal is balanced (or close to balanced) events. For squarks and gluinos, the signal is *very* unbalanced ($\not\!\!E_T$ of at least 75 GeV is required). An event of this type will typically have most of the jets on one side of the calorimeter (in ϕ) with the $\not\!\!E_T$ vector pointing on the other side. If a jet is reduced by a removal of a cell, the $\not\!\!E_T$ will decrease (opposite to that of a balanced event). When the cell is added back in, the corrected $\not\!\!E_T$ will increase back to the true value. Using the procedure of cutting on the minimum of the hot cell corrected and uncorrected $\not\!\!E_T$ will often result in use of the wrong $\not\!\!E_T$ value, as shown in Figure 6.

One may consider correcting the event if a hot cell is found within a jet and always using

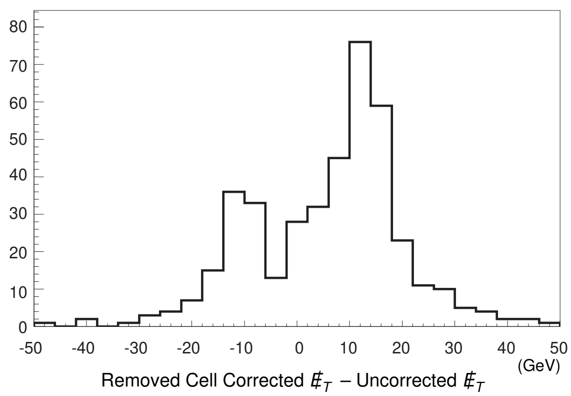

Figure 6: Removed cell corrected $\not{E}_T$ $-$ uncorrected $\not{E}_T$ for SUGRA MC. Note the larger peak when the difference is positive. In that region, the $\not{E}_T$ increases when the removed cell is added back into the event. The distribution shown is from an `isajet` SUGRA sample with $M_0 = 150$ GeV and $M_{1/2} = 80$ GeV. Distributions for other values of M_0 and $M_{1/2}$ are similar.

the hot cell corrected $\not{E}_T$ for cutting on. But the hot cell killer sometimes does do its job correctly. Always using the hot cell corrected $\not{E}_T$ would possibly introduce events with real hot cells; a background that is hard to model.

Since this analysis is extremely sensitive to the $\not{E}_T$ tail of QCD multijet events, events with hot cells in jets are rejected altogether. The following criteria must be met to reject such events:

- A cell that was removed by `aida` must be within $DR = 0.5$ (in $\eta \times \phi$ space) of the axis of a jet.

- That jet must have E_T >15 GeV and be within $|\eta| < 3.5$.

2.3.1 Efficiency of Removed Cells from Jets Requirement

A squark and gluino event will be rejected if a jet has a cell removed by `aida`, so an efficiency must be calculated. In fact, unless the event is corrected by putting the removed cell back into the jet, this efficiency is always present since removing a cell from a jet in a very unbalanced event acts to lower the $\not\!\!E_T$ that goes into `PNUT(4)` bank, possibly causing the event to fail the $\not\!\!E_T$ requirement. To obtain a measurement of the efficiency from the data, one would like to start with a sample of clean events that are not enhanced in hot cells. QCD jet triggers are unsuitable since they will fire on a hot cell. In order to get an unbiased jet sample, the `ele_1_mon` trigger is used, requiring a cluster in the electromagnetic calorimeter passing some electron shape requirements. An electron passing the Top group tight criteria is then required. About 6000 events pass and there are approximately 4000 total jets in the sample. Since it is unlikely that a hot cell could masquerade as a good quality electron that triggered the taking of the event, this sample should be as clean as possible. Out of the nearly 4000 jets, twelve are flagged as having a hot cell within a jet that would cause the event to be removed by the hot cell in jet criteria. This information is displayed in Figure 7.

The filled points of Figure 8 show the cell removal rate derived from Figure 7. Since the statistics for the last few bins are very low, the last point at $\sim$82 GeV is the sum of bins from Figure 7 over 60 GeV. Its E_T position is the weighted mean of the E_T of the entries. The solid line is a straight line fit to those points with slope and intercept shown in the solid lined box. To simulate the effects of `aida` removing cells from jets, each MC event (signal and background) is rejected with a probability determined by applying to each jet in the event the removed cell within jets frequency derived from the fit. With this procedure, about 5% of squark and gluino events are rejected.

2.3.2 Effect of Removed Cells from Jets on the Monte Carlo

One may ask why a Monte Carlo sample cannot be used to determine the hot cell within jets rate, since MC events without noise do not have real hot cells. The answer is that the detailed cell-by-cell structure of jets is not expected to be modeled correctly by showerlibrary Monte Carlo, and thus the rate at which cells are removed by `aida` in Monte Carlo does not match the data. The discrepancy can bee seen in Figure 8. The open circles are the fraction of jets that have a cell removed by `aida` in an `isajet` $t\bar{t}$ to all jets sample ($M_t = 170$ GeV/c^2). Such an all jets sample will have low intrinsic $\not\!\!E_T$. The Monte Carlo grossly overestimates the number of hot cells within jets. One is not even sure if the shape of the MC distribution is correct, since it is not suggested by the data.

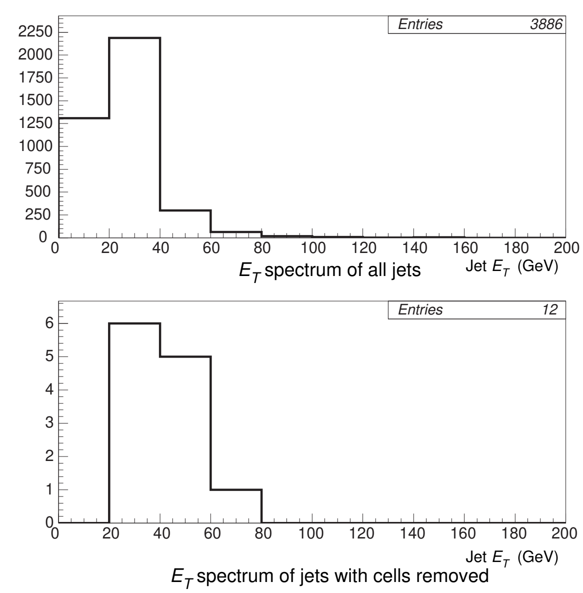

Figure 7: Jet E_T spectra for events with a good electron taken by `ele_1_mon`. The lower plot is the E_T spectra for jets that had a cell removed by `aida`. The jet E_Ts do *not* include the E_T of the removed cell.

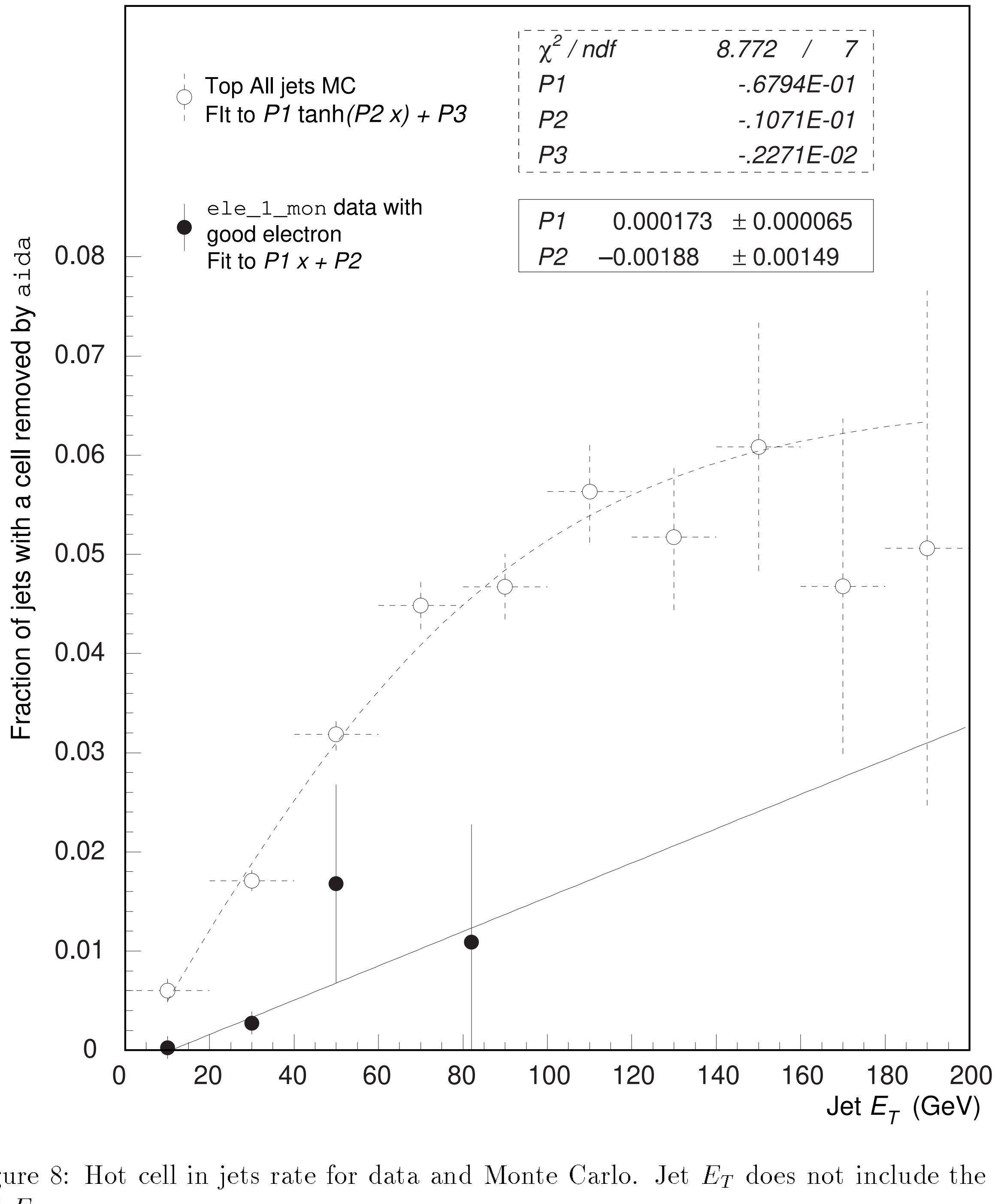

Figure 8: Hot cell in jets rate for data and Monte Carlo. Jet E_T does not include the hot cell E_T.

Since `aida` is run on MC samples, there will be cells removed from jets. Clearly, any hot cell found in a Monte Carlo event with no noise added is a mistake by `aida`. Therefore, for all Monte Carlo samples, cells removed from jets are added back into the event. Jet quantities and the $\not\!\!E_T$ are corrected accordingly.

One may worry that an entire jet can disappear when a cell containing most of its energy is removed and the remains of the jet has E_T below the reconstruction threshold of 8 GeV. An isolated hot cell in a Monte Carlo event would indicate an occurrence of this effect. Fewer than 1% of squark and gluino events passing the analysis requirements have such an isolated hot cell. Such events are deemed defective and are ignored (not counted in event tallies).

2.4 Jet Missing Energy Correlations (Angular Cuts)

One instrumental background to the squark and gluino signature comes from multijet events, where one or more jets are poorly measured creating missing transverse energy. This background can be reduced by examining the correlation between the directions of the jets and the $\not\!\!E_T$ vector. For example, if in a balanced event a jet's energy is mismeasured such that the jet becomes the leading jet, it will generate $\not\!\!E_T$ opposite to its direction (in ϕ). If a jet's energy is mismeasured low, it will tend to lie along the direction of the $\not\!\!E_T$. Figure 9 is a plot of $\phi_{\mathrm{2nd\,jet}} - \phi_{\not E_T}$ vs. $\phi_{\mathrm{Leading\,jet}} - \phi_{\not E_T}$ for QCD multijet events taken by the `jet85` trigger, $t\bar{t}$ Monte Carlo events ($m_{\mathrm{top}} = 170$ GeV$/c^2$), and two SUGRA signal Monte Carlo samples. Events displayed were required to have at least three good jets with $E_T > 25$ GeV, no other bad jets with $E_T > 15$ GeV (see Section 2.7 for the good jet requirements), $\not\!\!E_T > 25$ GeV, and no removed cells from jets. Note the clumping of events in the corners of the QCD multijet plot due to poorly measured jets. No pronounced clustering of events is seen in any

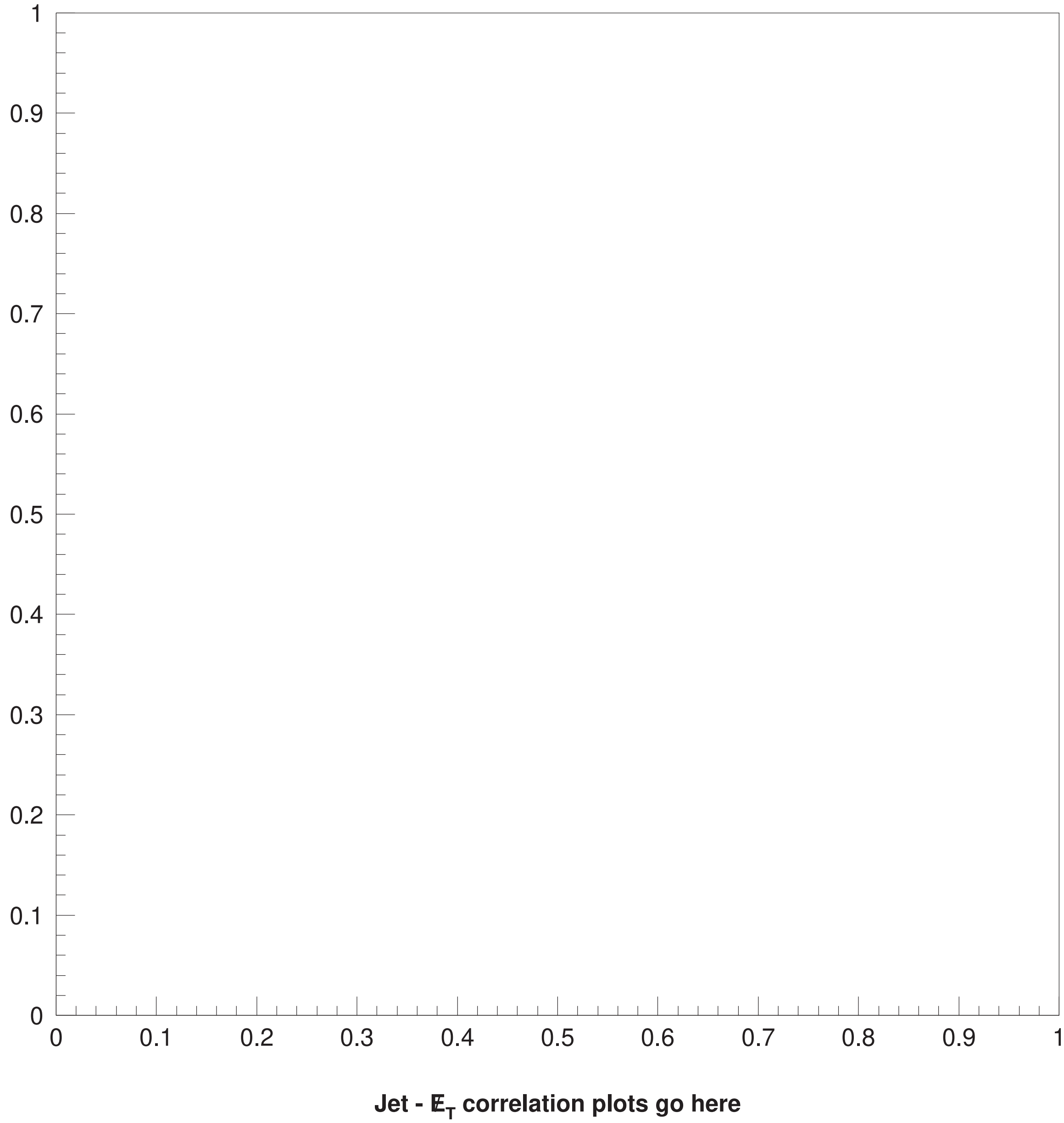

Figure 9: Jet – $\not{E}_T$ correlations. The angle differences are in radians. The solid line indicates the placement of the angular cuts described in the text. All samples were required to have three good jets, no bad jets, no removed cells from jets, and $\not{E}_T > 25$ GeV.

of the signal, top quark, or vector boson background Monte Carlo samples.

To eliminate the poorly measured QCD multijet events, an event is rejected if any jet with $E_T > 25$ GeV is either along or opposite in ϕ to within 0.1 radian of the direction of the $\not{E}_T$ vector. In order to reject events where a fluctuation of the second jet masks the correlation with the leading jet, events are required to have $\sqrt{(\delta\phi_1 - \pi)^2 - (\delta\phi_2)^2} \geq 0.5$ where $\delta\phi_i$ is the azimuthal angle between the i^{th} jet and the direction of $\not{E}_T$. The placement of the cuts are displayed in Figure 9. An event falling outside of the heavy solid line is rejected. All of these angular requirements are applied to the signal and background Monte Carlo samples, but the background from multijet events passing is estimated from data (see Section 4.2.1).

2.5 Muon Veto

Since only squark and gluino events with hadronic cascade decays are sought, events with muons are vetoed (electrons are vetoed with the good jet requirements discussed in Section 2.7). An event is rejected if it has a muon meeting the criteria in Table 2. These requirements are the standard loose muon criteria used by the Top group [10, 11] and are explained in more detail below.

Prezap/Postzap: Only CF muons are vetoed for the Prezap era (Run # < 89,000) when forward muon chambers suffered low efficiency due to accelerated aging. [12, 13]

`ifw4` **muon quality word:** `ifw4` starts at zero and is incremented for each failure of the WAMUS muon track to meet the following quality criteria [14],

- Every WAMUS module along the track contributes hits.

Prezap	Postzap	
CF μ	CF μ	EF μ
Quadrant ≤ 4	Quadrant ≤ 4	$4 <$ Quadrant ≤ 12
`ifw4` ≤ 1	`ifw4` ≤ 1	`ifw4` $= 0$
$P_T > 15$ GeV		
`Hfrac` > 0.6 and `Efrac(H1)` > 0 or `Hfrac` $= 1$		
`ifw1` $\neq 5$		

Table 2: Requirements for muon rejection. An event will be rejected if it contains a muon meeting the criteria shown here.

- Nonbend view impact parameter ≤ 100 cm.
- Bend view impact parameter ≤ 80 cm.
- Nonbend view track fit has hit residual RMS ≤ 7 cm.
- Bend view track fit has hit residual RMS ≤ 1 cm.

`MTC` quantities (`Hfrac` and `Efrac`): `MTC` [15] is a package run during reconstruction that performs muon tracking in the calorimeter. It starts by forming a 5 cell $\times$ 5 cell road centered about the muon track from WAMUS projected into the calorimeter. The road extends through all electromagnetic and hadronic layers. Tracking begins at the hit cell closest to the center of the road in the last layer of the calorimeter before the muon system. Hit cells in inner layers are added to the track if they are transversely offset by no more than one cell in η or ϕ compared to a hit cell in the layer above. If a layer has no hit cells meeting the neighbor criteria, the layer is skipped.

The `Hfrac` value is the fraction of hadronic layers that have a cell contributing to the muon track out of the total number of hadronic layers the track traverses.

Quadrant	Multiplicative Efficiency	
	`musmear` Postzap Monte Carlo	non-`musmear` MC
CF	0.937	0.815
EF	0.400	0.337

Table 3: Corrections to Monte Carlo muon efficiencies. [10, 11]

Along with the standard 5×5 road, a 3 cell $\times$ 3 cell "core" road is also constructed. `Efrac(H1)` is the fraction of energy in the outer most layer of the calorimeter within the core road out of the total energy (sum of all layers) within the core.

The special case of `Hfrac` $= 1$ is to allow vetoing of muons with a very good track (a hit in every calorimeter layer) that lies outside the 3 cell $\times$ 3 cell core cone and fails the `Efrac(H1)` requirement.

`ifw1` **missed layer word:** `ifw1` indicates if the muon is an "A–stub" with only hits in the first layer of WAMUS (A layer) before the toroid magnet. If `ifw1` $\neq 5$, then the muon is not an A–stub.

The muon veto is applied to all signal and background samples. For Monte Carlo, there is a correction to the efficiency. If a muon meeting the requirements in Table 2 is found in a Monte Carlo event, the event to be rejected at a rate [10, 11] given in Table 3.

2.6 Missing Transverse Energy Requirement

Missing transverse energy is one of the key event quantities used in selecting squark and gluino events and reducing backgrounds. The value used by this analysis is from the `PNUT(4)` bank, that is calorimeter $\not\!\!E_T$ after jet corrections. The $\not\!\!E_T$ thresholds are optimized for each

SUGRA point that was tested. See Section 5.2 for details of the optimization procedure. The $\not\!\!E_T$ thresholds used are $\not\!\!E_T > 75$, 90, and 100 GeV. This requirement is applied to all signal and background Monte Carlo samples. Several example spectra from Monte Carlo are shown in Figure 10.

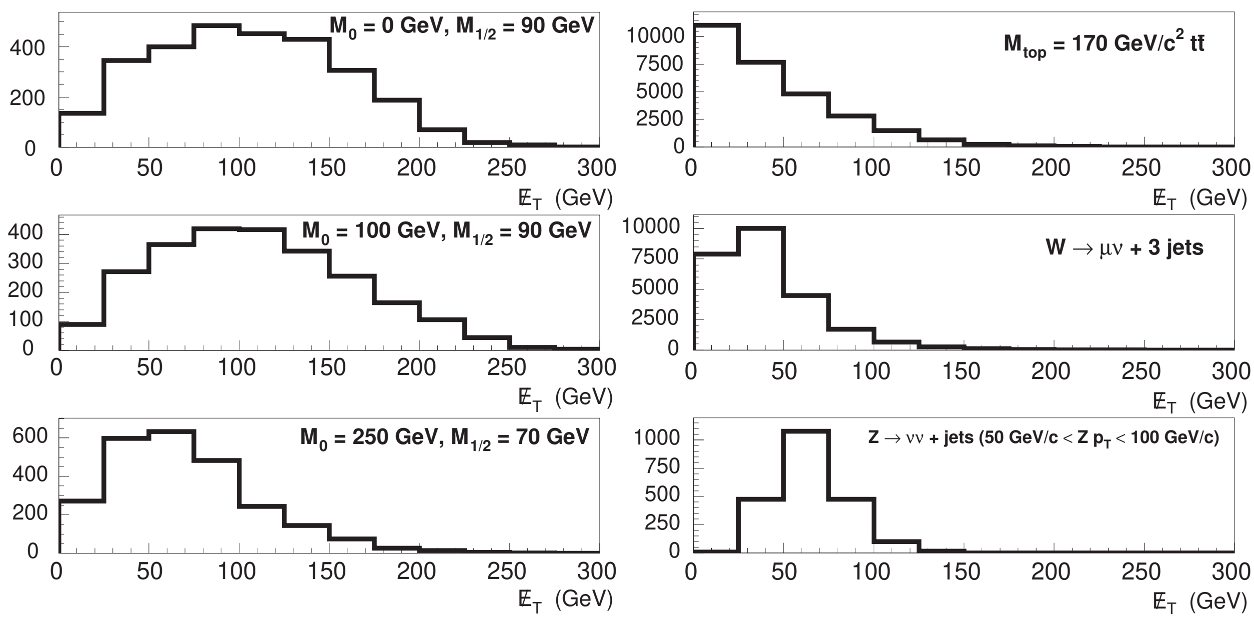

Figure 10: $\not\!\!E_T$ spectra. All distributions are from Monte Carlo. The $Z \to \nu\nu$ sample has a generator $\not\!\!E_T > 40$ GeV requirement applied (calculated from `isp1` banks).

2.7 Good Jet Requirements

Along with large $\not\!\!E_T$, the squark and gluino signature stipulates that such events should have a large jet multiplicity due to the cascade decays. To be as inclusive as possible while providing background rejection, the jet requirements are that an event must contain at least three good jets of corrected $E_T \geq 25$ GeV. Jets of cone size 0.5 in $\eta \times \phi$ space are used for this analysis. The 25 GeV requirement is placed beyond where the reconstruction of 0.5 cone jets is fully efficient.

A good jet must pass the clean jet requirements shown in Table 4 where EM fraction and CH fraction are the fraction of the jet's E_T deposited in the electromagnetic and coarse hadronic layers of the calorimeter respectively. Several example jet E_T spectra from Monte Carlo are shown in Figure 15.

$$\begin{aligned} 0.1 \leq \text{EM Fraction} &\leq 0.9 \\ \text{CH Fraction} &\leq 0.4 \\ |\eta| &\leq 3.5 \end{aligned}$$

Table 4: Good jet requirements.

The low end EM fraction requirement eliminates jets formed from hot cells in the hadronic calorimeter. The high EM fraction cut eliminates electrons and photons, since they deposit nearly all of their energy in the EM calorimeter. The calorimeter was built so that hadronic jets shower in the FH with the CH catching the tails. A jet showering predominately in the CH is in reality probably noise in a CH module or losses from the Main Ring accelerator, thus the purpose of the CH fraction requirement. The large η requirement assures that the jet is not extremely forward and close to the beam pipe. Figure 11 displays the number of good jets passing these requirements with $E_T \geq 25$ GeV for various signal and background samples.

Because of degraded jet energy resolution and lack of good EM coverage, events with the leading jet pointing to the intercryostat region ($1.1 \leq |\eta_{\text{detector}}| \leq 1.4$) are also rejected.

Another requirement taken from the Run 1a analysis is bad jet rejection. All jets in

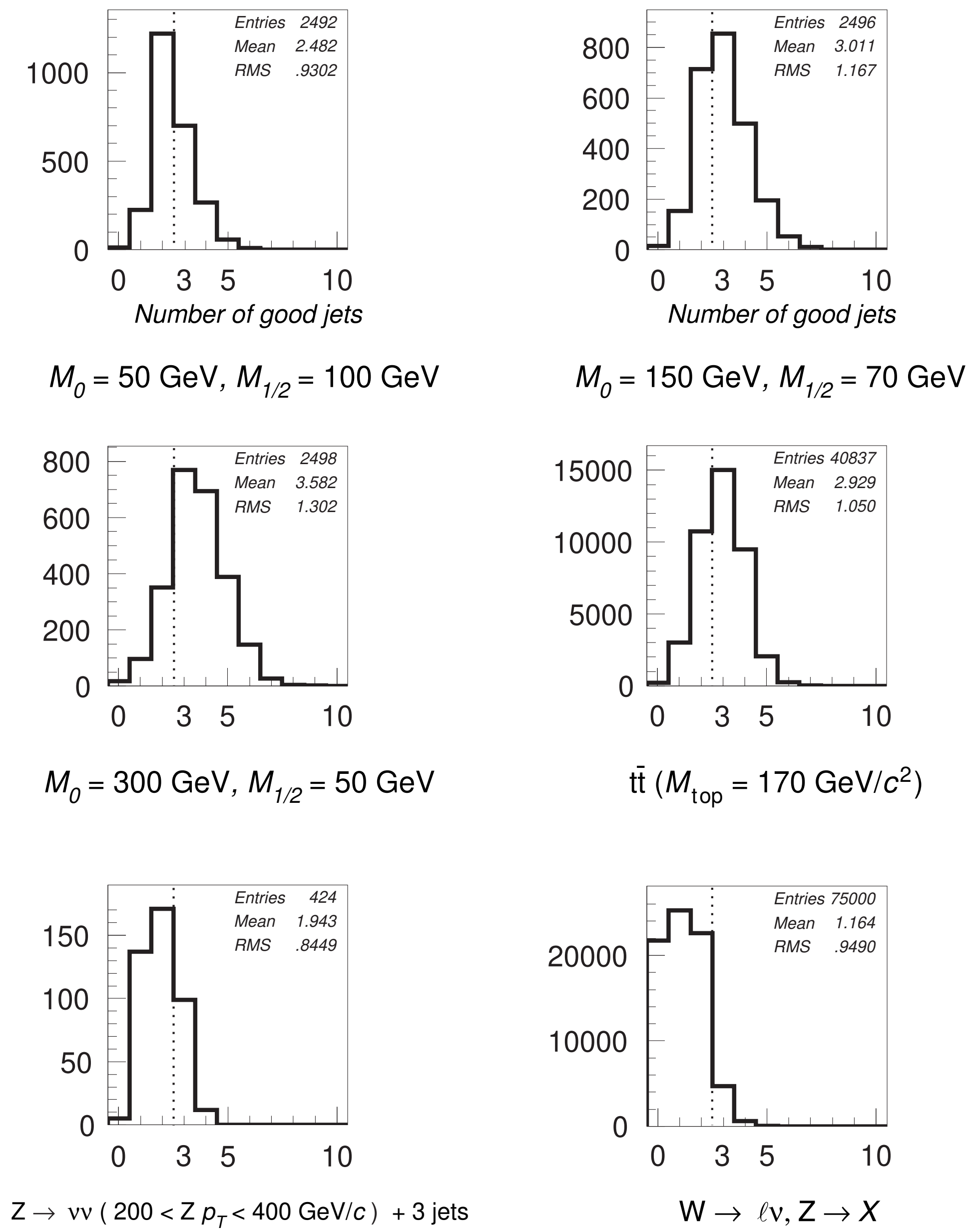

Figure 11: Number of good jets with $E_T > 25$ GeV. The dashed lines indicate the three jet requirement. Note that the $Z \to \nu\nu$ sample has a 3 `pjets` with $E_T > 7$ GeV requirement at the generator level.

the event with E_T over 15 GeV are required to pass the good jet tests, or else the event is rejected. The intention from Run 1a was that this cut would eliminate events with poorly measured jets and events with $\not{E}_T$ due to main ring noise or many interactions. In this analysis, it also acts as a very efficient electron veto.

All of the conditions described here are applied to the signal and background Monte Carlo samples. The last requirement described above (bad jets) was not applied to the Monte Carlo samples for the Run 1a analysis because the QCD group had measured an efficiency close to 100% for jets with $\not{E}_T > 15$ GeV. [16] However, in Run 1b there is no explicit electron veto, and so this requirement eliminates electrons. Thus, the efficiency will be much less than perfect. Since the showerlibrary Monte Carlo appears to model the jet EM fraction distribution correctly (when compared with QCD multijet data), that requirement is now applied to all Monte Carlo background and signal samples.

2.8 $\mathbf{H_T}$ Requirement

A large H_T requirement is used to severely reduce the Standard Model vector boson plus jets backgrounds. It is defined as follows,

$$H_T = \sum_{i=2}^{N} E_{T_{\mathrm{jet}\,i}} \tag{2}$$

where the sum is over the number N of good jets with $E_T \geq 25$ GeV *excluding* the leading jet. The good jet requirements are the same as in Table 4 except that the Top group's requirement of $|\eta| \leq 2.5$ is applied. An H_T requirement of at least 150 GeV is approximately 50% efficient for the signal for the worst case and reduces the vector boson background by nearly a factor of ten, leaving $t\bar{t}$ production as the dominant SM background. Shown in Figure 12 are histograms of H_T for various signal and background Monte Carlo samples.

Along with $\not\!\!E_T$, the H_T threshold is optimized for each signal point (see Section 5.2). H_T thresholds of $H_T > 100$, 120, 140, 150, and 160 GeV are used.

2.9 Leading Jet $\mathbf{E_T}$ Requirement

A data sample of events passing the `jet85` trigger and filter is used to determine the background from mismeasured QCD multijet events (see Section 4.2.1). `jet85` is the only sample suitable, since other jet triggers were heavily prescaled and have little collected luminosity or have undesirable extra requirements such as passing only events with a single interaction. In order to use the `jet85` sample for determining backgrounds, all candidate events must pass the `jet85` requirements, that is a level 2 jet with $E_T > 85$ GeV. This threshold translates to requiring a jet with $E_T > 115$ GeV, which is where `jet85` becomes fully efficient as shown in Figure 13. The turn on curve is best parameterized by the following formula:

$$\mathrm{PassingFraction}(E_T) = 1 - e^{-\left(\frac{E_T}{P_2}\right)^{P_1} - P_3} \tag{3}$$

This requirement is applied to all signal and background samples.

2.10 Confirmation of the Primary Vertex

In the Run 1a analysis, it was discovered that some multiple interaction events contribute a large instrumental background to the squark and gluino signature. Such events are nearly always QCD multijet events with very low true $\not\!\!E_T$ but large measured $\not\!\!E_T$. The cause of

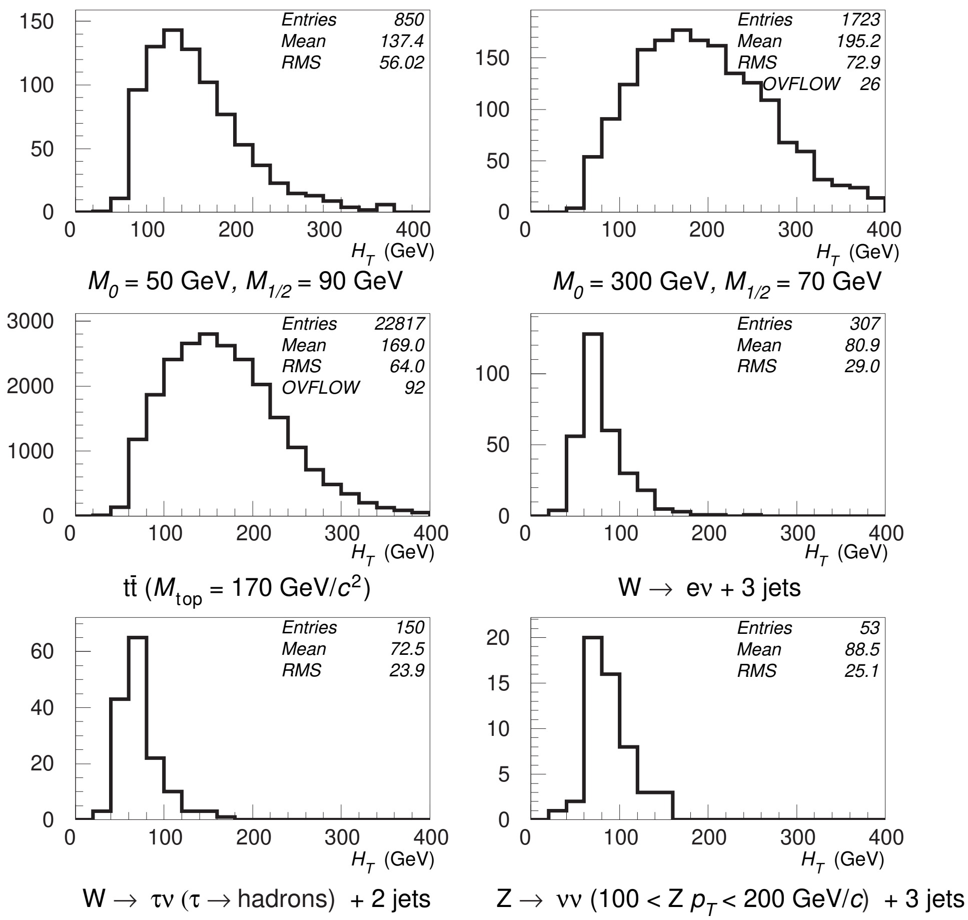

Figure 12: H_T spectra for signal and background Monte Carlo samples. 3 good jets are required.

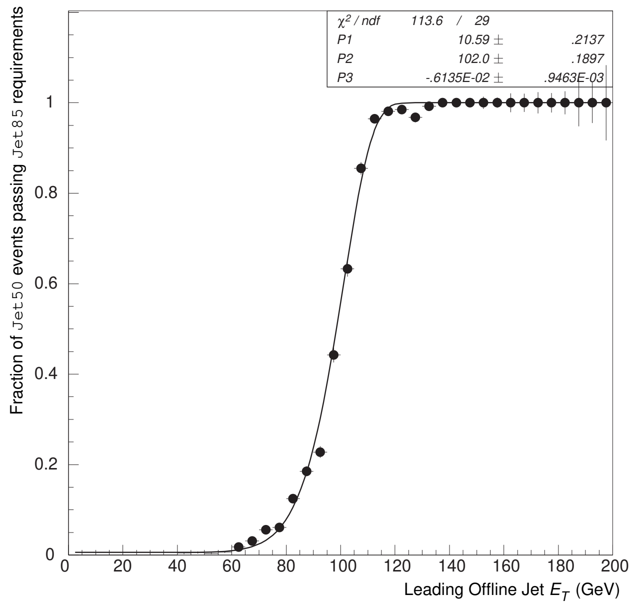

Figure 13: `jet85` turn on curve measured by the ratio of events taken by the `jet50` filter that pass `jet85` requirements. The parameterization is described in the text.

the mismeasurement is due to misplaced vertices. If an additional minbias event produces enough tracks, its interaction point will be assigned as the primary vertex from where the event is reconstructed. If the true hard scattering vertex is far enough from the misplaced primary vertex, the $\not\!\!E_T$ can be grossly mismeasured to a very high value.

These events with misplaced vertices are rare, but they are preferentially selected by this analysis due to the large $\not\!\!E_T$ requirement. The trigger and filter use `fastZ` and `slowZ` vertices respectively which are generated by timing information from the level 0 hodoscopes, not the tracking system. However, in events where the primary vertex is far from the true hard scattering vertex, the `fastZ`/`slowZ` vertex is still correlated with the incorrect primary vertex position as shown in Figure 14. Thus not only will the offline requirements accept these events, but the trigger will take them as well. Such balanced misvertexed events with

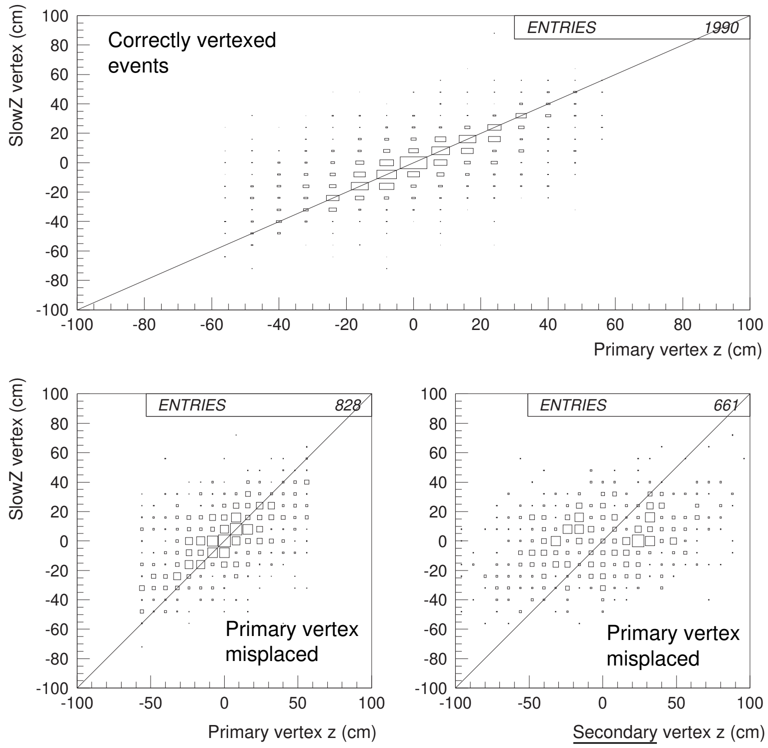

Figure 14: Trigger and offline vertex correlation. Data is from the `jet85` filter passing E_T and H_T requirements. The top plot is for events passing jet pointing (described in the text). The bottom two plots are those events that fail. Note how `slowZ` and the incorrect primary vertex are still quite correlated.

large measured $\not\!\!E_T$ swamp the candidate sample.

The solution of this problem for the Run 1a analysis was to impose a single interaction requirement on the data using the multiple interaction tool (`mi_tool`). [?] Any event with `mi_tool` value over 2, indicating a probable multiple interaction, was rejected. This cut reduced the observed integrated luminosity from ~13 pb^{-1} to ~7 pb^{-1}, for a loss of just less than half of the data. In Run 1b, the average instantaneous luminosity was much greater than in Run 1a ($\sim 10^{31}\,\mathrm{cm}^{-2}\,\mathrm{s}^{-1}$ in Run 1b). Requiring only single interactions would result in discarding a much larger fraction of the collected luminosity (approximately 2/3).

Most multiple interaction events are not a problem; rather it is only those where the vertex has been misidentified that give rise to mismeasured large $\not\!\!E_T$ events and constitute the instrumental background. In order to eliminate such events, the leading E_T central jet is required to emanate from the *primary* vertex selected by `reco`. This confirms that vertex as the true interaction point. This requirement is executed by using a technique for jet pointing [17] adapted and tuned for this analysis.

The procedures works in the following manner. Tracks within $DR = 0.4$ (in $\eta \times \phi$ space) of the axis of the leading E_T central jet projected into the Central Drift Chamber (CDC) are marked as associated with that jet. The origin of each of those tracks is determined by extrapolating them to the z axis (at $r = 0$). If a track extrapolates to within 10 cm of a reconstructed vertex, it is recorded as emanating from that vertex. An event will be rejected if the leading E_T central jet does not confirm the primary vertex as stipulated by the following criteria,

- The primary vertex is not confirmed if there are no tracks associated with the leading E_T central jet, or none of the tracks emanate from any reconstructed vertex. In the latter case, one has no faith that the primary vertex is correct. If no tracks are found close to the jet, as in the former case, it is unclear how the primary vertex was even determined.

- The primary vertex is not confirmed if 50% or more tracks associated with the leading E_T central jet emanate from a different vertex.

- The primary vertex is not confirmed if half or more of the tracks associated with the leading E_T central jet emanate from $|z| > 60$ cm. This requirement handles the case where the true interaction point falls in the region where vertex finding is less efficient or outside of the region where vertices are reconstructed.

Because full tracking is only performed for the CDC, only central jets can be used for this jet pointing technique. Using only the leading E_T central jet is sufficient to confirm the primary vertex and retains high signal efficiency. Nearly 100% of squark and gluino events have at least one central jet. Requiring a second central jet has an efficiency of approximately 90%.

This requirement is performed last in the analysis because more event information is needed than what is available on `microdsts`. See Section 3.2.

2.10.1 Details of Jet Pointing

In order to tune the jet pointing procedure and determine its efficiency, a data sample is needed. The goal is to keep the probability of rejecting a correctly vertexed event small while reducing as much of the misvertexed events background as possible.

Since activity in the CDC increases as the instantaneous luminosity increases, the jet pointing method will fail good events more often in periods of high instantaneous luminosity. Therefore, a sample of events is needed at a variety of instantaneous luminosities to measure the luminosity dependent efficiency. Ideally, one would like to use a sample with a low E_T jet trigger threshold so that the cross section for production of SUSY particles will be negligible compared to the QCD cross section. Unfortunately, the trigger with the lowest threshold, `jetmin`, was heavily prescaled and eliminated altogether after about 3/4 of Run 1b. Other slightly higher threshold jet triggers appeared for only a short time or included a Level Zero single interaction requirement. The only jet triggers that are usable are `jet85` (one large tile with E_T over 45 GeV and two large tiles over 10 GeV at level 1; level 2 jet over 85 GeV) and `jetmax` (one level 1 large tile over 35 GeV as well as two large tiles over 6 GeV; level 2 jet over 115 GeV). Fortunately, it appears that jet spectra of the leading jet from squark and gluino events resemble the leading jet spectra from these triggers, as shown in Figure 15.

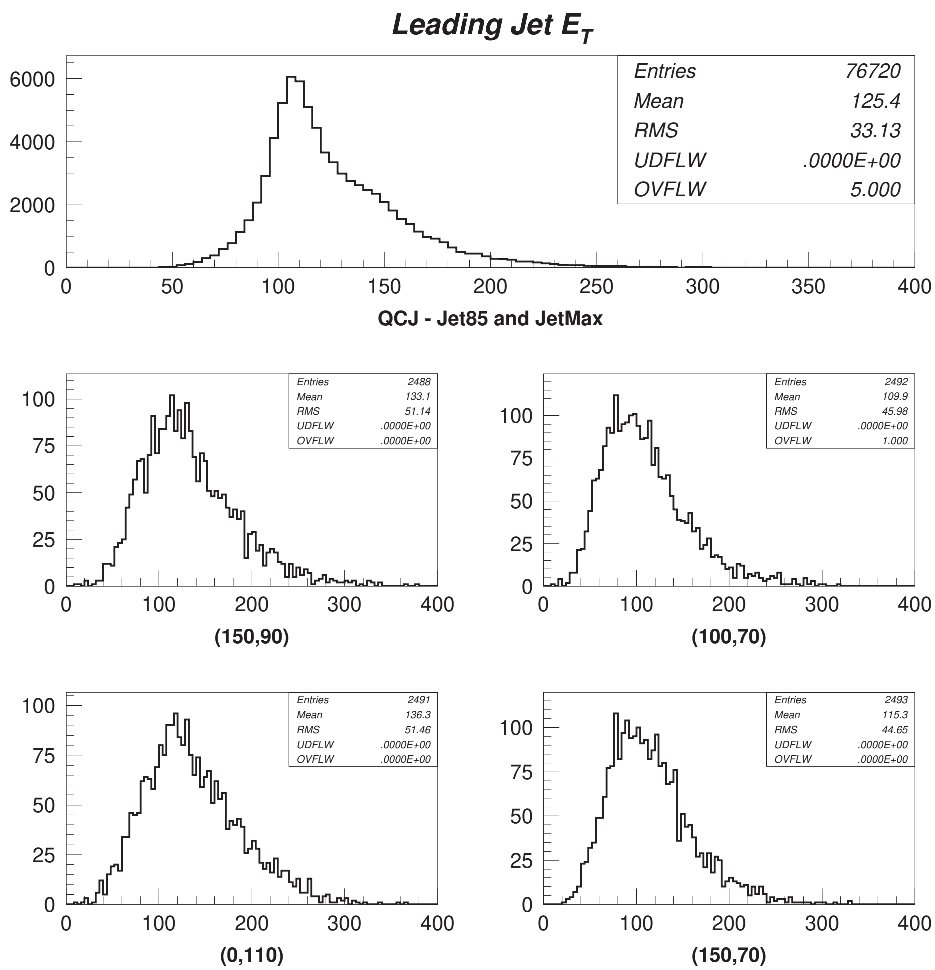

Figure 15: Leading jet E_T spectra. The lower four plots are from SUGRA MC samples with $(M_0, M_{1/2})$ as denoted.

Events from these triggers containing at least three good jets are used to tune and determine the efficiency of jet pointing. One still expects the SUSY cross section to be tiny compared to QCD when examining events at the low end of the $\not\!\!E_T$ spectrum.

As mentioned, the jet pointing method involves drawing a cone about the jet axis extrapolated into the CDC tracking volume. Any good track found within this cone is associated with that jet. Tracks are bad if they have no $r-z$ view (tracking is done in $r-\phi$ first, then $r-z$), have only two or fewer hits, have a bad χ^2 from fitting the hits, or have an $x-y$ impact parameter indicating that the track emanates from outside of the beam pipe.

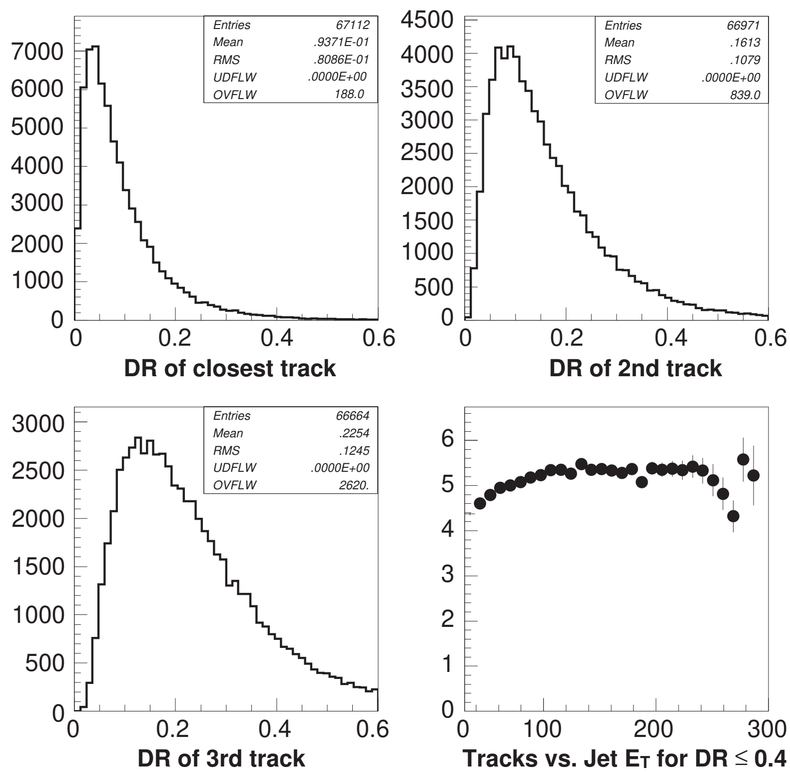

Figure 16: Jet – track matching. The first three plots show how close tracks come to the jet axis in $\eta \times \phi$ space. The lower right plot displays the average number of tracks found in a $DR = 0.4$ cone about the jet axis vs. jet E_T.

Figure 16 shows histograms of the distance that the closest, next closest and third closest tracks come to the jet axis. The jets are only from the central region ($|\eta_{\mathrm{detector}}| < 1.1$). A cone size of $DR = 0.4$ about the jet axis, where DR is the distance in $\eta \times \phi$ space, is appropriate to associate tracks with jets of 0.5 cone size. Enlarging this cone increases the probability that a stray track will be associated with the jet and thus will decrease the jet pointing efficiency.

The bottom right plot of Figure 16 shows the average number of tracks associated with a jet (found within the $DR = 0.4$ cone) vs. jet E_T. One would expect to find more tracks within higher E_T jets, since they can be made up of more particles than jets of low E_T. The plot does not show that behavior and seems to indicate that the CDC and/or tracking algorithm saturates if too many particles are present. Further indication of this saturation effect can be seen in Figure 17, showing the average number of tracks associated with the leading E_T central jet vs. instantaneous luminosity.

Now that the size of the cone to use for associating tracks is set, the efficiency of the jet pointing requirement must be determined. Multiple interactions are not included in the

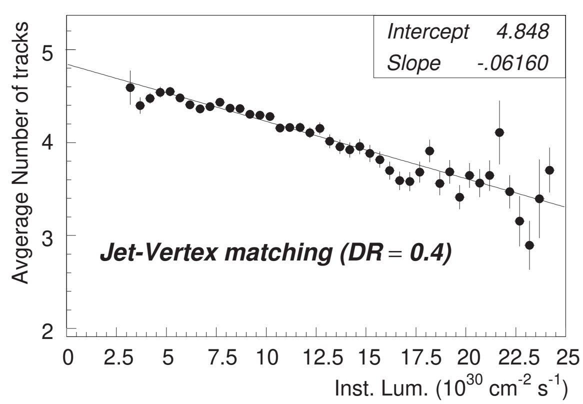

Figure 17: Average number of tracks in jets vs. instantaneous luminosity.

Monte Carlo samples, and the MC tracking efficiency is probably too high to accurately model high occupancy regions of the CDC, therefore the QCD multijet data are used to determine the jet pointing efficiency. Events from the QCD multijet sample are required to have at least three good jets (see the good jet requirements in Section 2.7) and $\not\!\!E_T <$ 25 GeV. The low $\not\!\!E_T$ requirement is used to assure that the events examined are less likely to suffer from misvertexing, since the efficiency should indicate how often correctly vertexed events are mistakenly rejected by the jet pointing requirement. This efficiency is shown vs. instantaneous luminosity in the plots displayed in Figure 18.

The top histogram in Figure 18 shows the instantaneous luminosity distribution for the QCD multijet events (after the good jet and low $\not\!\!E_T$ requirements are applied). The remaining plots show the fraction of events in each luminosity bin yielding a particular outcome of the jet pointing algorithm. The fractions for the same luminosity bin sum across the plots to one.

- Upper left plot: fraction of events where the primary vertex is confirmed, because the tracks in the central jet point to the primary vertex. Events shown here pass the jet pointing requirement, and the fractions are thus the efficiency of jet pointing vs. instantaneous luminosity. All events in the other plots fail jet pointing.

- Upper right: fraction of events where the jet had more tracks emanating from the secondary vertex than the primary.

- Middle left: fraction of events where the jet had more tracks emanating from the tertiary vertex than the primary. Only a few events have three vertices found.

- Middle right: fraction of events where none of the tracks associated with the jet point to a reconstructed vertex.

- Lower left: fraction of events where no tracks could be associated with the leading E_T central jet.

- Lower right: fraction of events where the jet had half or more of its associated tracks emanating from beyond $|z| = 60$ cm.

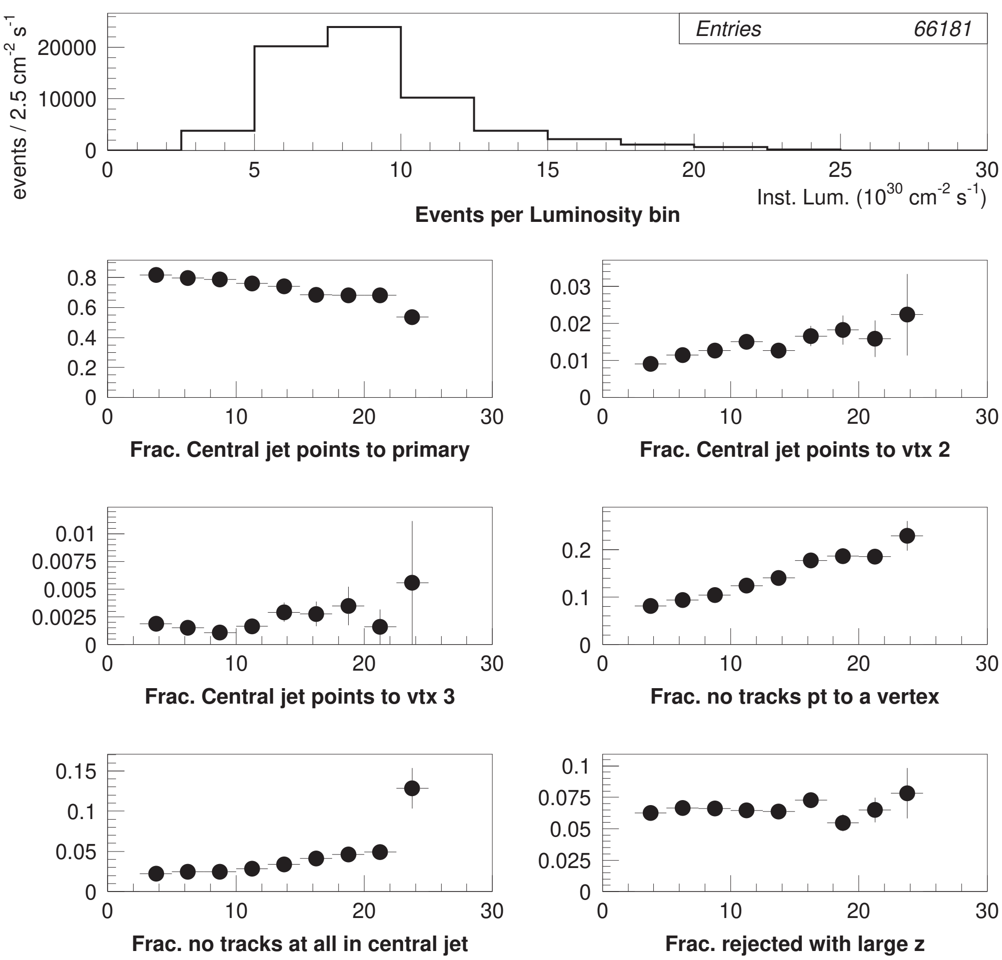

Figure 18: Efficiency of jet pointing. Plots are described in the text.

The jet pointing efficiency ranges from 82% for very low instantaneous luminosity to 68% for very large instantaneous luminosity (the last two bins displayed in the efficiency plots are for instantaneous luminosities where a minuscule amount of data were collected). When the luminosity profile of the data run (integrated luminosity vs. instantaneous luminosity, see Figure 22) is taken into account, the jet pointing method is 80% efficient overall.

Figure 19 shows at some level the effectiveness of the jet pointing procedure. The data come from a `jet85` QCD multijet sample passing most of the analysis cuts (except $\not\!\!E_T$ and leading jet E_T). The log plot shows three $\not\!\!E_T$ spectra, each normalized to its area. The filled circles denote the spectrum for all events. The grey triangles are for events passing the single interaction requirement of `mitool` (Run 1b version) < 2. Note that only a small fraction of the data passes this condition, as seen by the large error bars on the single interaction points. The filled squares are the data passing the jet pointing algorithm. At low $\not\!\!E_T$, all three types of points track together. As $\not\!\!E_T$ increases, the "all data" points develop the enhanced tail due to the misplaced vertex events. The "pass jet pointing" points tend to lie well below the "all data" points for large $\not\!\!E_T$.

The expected background, that is misvertexed events that pass the jet pointing requirement, is not explicitly determined since such events will contribute to the calculated QCD multijet background (see Section 4.2.1). An examination of the final event sample yielded no such mistakes by the jet pointing algorithm, indicating that the background is probably quite small.

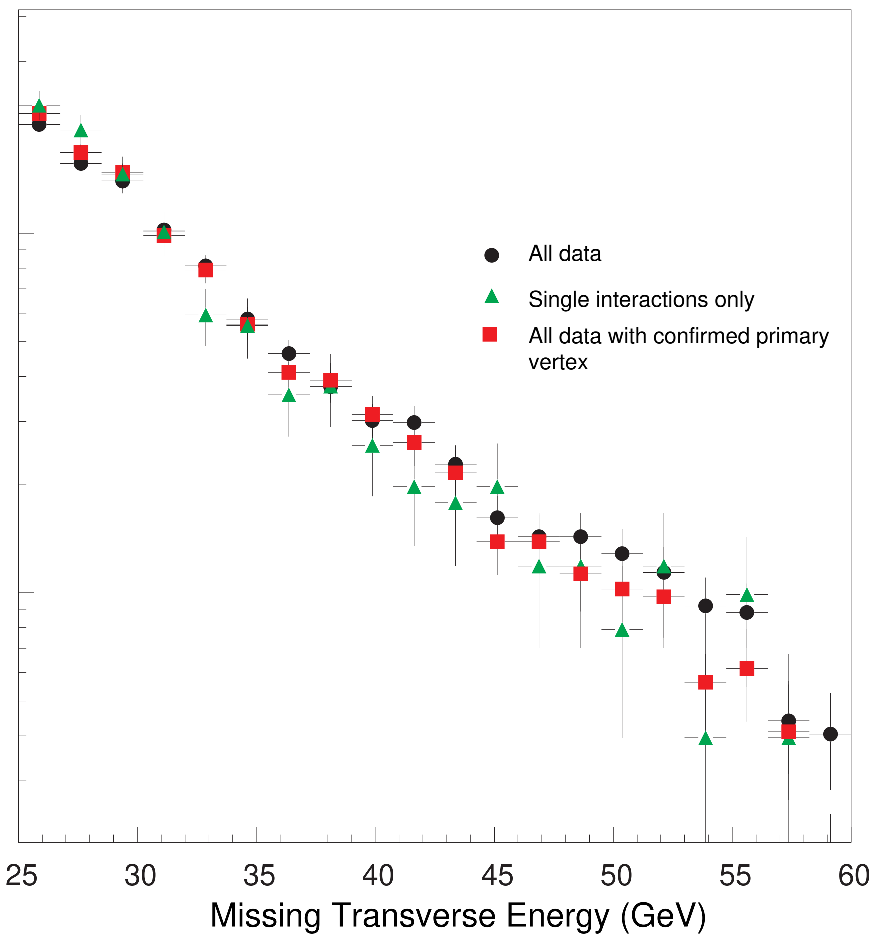

Figure 19: Effectiveness of jet pointing.

3 Collider Data

The data taken for this analysis correspond to an integrated luminosity of 79.2 pb^{-1}. Data were collected by an unprescaled trigger and then streamed into manageable file sets. An ntuple was made from those files with very loose $\not\!\!E_T$ and jet requirements. Most of the analysis cuts are performed on that ntuple, but since it is made from `microdst` files, there is not enough information to do the confirmation of the primary vertex step. A list of events passing the other requirements is generated and those events are picked to obtain `stas` or `dsts`. Running jet pointing on those events yields the final candidate sample consisting of 49 events (with $\not\!\!E_T > 50$ GeV and $H_T > 100$ GeV required). A full breakdown of the cuts on the data is given in Section 3.2.

3.1 Trigger and Filter

Events were collected for this analysis with the `missing_et` trigger and filter. This trigger was not prescaled at any time during Run 1b. The requirements of the trigger and filter are,

Level 1: L1 $\not\!\!E_T > 40$ GeV and at least one calorimeter trigger tower with $E_T > 5$ GeV and $|\eta_{\rm detector}| < 2$

Level 2: L2 $\not\!\!E_T > 40$ GeV

Level 1 calculates $\not\!\!E_T$ from trigger towers within $|\eta_{\rm detector}| < 1.6$, and does not include energy in the ICD and CH layers of the calorimeter. Since the CH is excluded, the `missing_et` trigger will not usually fire on events with only negative energy. Level 2 uses the entire calorimeter for its calculation and may remove at most one cell flagged as hot by the hot cell

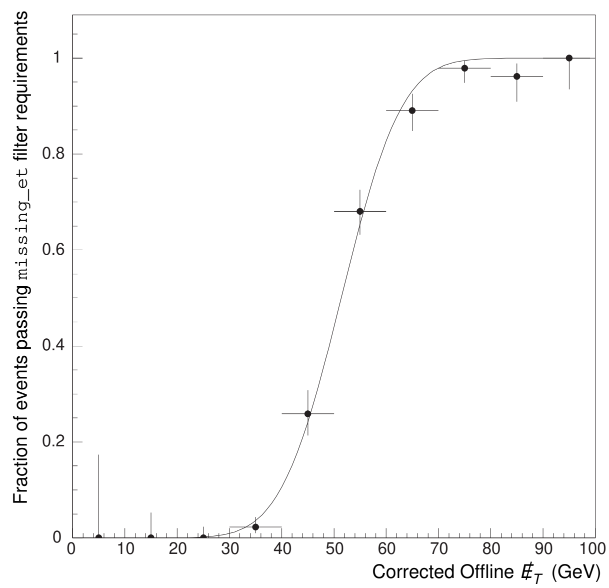

Figure 20: Turn on curve for the `missing_et` trigger from the "jet erasure" procedure.

killer (see Section 2.3). The trigger also requires `good_cal`, which means that the trigger is inhibited from taking data while the Main Ring is in injection or transition (`mrbs`) or while Main Ring protons are passing through the DØ calorimeter (`micro-blank`).

Figure 20 shows the turn on curve for the `missing_et` trigger. Obtaining a turn on curve for $\not\!\!E_T$ is nontrivial since there are many sources of $\not\!\!E_T$ in events (some instrumental). One would like to measure the turn on characteristics for events with true $\not\!\!E_T$ caused by physics processes (neutrinos). Two procedures are used.

One method [18] is used to generate the curve in Figure 20. The procedure is to take balanced multijet events collected by QCD jet triggers and replace one jet cell by cell with calorimeter noise. This "erases" the jet from the event, generating $\not\!\!E_T$ as if the jet were a neutrino. The altered events are then passed through `reco` (version 12.20) and the trigger simulator (version ??). The remaining jets and $\not\!\!E_T$ are corrected with `cafix` version 5.0.

The trigger simulator was designed to *exactly* mimic the online Level 1 and Level 2 systems, giving the $\not\!\!E_T$ that Level 1 and Level 2 would have seen. Figure 20 displays the fraction of events passing the `missing_et` trigger and filter requirements vs. corrected calorimeter $\not\!\!E_T$.

The other method involves a sample with high P_T muons. Since muons pass through the calorimeter leaving little energy, they generate calorimeter $\not\!\!E_T$. The statistics for the muon sample are very small, but the turn on curve is consistent with what is measured by the jet erasure method.

As seen in Figure 20, the `missing_et` trigger is fully efficient at ~75 GeV. The curve is parameterized by the function in Equation (4).

$$f(\not\!\!E_T) = \frac{1}{2}\left[\mathrm{erf}\left(\frac{\not\!\!E_T - x_0}{\sqrt{2}\sigma}\right) + 1\right] \tag{4}$$

The fit parameters are,

$$x_0 = 51.4 \pm 0.4$$

$$\sqrt{2}\sigma = 12.9 \pm 1.4$$

The χ^2 is 0.5.

The parameterization of the `missing_et` turn on curve is only used to calculate efficiencies and backgrounds for $\not\!\!E_T < 75$ GeV. Since the QCD background rises dramatically in between 50 and 75 GeV, the offline $\not\!\!E_T$ threshold is always in the region where `missing_et` is fully efficient.

3.2 Applying Analysis Requirements to the Data

All data were reconstructed with version 12 of the DØ reconstruction program (`reco`). Jets and $\not\!\!E_T$ were corrected by `cafix` 5.0. Table 5 shows the effects of each of the analysis requirements on the data. The initial sample comes from the `run1b_np_met d∅dad` stream. `d∅dad` streams are files of run and event pointers, allowing direct access to `ALL` stream `microdsts`. The `run1b_np_met d∅dad` stream contains the same events as the physical `np_met` STA stream. Any event passing the `missing_et`, `scalar_et`, or `jet_1_miss` triggers is included in the `run1b_np_met` stream.

Some events from the `run1b_np_met d∅dad` stream meeting loose requirements are extracted into an ntuple (see Appendix **??** for information on where to find data files used in this analysis). The ntuple requirements are that events must have corrected $\not\!\!E_T > 40$ GeV and at least two jet banks (any quality jets with E_T over 8 GeV). All of the analysis requirements except confirmation of the primary vertex are made on this ntuple. Note that the `missing_et` trigger requirement was not made when filling the ntuple to make it more usable to others.

The `microdsts` do not contain enough information to do the jet pointing procedure to confirm the primary vertex, since information about all of the tracks in the CDC is needed. The `microdst` only has information on CDC tracks that lie in roads pointing to an EM cluster. Therefore, a small sample of events passing all analysis requirements except for primary vertex confirmation is picked using the `pick events` facility [**?**]. `sta` or `dst` files of these events are obtained and are used to complete the analysis. A summary of the number of events passing for different $\not\!\!E_T$ thresholds is shown in Table 7. Some distributions of the data passing the analysis requirements are shown in Figure 21.

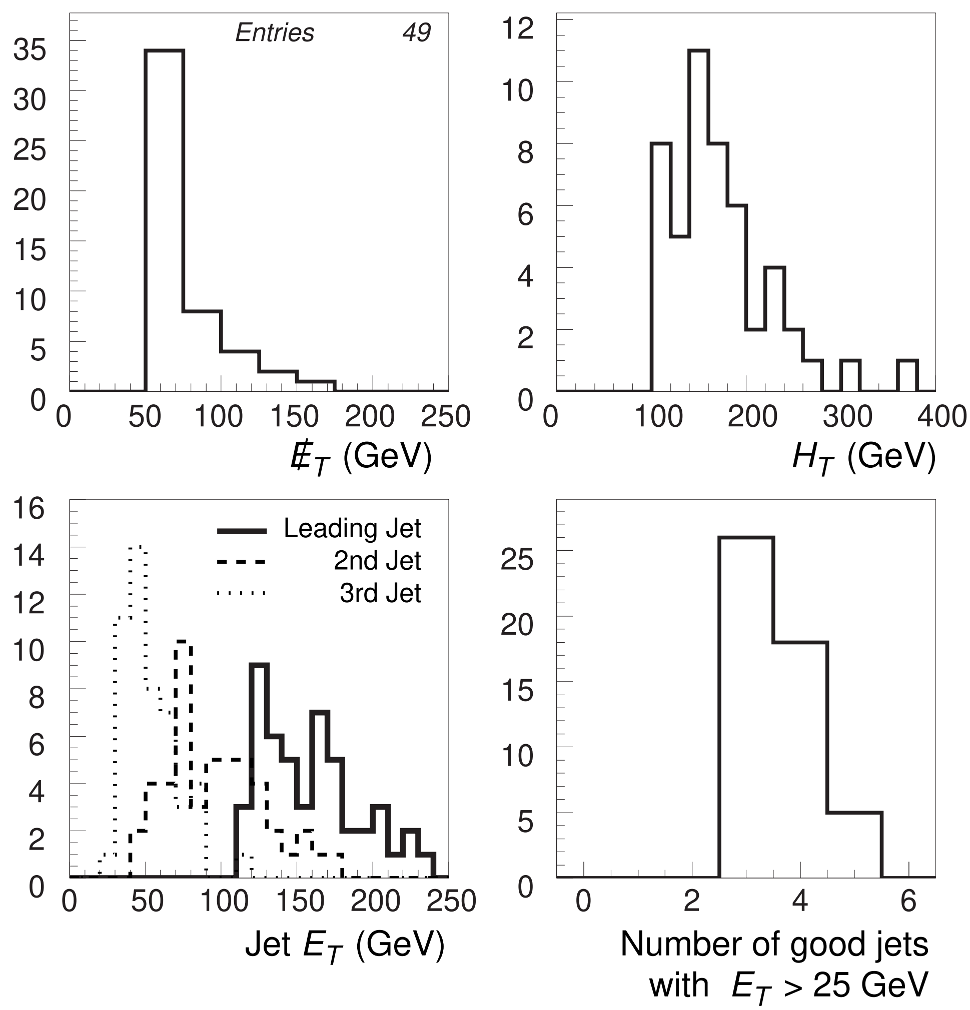

Figure 21: $\not{E}_T$, H_T, jet E_T distributions, and the number of jets for `missing_et` data passing $\not{E}_T > 50$ GeV and $H_T > 100$ GeV.

Analysis Requirement	*Events remaining*
Events in `run1b_np_met` stream	1,628,939
Events passing ntuple selection ($\not\!\!E_T$ > 40 GeV, 2 jet banks)	682,399
Pass `missing_et` filter	173,724
$0 < E_T^{\mathrm{scalar}} < 1800$ GeV	171,270
$-60 \leq$ primary vertex z position ≤ 60 cm	150,828
No cells removed from jets	118,762
All jets of $E_T > 15$ GeV pass good jet requirements	79,190
Leading jet not pointing towards ICR	71,023
At least 3 jets with $E_T > 25$ GeV	9,012
Jets not correlated with $\not\!\!E_T$ vector	2,838
$\not\!\!E_T > 50$ GeV	1,218
$H_T > 100$ GeV	418
Leading jet $E_T > 115$ GeV	136
No isolated muons with $E_T > 15$ GeV	135
Leading E_T central jet confirms primary vertex	49

Table 5: Analysis requirements on the data

3.2.1 Discrepancies Between `stas` and `microdsts`

One must use caution when switching from `microdsts` to `stas` and `dsts`. A part of the jet correction algorithm in `cafix` subtracts a jet's energy that is associated with electrons and photons (`pelcs` and `pphos`) found within the jet cone. On `stas` and `dsts`, a maximum of four such electrons or photons are recorded for each jet, while `microdsts` only keep track of at most two. Therefore, the $\not\!\!E_T$ values of some events will be slightly different between `microdsts` and `dsts` / `stas`. Because of this discrepancy, the cuts performed before picking

missing_et	jet85	jet50
79.2 ± 4.2 pb^{-1}	55.9 ± 3.0 pb^{-1}	4.7 ± 0.2 pb^{-1}

Table 6: Luminosity for triggers used in this analysis.

the events are not reapplied to the `dst` / `sta` sample.

3.3 Luminosity

The observed luminosity is determined by running the production data base utility `get_filt_lum` over the list of data files that were examined in the analysis. This file list is extracted from the `dødad` file catalog, `run1b_mds.filecat` dated November 1996. The total luminosity seen by the `missing_et` trigger is 84.3 pb^{-1}. 3.4 pb^{-1} of luminosity from runs flagged as "bad" are subtracted as well as 1.6 pb^{-1} from files that `dødad` failed to load. 79.2 pb^{-1} remains. A summary of the luminosity information is given in Table 6. The systematic error on the luminosity is 5.3% [?].

A plot of the instantaneous luminosity profile is given in Figure 22. The average instantaneous luminosity for Run 1b for events collected in the `missing_et` stream is 8.76×10^{30} cm^{-2} s^{-1}.

3.4 Candidates

Table 7 displays the number of events in the data passing the analysis requirements for different $\not\!\!E_T$ and H_T thresholds. The points with $\not\!\!E_T$ threshold of 50 GeV are not used in the analysis.

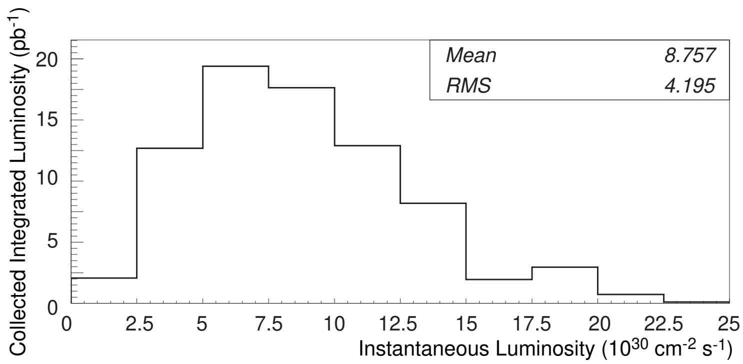

Figure 22: Luminosity profile for the Run 1b `missing_et` trigger.

$\not\!\!E_T >$ (GeV)	$H_T >$ (GeV)	Candidates	$\not\!\!E_T >$ (GeV)	$H_T >$ (GeV)	Candidates
50	100	49	50	150	31
75	100	15	75	120	12
75	140	11	75	150	8
75	160	6	90	100	8
100	100	7	100	150	3

Table 7: Number of candidate events passing all requirements with varying $\not\!\!E_T$ and H_T thresholds.

4 Background Estimation

A disadvantage of the jets and missing energy signature is the large backgrounds that must be dealt with. Section 2 describes the requirements on the analysis designed to reduce the backgrounds as much as possible while still retaining signal efficiency. There are two types of background sources: those with $\not\!\!E_T$ due to one or more neutrinos produced in the event and those with $\not\!\!E_T$ from purely instrumental effects. Many background sources are considered. Details of the background estimates are shown in Tables 10 through 19.

4.1 Physics Backgrounds

The examined SM processes that have $\not\!\!E_T$ due to one or more neutrinos in the final state are:

- $t\bar{t}$ decays
- $W \to e\nu$ + jets
- $W \to \mu\nu$ + jets
- $W \to \tau\nu$ + jets, $\tau \to \ell\nu$
- $W \to \tau\nu$ + jets, $\tau \to$ hadrons
- $W \to \ell\nu$, $Z \to X$
- $W \to \ell\nu$, $W \to qq'$
- $Z \to \tau\tau$ + jets

Process	σ_{vis} (pb)	$\pm\delta\sigma_{vis}$ (pb)	MC events generated
$t\bar{t} \to X$	5.77	1.75	39512
$W \to e\nu + \geq 3$ jets	95.67	28.70	18052
$W \to \mu\nu + \geq 3$ jets	95.67	28.70	18205
$W \to \tau\nu + \geq 3$ jets, $\tau \to \ell\nu$	34.15	10.24	6665
$W \to \tau\nu + \geq 2$ jets, $\tau \to$ hadrons	173.82	34.76	11165
$W \to \ell\nu$, $W \to qq'$	5.54	1.66	47579
$W \to \ell\nu$, $Z \to X$	0.32	0.10	48121
$Z \to \mu\mu + \geq 3$ jets	3.19	0.96	11987
$Z \to \tau\tau$, $25 < Z\,p_T < 50$	18.50	5.55	11932
$Z \to \tau\tau$, $50 < Z\,p_T < 100$	4.10	1.30	2971
$Z \to \tau\tau$, $100 < Z\,p_T < 200$	0.48	0.14	988
$Z \to \tau\tau$, $200 < Z\,p_T < 400$	0.02	0.006	982
$Z \to \nu\nu$, $25 < Z\,p_T < 50$	70.00	21.00	39929
$Z \to \nu\nu$, $50 < Z\,p_T < 100$	20.00	6.00	9976
$Z \to \nu\nu$, $100 < Z\,p_T < 200$	2.50	0.75	999
$Z \to \nu\nu$, $200 < Z\,p_T < 400$	0.08	0.02	981

Table 8: Background information. Cross sections and errors are shown for the processes generated with Monte Carlo. Events with hot cells are not counted.

- $Z \to \nu\nu$ + jets

The background summary tables indicate the background estimates for different $\not\!\!E_T$ and H_T requirements.

The analysis requirements as described in Section 2 are applied to all background Monte Carlo samples. Events where `aida` removed a cell from a jet are corrected by putting the cell back into the event and adjusting the jet quantities and $\not\!\!E_T$ accordingly. Events that have an isolated hot cell, indicating that a jet was lost to the hot cell killer, are not counted. Furthermore, the removed cell efficiency as described in Sections 2.3.1 and 2.3.2 is applied to all Monte Carlo events. A summary of the background Monte Carlo information is given in Table 8. Each background is discussed in subsequent sections.

All Monte Carlo samples produced were processed by `showerlibrary` `geant` and `reco`.

4.1.1 $t\bar{t}$ decays

Production and decays of top quarks is the most significant standard model background, because the process of two heavy objects decaying through W bosons is very similar to squark and gluino cascade decays. The most prevalent $t\bar{t}$ decay mode that passes the analysis requirements is $t\bar{t} \rightarrow \ell +$ jets (one W decays to jets, the other decays to a lepton plus a neutrino), since the many jets may have large E_T and there is significant $\not\!\!E_T$ due to the neutrino from the W decay. The fact that the lepton must not be found can also act to enhance the $\not\!\!E_T$. The $t\bar{t} \rightarrow$ all jets type events have little intrinsic $\not\!\!E_T$ and very rarely pass the analysis requirements.

The $t\bar{t}$ background is estimated from a 40,000 event Monte Carlo sample produced by `herwig` [?] with the top quark mass set at 170 GeV/c^2, close to the DØ measured value of 172 GeV/c^2 [?]. The DØ measured cross section at that mass is 5.77 ± 1.82 pb [?]. So that errors are not applied twice, luminosity and energy scale errors are removed from the error on the cross section, resulting in an error of 1.72 pb.

Figure 23 displays the number of events from different $t\bar{t}$ decay modes passing the analysis requirements. The sample used there is from `isajet` instead of `herwig`, because the `herwig` events do not contain enough information to determine the parents of all of the daughter particles.

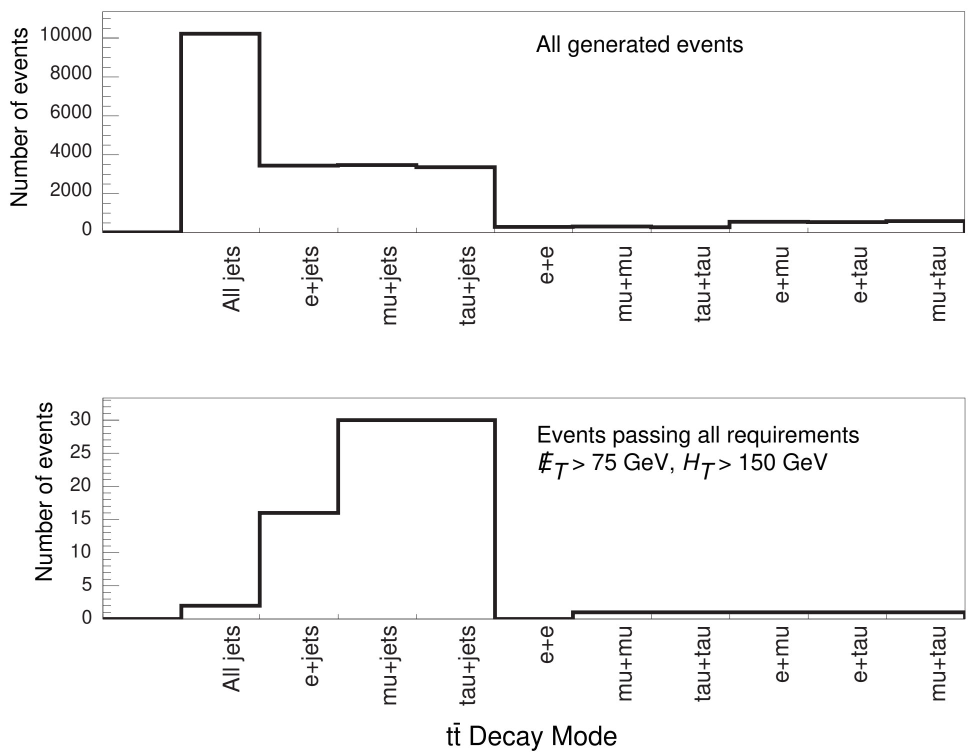

Figure 23: $t\bar{t}$ decay modes. The top plots shows the number of events generated in an `isajet` top quark to everything Monte Carlo sample ($M_{\rm top} = 170$ GeV/c^2). The bottom plot shows the number of events passing all of the analysis requirements ($\not\!\!E_T > 75$ GeV and $H_T >$ 150 GeV).

Single top

Although single top quark production has not been observed, one may imagine that such events can mimic the squark and gluino jets and missing energy signature. However, single top events typically do not have enough high E_T jets to pass the analysis requirements. With the low theoretical cross section for single top production, there is zero contribution to this analysis.

4.1.2 $\mathbf{W} \to \ell\nu$

W boson decays can be an important background since the neutrino can make substantial $\not\!\!E_T$ in the event along with energy that went with a lost lepton. Though the leading jet produced in initial or final state radiation may have substantial E_T, the other jets are typically soft. By excluding the leading jet from the H_T calculation as described in Section 2.8, the H_T requirement severely reduces the contribution from these sources to the analysis background.

Large W + jets `vecbos` Monte Carlo samples produced by the Top group (~20,000 events per decay type) and hadronized by `isajet` are used. For all W decays except for hadronic decays of the tau, a $W \to \ell\nu + \geq 3$ jets sample is used. Since a tau decaying to hadrons will look like a jet, a $W \to \ell\nu + \geq 2$ jets sample is used to get the $W \to \tau\nu$, $\tau \to$ hadrons estimate (only W's decaying to taus decaying to hadrons are examined).

The `vecbos` cross sections are used with a 30% error applied for the 3 jet samples and 20% for the two jet sample (10% per generated jet). [6]

4.1.3 WW and WZ

Events with vector boson pairs are considered because the final states are somewhat close to those of top decays though with less jets produced. Although the cross section for production of WW is close that of $t\bar{t}$, there are not enough high E_T jets for events to pass the analysis requirements.

Two `isajet` samples with ~50,000 events each produced by the Top group are used for this estimate: one for $W \to \ell\nu$, $W \to qq'$ events and another for $W \to \ell\nu$, $Z \to X$ events. The WW cross section is 5.54 ± 1.66 pb and the WZ cross section is 0.32 ± 0.10 pb. Only a handful of Monte Carlo events pass the analysis requirements, yielding no contribution to the background.

4.1.4 $\mathbf{Z} \to \nu\nu$ and $\mathbf{Z} \to \tau\tau$

Decays of the Z boson do not normally involve large missing energy except perhaps in the invisible mode ($Z \to \nu\nu$) but even then, the neutrinos are back to back if the Z is not boosted. Therefore, for Z events to mimic the SUSY signal, the Z must be heavily boosted and a lepton must be lost for the visible modes.

The $Z \to \nu\nu$ and $Z \to \tau\tau$ backgrounds are estimated with `pythia`. As seen in Table 8, several large samples of such events with varying ZP_T were produced. In order to reduce the number of events going through `geant` and `reco`, events were required to have three generator level jets with $E_T > 7$ GeV and generator $\not{E}_T > 40$ GeV. The larger the ZP_T, the more events that pass, but the cross section also drops. For $ZP_T > 400$ GeV, the cross section is so small that the contribution to this analysis is negligible. The cross sections are determined by `pythia` with an assumed error of 30%.

The H_T requirement severely reduces the amount of these backgrounds, since the secondary jets are typically soft like the W backgrounds.

4.2 Instrumental Backgrounds

Instrumental backgrounds arise from events where the $\not\!\!E_T$ is solely due to mismeasurements. Examples of possible sources are:

- QCD multijet events with mismeasured jets
- $t\bar{t} \rightarrow$ all jets events with mismeasured jets
- $Z \rightarrow ee$ + jets, $Z \rightarrow \mu\mu$ + jets events where both leptons are lost or mismeasured.

The Z sources yield little contribution (< 0.04 event for the loosest requirements of $\not\!\!E_T > 75$ GeV and $H_T > 100$ GeV). A 12,000 event $Z \rightarrow \mu\mu + \geq 3$ jets `vecbos` Monte Carlo sample was used to check the estimate. Although such events could rarely have substantial $\not\!\!E_T$ when a muon is lost, the H_T requirement eliminates them.

The $t\bar{t} \rightarrow$ all jets source is essentially identical to mismeasured QCD multijet events. QCD has a huge cross section, however, so it is expected that the $t\bar{t} \rightarrow$ all jets contribution is small compared to QCD.

4.2.1 Mismeasured QCD Multijet Events

QCD multijet events can be a background when one or more jets fluctuate and are mismeasured, potentially generating $\not\!\!E_T$ in what should be a balanced event. The jet – $\not\!\!E_T$ direction correlation requirements described in Section 2.4 eliminate much of this background, but there is still some left over. The background is difficult to estimate, since one does not expect a Monte Carlo to correctly model the extreme tails of the QCD multijet $\not{E}_T$ spectrum where the jet fluctuations are large. Therefore, collider data is used to estimate the QCD multijet background.

One cannot use QCD multijet data with very large $\not{E}_T$, since that overlaps with the signal region and the events would be the same as those passing the analysis `missing_et` trigger. In order to stay in the region where the QCD cross section dominates over SUSY, some characteristic of low $\not{E}_T$ QCD data must be extrapolated into the signal region to estimate the background. Two procedures are used: a shape fit and an extrapolation of the QCD multijet $\not{E}_T$ spectrum.

The shape fit is the primary method used for this analysis. The procedure involves taking histograms of a certain distribution from data and background/signal sources and then use a histogram shape fitter to estimate the contribution of each source to the data. The histogram shape fitter itself is described in Appendix A and Reference 19. The distribution that is fit is derived from the two dimensional plot of $\phi_{\mathrm{2nd\,jet}} - \phi_{\not{E}_T}$ vs. $\phi_{\mathrm{Leading\,jet}} - \phi_{\not{E}_T}$ shown in Figure 9. The distance of each point from the upper right hand corner at (π, π) is histogrammed for the data, QCD multijet events, $t\bar{t}$ Monte Carlo, and a squark and gluino signal sample as shown in Figure 24. Note that the histograms have variable sized bins so that when random angles are plotted, the resulting histogram is flat. This rather peculiar distribution (henceforth referred to as "distance from (π, π)") was chosen because the histograms from QCD multijet events and $t\bar{t}$/ SUSY events are markedly different. Since the QCD multijet background is the goal of the fit, it is important to use a distribution where the QCD events are distinct. The fact that $t\bar{t}$ and SUSY histograms appear very similar (as expected since $t\bar{t}$ decays are

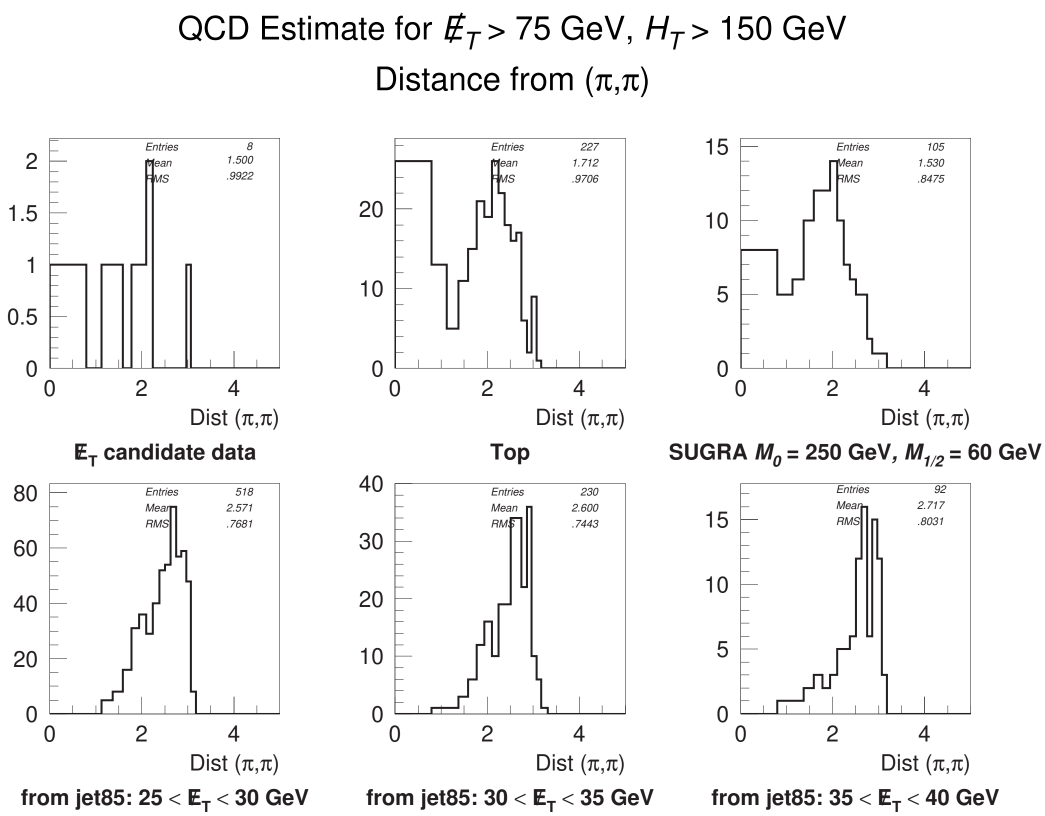

Figure 24: The "Distance from (π, π)" distributions.

similar to squark and gluino decays) will mean that the fitter will attribute left over data to both $t\bar{t}$ and SUSY about evenly. That is of no concern, since $t\bar{t}$ background and SUSY efficiencies are determined by other means.

The QCD multijet data used in the shape fit are from the `jet85` trigger. In order for the extrapolating methods to work well, there must be a large amount of multijet data in various $\not\!\!E_T$ bins. A sample taken by the `jet85` trigger which was only prescaled at the highest luminosities provides the largest amount of data. The trigger with the next lower jet threshold, `jet50` yields a sample with less than one tenth the size of the `jet85` sample. The lower threshold jet triggers were either severely prescaled, eliminated altogether after a fraction of the run, or had some additional unwanted requirements such as single interactions. The sample from `jet85` is the only viable option. In order for the `jet85` sample to be a proper model of the background, the leading jet requirement of $E_T > 115$ GeV is made in the analysis as described in Section 2.9.*

All of the analysis requirements except for $\not\!\!E_T$ are made on events from the `jet85` trigger. The events are then binned by $\not\!\!E_T$, and histograms of the distance from (π, π) distribution are made. A good feature of the distance from (π, π) distribution for QCD multijet events is that it only changes slightly as $\not\!\!E_T$ is increased, thus the shape most likely holds for large $\not\!\!E_T$. Three or four $\not\!\!E_T$ bins are used: $25 < \not\!\!E_T < 30$ GeV, $30 < \not\!\!E_T < 35$ GeV, $35 < \not\!\!E_T < 40$ GeV, and for some samples $40 < \not\!\!E_T < 45$ GeV. The last sample is omitted if it is populated with less than 30 events.

*In order to generate a very large sample of low threshold jets in Run II, it may be feasible to produce distributions in the level 3 trigger system instead of collecting and writing out each event. That procedure will work so long as complicated event-by-event information and corrections are not needed. For Run I, events that are misvertexed contaminate the jet samples and are removed by the primary vertex confirmation method described in Section 2.10; a procedure too complex to run in the level 2 filter nodes.

Each of the QCD multijet histograms are independently fed into the histogram shape fitter along with histograms from `missing_et` stream data (the data histogram) , $t\bar{t}$ Monte Carlo and a SUSY signal Monte Carlo sample. The latter three samples also have all analysis requirements applied including the various $\not{E}_T$ and H_T requirements.

The result of this procedure is a posterior probability distribution of the expected QCD multijet contribution to the data done for each of the QCD multijet $\not{E}_T$ bins. The distributions shown in Figure 25 are all similar. They are peaked at or near zero with large tails. The estimate for the expected number of QCD multijet events is taken to be the average of the means of the three (or four) distributions with the error given by the average of the RMS values. The means of the distributions are all within errors of each other.

The histogram fitter can only handle three source histograms plus the data histogram. Though one would like to include all of the backgrounds in the fit, that is difficult to do since there must be a more events in the histograms than the number of bins. For most of the backgrounds determined from Monte Carlo other than $t\bar{t}$, very few events pass. Since $t\bar{t}$ is the dominant physics background, adding in the others would have little affect. In fact, replacing the SUSY signal sample with the $W \rightarrow e\nu + \geq 3$ jets histogram only changes the result by 0.1 event. Replacing the SUSY histogram with ones from other SUGRA points also has little affect on the QCD estimate, since the distance from (π, π) distributions are similar.

To verify that the QCD multijet background estimate is valid, an extrapolation of the QCD multijet $\not{E}_T$ spectrum is also performed, again using `jet85` data with all the require-

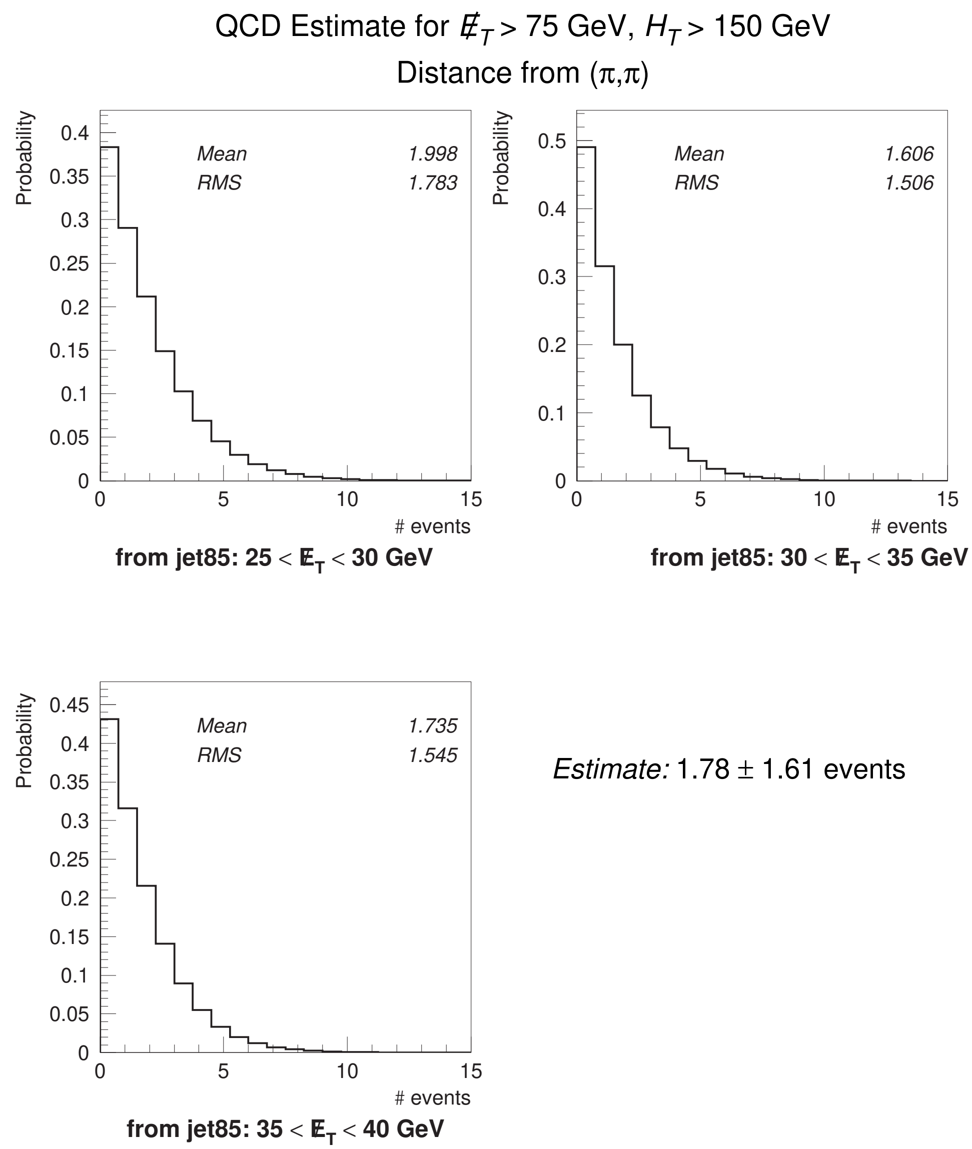

Figure 25: Posterior probability distributions for QCD estimate.

ments except $\not\!\!E_T$ applied. Figure 26 shows a $\not\!\!E_T$ spectrum and a fit with the function,

$$f(\not\!\!E_T) = \frac{N\beta e^{-\left(\sqrt{\beta \not\!\!E_T} - \sqrt{\beta \not\!\!E_{T\mathrm{cut}}}\right)}}{2\left(1 + \sqrt{\beta \not\!\!E_{T\mathrm{cut}}}\right)} \tag{5}$$

This function is essentially $f(x) = e^{-\sqrt{x}}$ with extra constants so that for a value of $\not\!\!E_{T\mathrm{cut}}$, the fit parameter N is almost the number of events expected for $\not\!\!E_T > \not\!\!E_{T\mathrm{cut}}$ (N is $f(\not\!\!E_T)$ integrated from $\not\!\!E_{T\mathrm{cut}}$ to infinity). The estimate is obtained by dividing N by the bin width (5 GeV) and then multiplying by the ratio of the `missing_et` luminosity to the `jet85` luminosity (79.2/55.9). The estimate for the extrapolation in Figure 26 is 1.7 ± 0.3 events. One has no evidence that the very small errors are correct, especially since the χ^2 of the fit would seem to indicate that the errors on the points are too small.

The QCD estimates from the shape fit shown in Figure 24 and Figure 25 agree well with the $\not\!\!E_T$ extrapolation in Figure 26. Table 9 compares the estimates for some other $\not\!\!E_T$/ H_T requirements.

For the QCD multijet background prediction at $\not\!\!E_T > 50$ GeV, the histogram shape fitting procedure cannot be used, because it is not designed to handle accounting for the `missing_et` turn on curve (the trigger is inefficient for $\not\!\!E_T < 75$ GeV). Therefore, the extrapolation of the $\not\!\!E_T$ spectrum with the turn on curve folded in is used to obtain that background estimate. The estimates are displayed in Tables 10 and 11.

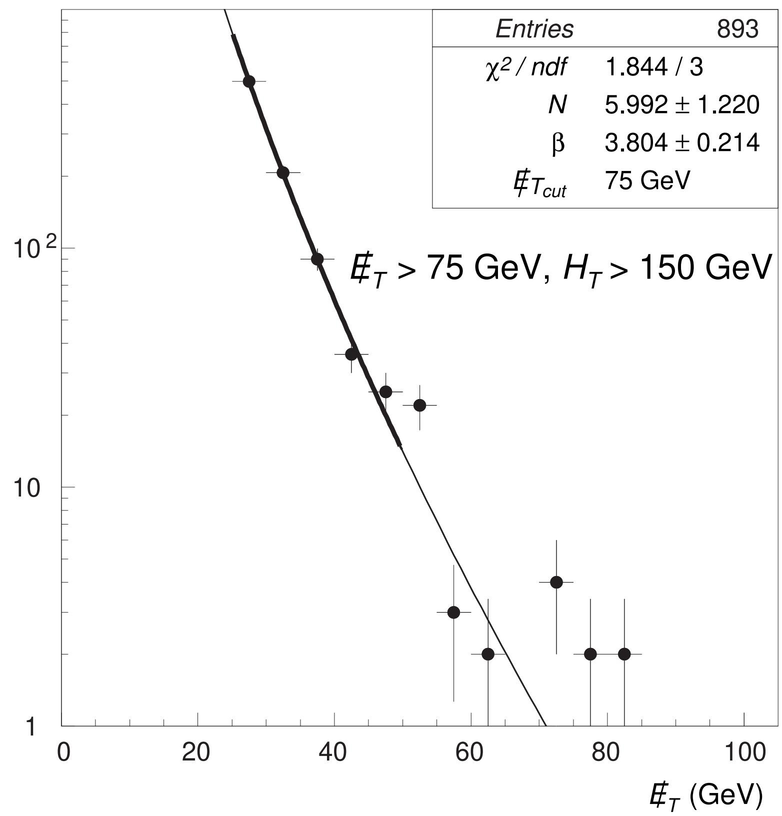

Figure 26: Extrapolation of the QCD multijet $\not\!\!E_T$ spectrum from `jet85`. The fit region is $25 < \not\!\!E_T < 45$ GeV. The parameters for the expected QCD background at $\not\!\!E_T > 75$ GeV are described in the text.

$\not\!\!E_T >$ (GeV)	$H_T >$ (GeV)	Shape fit Estimate	Extrapolation Estimate
75	100	3.5 ± 2.6	2.8 ± 0.9
75	150	1.8 ± 1.6	1.7 ± 0.3
100	100	1.7 ± 1.6	0.6 ± 0.1

Table 9: QCD background estimates from the shape fit and $\not\!\!E_T$ spectrum extrapolation.

4.3 Background Estimates

The background estimates for all the analysis requirements and varying $\not\!\!E_T$ and H_T thresholds are shown in Tables 10 through 19. The expected background, $< N >$, is given for 79.2 pb^{-1} of data. E–scale indicates the error due to the energy scale. The energy scale error [20] is calculated from the change in the number of events passing the cuts when each jet in every event is modified according to

$$E_{T_{\rm new}} = (\pm 4\%)\, E_T \pm 1 \text{ GeV} \tag{6}$$

where (+) and (−) are for the high and low energy scale errors respectively. δLum is the error due to the luminosity and $\delta\sigma$ is the error due to the cross section. Only the backgrounds that contribute events are shown. The total background expected without QCD is given at the bottom of the first block. The QCD background with its error is then shown.

The bottom block shows the total background. The first error is the total statistical error. The upper and lower errors are the sum of the upper and lower systematic errors. The systematic errors are added in the following manner:

- Energy scale errors are added linearly.
- Luminosity errors are added linearly.
- All `vecbos` and `pythia` cross section errors are added linearly. The $t\bar{t}$ cross section error is then added in quadrature to form the cross section error.
- The energy scale, luminosity, cross section, and error on the QCD estimate are added in quadrature to form the final error.

The "95% CL No Pass" value indicates the 95% upper limit on the number of events that could be contributed from background sources that have a zero efficiency for passing the analysis requirements. Finally, the number of events seen in the data is displayed.

Background	$< N >$	$\pm$ Stat	+ E–scale	− E–scale	$\pm$ δLum	$\pm$ $\delta\sigma$
$t\bar{t} \to X$	4.67	$\pm$ 0.21	+ 1.69	− 1.10	$\pm$ 0.25	$\pm$ 1.41
$W \to e\nu + \geq 3$ jets	1.35	$\pm$ 0.67	+ 0.03	− 0.03	$\pm$ 0.07	$\pm$ 0.40
$W \to \ell\nu$, $W \to qq'$	0.29	$\pm$ 0.05	+ 0.11	− 0.12	$\pm$ 0.02	$\pm$ 0.09
$Z \to \mu\mu + \geq 3$ jets	0.04	$\pm$ 0.03	+ 0.04	− 0.01	$\pm$ 0.00	$\pm$ 0.01
$Z \to \tau\tau$	0.22	$\pm$ 0.08	+ 0.01	− 0.09	$\pm$ 0.01	$\pm$ 0.07
$Z \to \nu\nu$	1.02	$\pm$ 0.34	+ 0.55	− 0.03	$\pm$ 0.05	$\pm$ 0.30
Total (w/o QCD)	7.59	$\pm$ 0.79	+ 2.45	− 1.39	$\pm$ 0.40	$\pm$ 1.49

$< N_{QCD} >$ 36.4 ± 7.9

Total $< N >$	95% CL No Pass	Events in Data
$44.0 \pm 0.8\ ^{+8.5}_{-8.2}$	0.8	49

Table 10: Backgrounds for $\not{E}_T > 50$ GeV and $H_T > 100$ GeV. The QCD background is from extrapolating the `jet85` $\not{E}_T$ spectrum.

Background	$< N >$	$\pm$ Stat	+ E–scale	− E–scale	$\pm$ δLum	$\pm$ $\delta\sigma$
$t\bar{t} \to X$	3.13	$\pm$ 0.17	+ 1.17	− 0.81	$\pm$ 0.17	$\pm$ 0.95
$W \to \ell\nu$, $W \to qq'$	0.09	$\pm$ 0.03	+ 0.08	− 0.03	$\pm$ 0.00	$\pm$ 0.03
$Z \to \nu\nu$	0.09	$\pm$ 0.02	+ 0.01	− 0.02	$\pm$ 0.01	$\pm$ 0.03
Total (w/o QCD)	3.35	$\pm$ 0.17	+ 1.29	− 0.86	$\pm$ 0.18	$\pm$ 0.95

$< N_{QCD} >$ 21.9 ± 5.14

Total $< N >$	95% CL No Pass	Events in Data
$25.2 \pm 0.2\ ^{+5.4}_{-5.3}$	0.8	31

Table 11: Backgrounds for $\not\!\!E_T > 50$ GeV and $H_T > 150$ GeV. The QCD background is from extrapolating the `jet85` $\not\!\!E_T$ spectrum.

Background	$< N >$	$\pm$ Stat	+ E–scale	− E–scale	$\pm$ δLum	$\pm$ $\delta\sigma$
$t\bar{t} \to X$	3.11	$\pm$ 0.17	+ 1.08	− 0.84	$\pm$ 0.17	$\pm$ 0.94
$W \to e\nu + \geq 3$ jets	1.35	$\pm$ 0.67	+ 0.03	− 0.03	$\pm$ 0.07	$\pm$ 0.40
$W \to \ell\nu$, $W \to qq'$	0.21	$\pm$ 0.04	+ 0.09	− 0.09	$\pm$ 0.01	$\pm$ 0.06
$Z \to \mu\mu + \geq 3$ jets	0.04	$\pm$ 0.02	+ 0.03	− 0.01	$\pm$ 0.00	$\pm$ 0.01
$Z \to \tau\tau$	0.14	$\pm$ 0.06	+ 0.01	− 0.06	$\pm$ 0.01	$\pm$ 0.05
$Z \to \nu\nu$	0.93	$\pm$ 0.33	+ 0.42	− 0.03	$\pm$ 0.04	$\pm$ 0.28
Total (w/o QCD)	5.79	$\pm$ 0.77	+ 1.67	− 1.08	$\pm$ 0.31	$\pm$ 1.04

$< N_{QCD} >$ 3.54 ± 2.64

Total $< N >$	95% CL No Pass	Events in Data
$9.3 \pm 0.8\,^{+3.4}_{-3.2}$	0.8	15

Table 12: Backgrounds for $\not\!\!E_T > 75$ GeV and $H_T > 100$ GeV.

Background	$< N >$	$\pm$ Stat	$+$ E–scale	$-$ E–scale	$\pm$ δLum	$\pm$ $\delta\sigma$
$t\bar{t} \to X$	2.65	$\pm$ 0.16	$+$ 1.02	$-$ 0.71	$\pm$ 0.14	$\pm$ 0.80
$W \to e\nu + \geq 3$ jets	0.34	$\pm$ 0.34	$+$ 0.03	$-$ 0.03	$\pm$ 0.02	$\pm$ 0.10
$W \to \ell\nu$, $W \to qq'$	0.13	$\pm$ 0.03	$+$ 0.05	$-$ 0.06	$\pm$ 0.01	$\pm$ 0.04
$Z \to \mu\mu + \geq 3$ jets	0.02	$\pm$ 0.02	$+$ 0.01	$-$ 0.02	$\pm$ 0.00	$\pm$ 0.01
$Z \to \tau\tau$	0.05	$\pm$ 0.03	$+$ 0.00	$-$ 0.00	$\pm$ 0.00	$\pm$ 0.02
$Z \to \nu\nu$	0.61	$\pm$ 0.27	$+$ 0.02	$-$ 0.02	$\pm$ 0.03	$\pm$ 0.18
Total (w/o QCD)	3.81	$\pm$ 0.46	$+$ 1.14	$-$ 0.84	$\pm$ 0.20	$\pm$ 0.82

$< N_{QCD} >$ 2.68 ± 2.23

Total $< N >$	95% CL No Pass	Events in Data
$6.5 \pm 0.5\,^{+2.7}_{-2.6}$	0.8	12

Table 13: Backgrounds for $\not{E}_T > 75$ GeV and $H_T > 120$ GeV.

Background	$< N >$	$\pm$ Stat	+ E–scale	− E–scale	$\pm$ δLum	$\pm$ $\delta\sigma$
$t\bar{t} \to X$	2.19	$\pm$ 0.14	+ 0.78	− 0.58	$\pm$ 0.12	$\pm$ 0.66
$W \to \ell\nu$, $W \to qq'$	0.08	$\pm$ 0.02	+ 0.03	− 0.04	$\pm$ 0.00	$\pm$ 0.03
$Z \to \tau\tau$	0.02	$\pm$ 0.00	+ 0.00	− 0.00	$\pm$ 0.00	$\pm$ 0.01
$Z \to \nu\nu$	0.25	$\pm$ 0.15	+ 0.05	− 0.10	$\pm$ 0.01	$\pm$ 0.07
Total (w/o QCD)	2.54	$\pm$ 0.21	+ 0.86	− 0.72	$\pm$ 0.13	$\pm$ 0.67

$< N_{QCD} >$ 2.05 ± 1.82

Total $< N >$	95% CL No Pass	Events in Data
$4.6 \pm 0.2\,^{+2.1}_{-2.1}$	0.7	11

Table 14: Backgrounds for $\not{E}_T > 75$ GeV and $H_T > 140$ GeV.

Background	$< N >$	$\pm$	Stat	$+$	E–scale	$-$	E–scale	$\pm$	δLum	$\pm$	$\delta\sigma$
$t\bar{t} \rightarrow X$	2.03	$\pm$	0.14	$+$	0.65	$-$	0.67	$\pm$	0.11	$\pm$	0.62
$W \rightarrow \ell\nu$, $W \rightarrow qq'$	0.06	$\pm$	0.02	$+$	0.04	$-$	0.02	$\pm$	0.00	$\pm$	0.02
$Z \rightarrow \tau\tau$	0.02	$\pm$	0.00	$+$	0.00	$-$	0.00	$\pm$	0.00	$\pm$	0.01
$Z \rightarrow \nu\nu$	0.09	$\pm$	0.02	$+$	0.01	$-$	0.02	$\pm$	0.01	$\pm$	0.03
Total (w/o QCD)	2.21	$\pm$	0.14	$+$	0.70	$-$	0.71	$\pm$	0.12	$\pm$	0.62

$< N_{QCD} >$ 1.78 ± 1.61

Total $< N >$	95% CL No Pass	Events in Data
$4.0 \pm 0.1\ ^{+1.9}_{-1.9}$	0.7	8

Table 15: Backgrounds for $\not\!\!E_T > 75$ GeV and $H_T > 150$ GeV.

Background	$<N>$	$\pm$	Stat	$+$	E–scale	$-$	E–scale	$\pm$	δLum	$\pm$	$\delta\sigma$
$t\bar{t} \to X$	1.73	$\pm$	0.13	$+$	0.72	$-$	0.53	$\pm$	0.09	$\pm$	0.53
$W \to \ell\nu$, $W \to qq'$	0.06	$\pm$	0.02	$+$	0.01	$-$	0.03	$\pm$	0.00	$\pm$	0.02
$Z \to \tau\tau$	0.02	$\pm$	0.00	$+$	0.00	$-$	0.00	$\pm$	0.00	$\pm$	0.00
$Z \to \nu\nu$	0.08	$\pm$	0.02	$+$	0.01	$-$	0.01	$\pm$	0.00	$\pm$	0.02
Total (w/o QCD)	1.89	$\pm$	0.13	$+$	0.74	$-$	0.58	$\pm$	0.10	$\pm$	0.53

$< N_{QCD} >$ 1.72 ± 1.54

Total $<N>$	95% CL No Pass	Events in Data
$3.6 \pm 0.1\ ^{+1.8}_{-1.7}$	0.7	6

Table 16: Backgrounds for $\not\!\!E_T > 75$ GeV and $H_T > 160$ GeV.

Background	$< N >$	$\pm$	Stat	+	E–scale	$-$	E–scale	$\pm$	δLum	$\pm$	$\delta\sigma$
$t\bar{t} \to X$	2.22	$\pm$	0.14	+	0.94	$-$	0.64	$\pm$	0.12	$\pm$	0.67
$W \to e\nu + \geq 3$ jets	1.01	$\pm$	0.58	+	0.03	$-$	0.03	$\pm$	0.05	$\pm$	0.30
$W \to \ell\nu$, $W \to qq'$	0.18	$\pm$	0.04	+	0.08	$-$	0.08	$\pm$	0.01	$\pm$	0.05
$Z \to \mu\mu + \geq 3$ jets	0.03	$\pm$	0.02	+	0.02	$-$	0.01	$\pm$	0.00	$\pm$	0.01
$Z \to \tau\tau$	0.11	$\pm$	0.05	+	0.01	$-$	0.03	$\pm$	0.01	$\pm$	0.03
$Z \to \nu\nu$	0.93	$\pm$	0.33	+	0.43	$-$	0.16	$\pm$	0.05	$\pm$	0.28
Total (w/o QCD)	4.47	$\pm$	0.69	+	1.51	$-$	0.96	$\pm$	0.24	$\pm$	0.76

$< N_{QCD} >$ 2.48 ± 2.01

Total $< N >$	95% CL No Pass	Events in Data
$7.0 \pm 0.7\ ^{+2.7}_{-2.5}$	0.8	8

Table 17: Backgrounds for $\not{E}_T > 90$ GeV and $H_T > 100$ GeV.

Background	$< N >$	$\pm$ Stat	+ E–scale	$-$ E–scale	$\pm$ δLum	$\pm$ $\delta\sigma$
$t\bar{t} \to X$	1.75	$\pm$ 0.13	+ 0.73	$-$ 0.54	$\pm$ 0.09	$\pm$ 0.53
$W \to e\nu + \geq 3$ jets	1.01	$\pm$ 0.58	+ 0.03	$-$ 0.03	$\pm$ 0.05	$\pm$ 0.30
$W \to \ell\nu$, $W \to qq'$	0.16	$\pm$ 0.03	+ 0.06	$-$ 0.08	$\pm$ 0.01	$\pm$ 0.05
$Z \to \mu\mu + \geq 3$ jets	0.02	$\pm$ 0.02	+ 0.02	$-$ 0.00	$\pm$ 0.00	$\pm$ 0.01
$Z \to \tau\tau$	0.08	$\pm$ 0.04	+ 0.00	$-$ 0.00	$\pm$ 0.00	$\pm$ 0.02
$Z \to \nu\nu$	0.79	$\pm$ 0.30	+ 0.28	$-$ 0.03	$\pm$ 0.04	$\pm$ 0.24
Total (w/o QCD)	3.81	$\pm$ 0.67	+ 1.15	$-$ 0.69	$\pm$ 0.20	$\pm$ 0.63

$< N_{QCD} >$ 1.77 ± 1.59

Total $< N >$	95% CL No Pass	Events in Data
$5.6 \pm 0.7\,^{+2.2}_{-2.0}$	0.8	7

Table 18: Backgrounds for $\not\!\!E_T > 100$ GeV and $H_T > 100$ GeV.

Background	$<N>$	$\pm$ Stat	+ E–scale	− E–scale	$\pm$ δLum	$\pm$ $\delta\sigma$
$t\bar{t} \to X$	1.04	$\pm$ 0.10	+ 0.44	− 0.40	$\pm$ 0.06	$\pm$ 0.32
$W \to \ell\nu$, $W \to qq'$	0.03	$\pm$ 0.02	+ 0.03	− 0.01	$\pm$ 0.00	$\pm$ 0.01
$Z \to \nu\nu$	0.09	$\pm$ 0.02	+ 0.02	− 0.02	$\pm$ 0.00	$\pm$ 0.03
Total (w/o QCD)	1.18	$\pm$ 0.10	+ 0.49	− 0.43	$\pm$ 0.06	$\pm$ 0.32

$< N_{QCD} >$ 1.15 ± 1.08

Total $<N>$	95% CL No Pass	Events in Data
$2.3 \pm 0.1\ ^{+1.2}_{-1.2}$	0.7	3

Table 19: Backgrounds for $\not{E}_T > 100$ GeV and $H_T > 150$ GeV.

5 Results

No significant excess over standard model backgrounds is observed for any of the $\not{E}_T$ and H_T thresholds. Since no new physics will be discovered with this analysis (oh well), cross section and mass limits are determined.

5.1 Sensitivity to the Signal

To determine the sensitivity of this analysis, production and decays of squarks and gluinos are simulated using `isajet` v7.13 [21]. Events are produced according to the SUGRA parameters described in Section 1.1. Three SUGRA parameters and the top quark mass are fixed to the following values:

- $\tan\beta = 2$,
- $A_0 = 0$,
- $\mathrm{sign}(\mu) < 0$,
- $M_{top} = 170$ GeV/c^2.

A_0 only affects the decay of SUSY light scalar top quarks. Since jets from the top squarks are soft, this analysis is not sensitive to them and so the value of A_0 has little effect. Changing μ to be positive dramatically decreases the mass difference between the charginos and neutralinos, so that cascade decays produce very soft jets and little $\not{E}_T$. The analysis is not attempted for $\mathrm{sign}(\mu) > 0$. Changing $\tan\beta$ alters the gauge and Higgs content of the charginos and neutralinos, thus changing the branching ratios in cascade decays. $\tan\beta = 2$

is a popular value among theorists. Altering $\tan\beta$ may be done as an extension of this analysis.

With those SUGRA parameters set, events are generated at 49 various points in the M_0 – $M_{1/2}$ plane as shown in Figure 27. The MC samples are processed by `showerlibrary geant` v3.14 and `reco` v12.15. All of the analysis requirements are applied to these samples. Events that have an isolated hot cell are not counted (see Section 2.3.2).

Although in principle all sparticles can contribute to this analysis, squarks and gluinos by far dominate the types of events that pass the requirements and also have the largest production cross sections. Therefore, only squark and gluino type events are produced by `isajet`. All decay modes are allowed.

Next-to-leading order cross sections [22] are calculated by the `prospino` program [23]. `prospino` determines the $\tilde{g}-\tilde{g}$, $\tilde{q}-\tilde{g}$, $\tilde{q}-\tilde{q}$, and $\tilde{q}-\bar{\tilde{q}}$ NLO cross sections. `prospino` does not include scalar tops in its calculation (that will be available in the near future from the program's authors). Therefore, any scalar tops produced by `isajet` are not counted. Typically, less than 1% of squark and gluino events produced contain scalar tops, and only up to a percent or two of them will pass the analysis requirements since jets and $\not\!\!E_T$ from scalar tops are soft.

`prospino` assumes that the squarks (except the scalar top) are mass degenerate. To obtain a cross section from `prospino` for a certain value of M_0 and $M_{1/2}$, the equivalent gluino and squark masses must be determined. The conversion is done with code within `isajet`, and the five squark masses are averaged to obtain the degenerate squark mass.

Typically, the NLO cross sections from `prospino` are anywhere from equal to double the cross sections returned by `isajet`. For a given M_0 and $M_{1/2}$, the ratios of the NLO squark

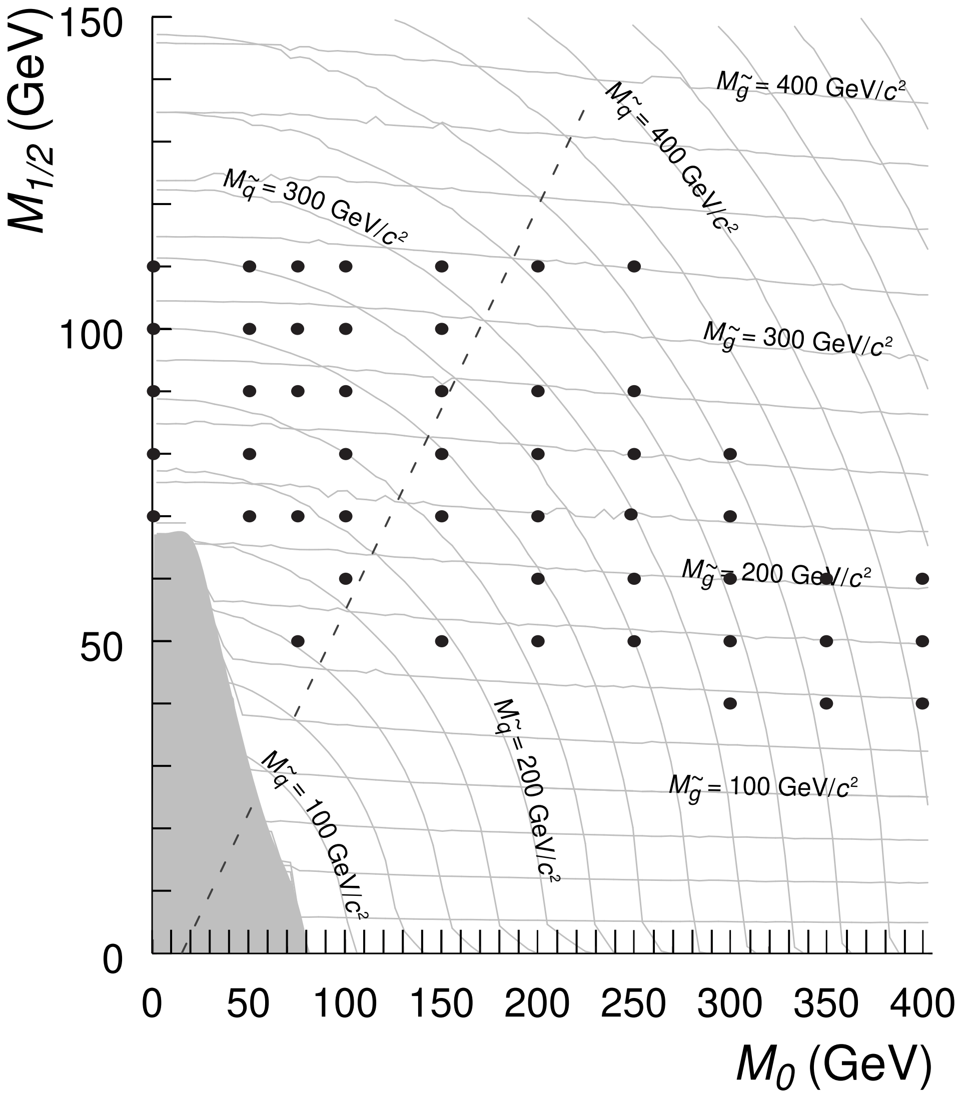

Figure 27: Monte Carlo signal points in the M_0 – $M_{1/2}$ plane. The light grey lines are contours of gluino and squark masses. The dashed line indicates where squarks and gluinos have equal mass. The shaded region is where SUGRA yields some unphysical condition.

and gluino production process cross sections (gluino–gluino, squark–squark, etc.) match ratios of the types of squark and gluino events that `isajet` produces to within 10%.

A list of total production cross sections is given in Tables 20 through 22.

5.2 Optimization of the $\not\!\!E_T$ and H_T requirements

As seen in the figures of Section 2, the characteristics of the signal changes as M_0 and $M_{1/2}$ are varied. Therefore, more than one set of analysis requirements will help maximize signal efficiency and background rejection for each SUGRA point. The two requirements that can be easily varied within some limits are $\not\!\!E_T$ and H_T.

For a given signal point, the efficiencies for passing the analysis requirements with $\not\!\!E_T$ ranging from 50 GeV to 150 GeV and H_T varying from 100 GeV to 250 GeV (both with 5 GeV steps) are recorded. A similar procedure is performed for all of the background efficiencies along with keeping track of their energy scale errors (or the QCD estimate error for the QCD background).

An "optimizing figure of merit" is calculated for each tested $\not\!\!E_T - H_T$ point,

$$F(\not\!\!E_T, H_T) = S/\sqrt{B + \sigma^2} \tag{7}$$

where S is the number of signal events expected, B is the number of background events expected, and σ is the average of the sum high and low energy scale errors for all of the backgrounds added in quadrature with the QCD background estimate error. The optimal $\not\!\!E_T - H_T$ thresholds are found by looking near the peak of the 2-D F distribution. Typically, the maximum of F is the center of a plateau in the $\not\!\!E_T - H_T$ plane where F only changes slightly. One chooses the lower edge of the plateau for greater signal efficiency to facilitate a discovery.

$\not{E}_T - H_T$ are optimized for all signal samples. Three example optimization plots are shown in Figures 28 through 30. As seen in the figures, the F value falls rapidly as $\not{E}_T$ drops below 75 GeV due to the rapidly increasing QCD background. An explanation of the general trends of the optimization is given in Section 5.3. Note that many signal samples have an optimized H_T of 100 GeV, the lower H_T limit. All of the SUGRA samples have H_T peaked beyond 100 GeV, so decreasing H_T will soon start the fall of the F parameter as little signal is being added while the backgrounds are increasing. The value of 100 GeV H_T is probably very near true optimal for those signal points where F in H_T does not show a full plateau.

Tables 20 through 22 include the optimized $\not{E}_T$ and H_T thresholds as well as the efficiency and number of events expected for each signal point. The errors on the efficiencies are the statistical and the high and low energy scale errors. The energy scale errors are calculated in the same manner as the backgrounds. The error on the expected number of events is the statistical and average of the energy scale errors added in quadrature.

5.3 Exclusion Contour

With no excess of events over standard model backgrounds, cross section and exclusion limits are calculated.

A 95% CL cross section limit is calculated in the manner described in Reference 8 for each of the SUGRA Monte Carlo points in the $M_0 - M_{1/2}$ plane† The appropriate background estimates associated with a M_0, $M_{1/2}$ point are used by the limit calculator, along with the

†At this time, the limit out to $M_0 = 300$ GeV has been determined.

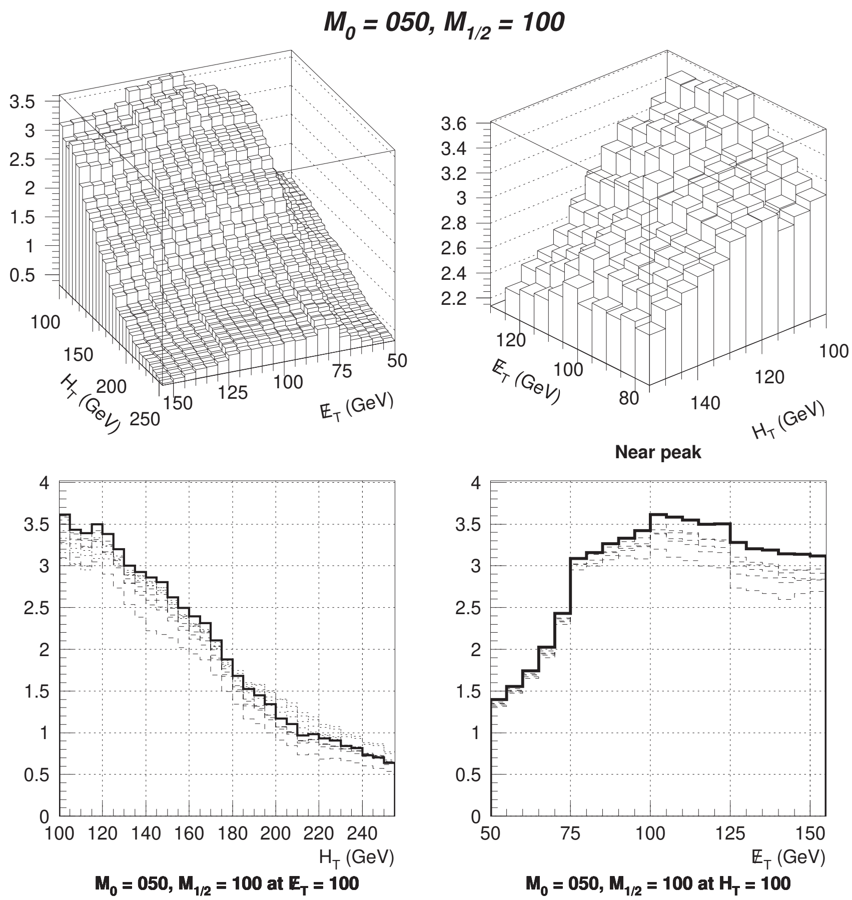

Figure 28: Optimizing figure of merit (F) for $M_0 = 50$ GeV and $M_{1/2} = 100$ GeV. The upper left plot shows F for the entire $\not\!\!E_T - H_T$ plane. The region around the peak of F is displayed in the upper right hand plot (note the different orientation of the plot). The lower two plots show the projection of F on the H_T axis (lower left) and the $\not\!\!E_T$ axis (lower right). The heavy solid line indicates the F trace for the $\not\!\!E_T$ or H_T slice that corresponds to the peak (and shown in the plot caption). The long dashed lines show F traces when the $\not\!\!E_T$ or H_T slice is moved higher the peak in five steps of 5 GeV. The dotted lines are for moving lower than the peak (obviously, there will be no dotted lines on the $\not\!\!E_T$ plot when the peak H_T value is at the lower limit of 100 GeV). For this signal point, the optimal thresholds are $\not\!\!E_T = 100$ GeV and $H_T = 100$ GeV.

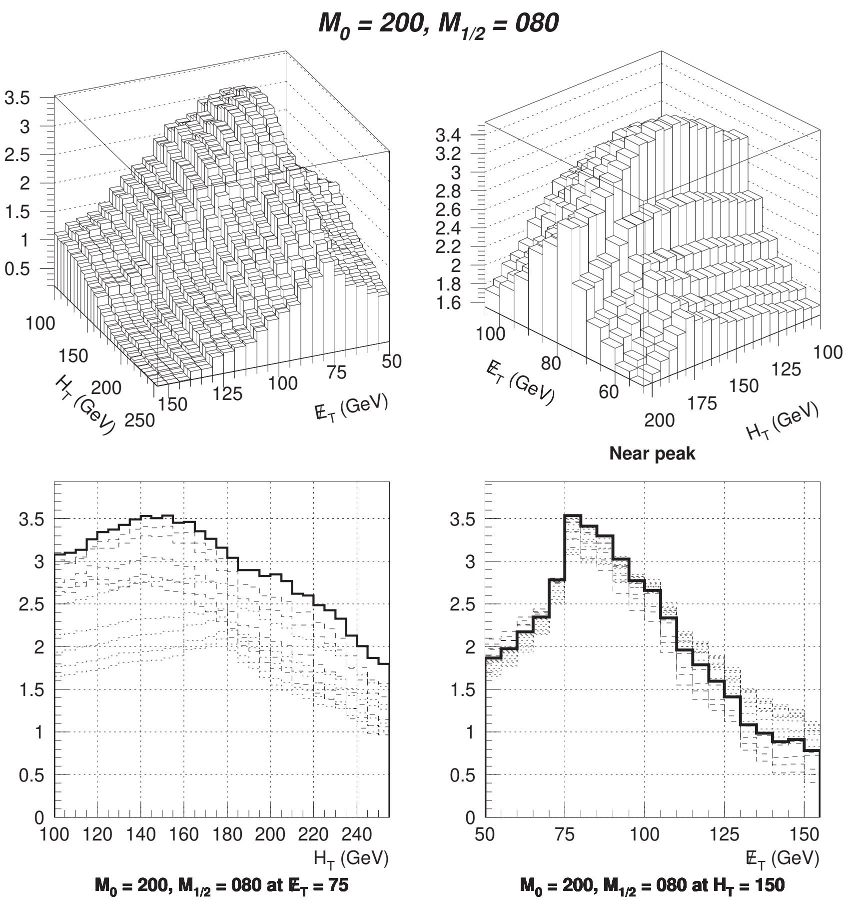

Figure 29: Optimizing figure of merit for $M_0 = 200$ GeV and $M_{1/2} = 80$ GeV. For this signal point, the optimal thresholds are $\not\!\!E_T = 75$ GeV and $H_T = 140$ GeV.

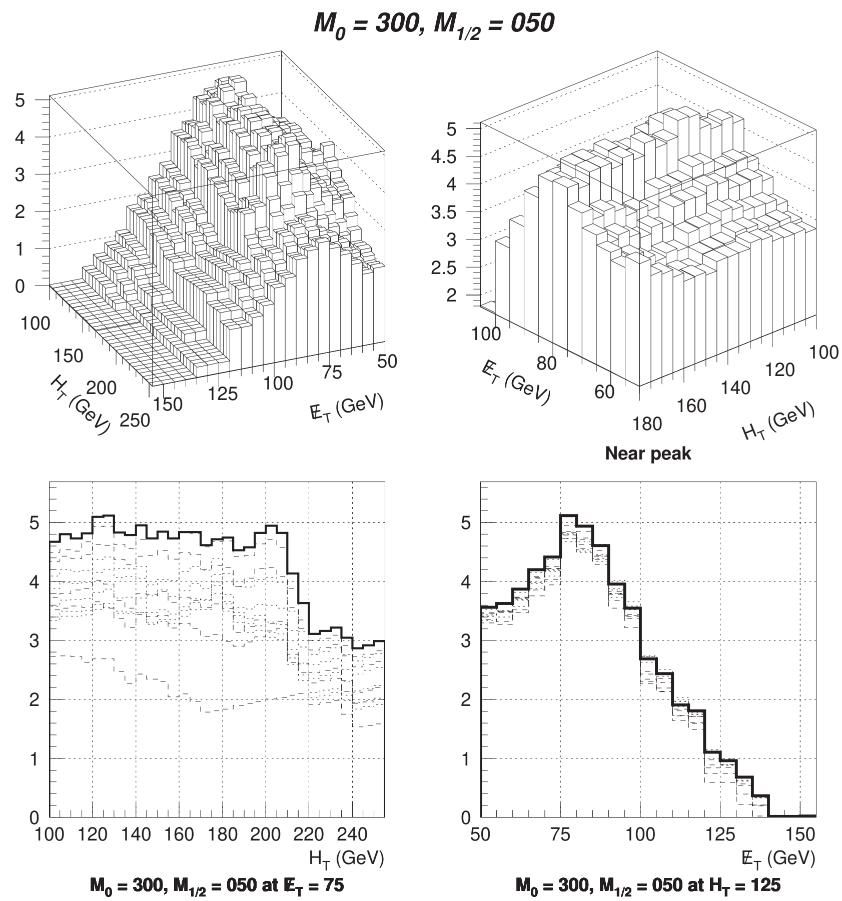

Figure 30: Optimizing figure of merit for $M_0 = 300$ GeV and $M_{1/2} = 50$ GeV. For this signal point, the optimal thresholds are $\not{E}_T = 75$ GeV and $H_T = 120$ GeV.

M_0 (GeV)	$M_{1/2}$ (GeV)	MC Events	$\not{E}_T >$ (GeV)	$H_T >$ (GeV)	σ_{NLO} (pb)	ϵ (%)	$< N >$
0	70	2468	75	100	30.1	$2.1 \pm 0.3 {}^{+0.5}_{-0.4}$	50.9 ± 13.2
0	80	2451	100	100	11.7	$2.8 \pm 0.3 {}^{+0.6}_{-0.5}$	25.7 ± 5.9
0	90	2428	100	100	5.8	$4.6 \pm 0.4 {}^{+0.8}_{-0.8}$	21.1 ± 3.9
0	100	2407	100	100	2.8	$4.9 \pm 0.4 {}^{+1.0}_{-1.1}$	10.8 ± 2.5
0	110	2389	100	100	1.3	$6.5 \pm 0.4 {}^{+0.5}_{-0.9}$	6.9 ± 0.9
50	70	2448	75	100	25.6	$2.7 \pm 0.3 {}^{+1.0}_{-0.6}$	54.5 ± 16.4
50	80	2454	100	100	11.3	$3.4 \pm 0.3 {}^{+1.1}_{-0.7}$	30.4 ± 8.5
50	90	2429	100	100	5.1	$4.3 \pm 0.4 {}^{+0.9}_{-1.0}$	17.3 ± 4.2
50	100	2406	100	100	2.5	$5.8 \pm 0.4 {}^{+0.9}_{-1.2}$	11.3 ± 2.2
50	110	2385	100	100	1.2	$6.7 \pm 0.5 {}^{+1.3}_{-1.2}$	6.5 ± 1.3
75	50	991	75	100	121.5	$1.1 \pm 0.3 {}^{+0.4}_{-0.4}$	107.5 ± 47.5
75	70	983	100	100	21.2	$2.2 \pm 0.4 {}^{+0.7}_{-0.5}$	37.7 ± 12.6
75	90	966	75	120	4.3	$5.9 \pm 0.7 {}^{+1.2}_{-0.9}$	19.9 ± 4.1
75	100	2408	100	100	2.2	$6.4 \pm 0.4 {}^{+1.3}_{-1.0}$	11.1 ± 2.1
75	110	963	100	100	1.1	$5.8 \pm 0.7 {}^{+1.8}_{-0.8}$	4.9 ± 1.2
100	60	2468	75	100	36.1	$2.2 \pm 0.3 {}^{+0.8}_{-0.5}$	62.2 ± 19.7
100	70	2438	75	100	16.7	$3.7 \pm 0.3 {}^{+1.3}_{-0.9}$	49.6 ± 14.9
100	80	2418	100	100	7.7	$4.1 \pm 0.4 {}^{+1.3}_{-1.1}$	24.9 ± 7.5
100	90	2425	90	100	3.7	$6.2 \pm 0.4 {}^{+0.9}_{-1.2}$	18.1 ± 3.3
100	100	2417	90	100	1.8	$7.7 \pm 0.5 {}^{+1.4}_{-1.5}$	11.1 ± 2.2
100	110	2358	100	100	0.9	$8.8 \pm 0.5 {}^{+1.3}_{-1.5}$	6.4 ± 1.1

Table 20: Signal information (small M_0). Details of the errors are given in the text. The cross sections are calculated by `prospino`, also discussed in the text.

M_0 (GeV)	$M_{1/2}$ (GeV)	MC Events	$\not\!\!E_T >$ (GeV)	$H_T >$ (GeV)	σ_{NLO} (pb)	ϵ (%)	$< N >$
150	50	2120	75	100	48.6	$1.5 \pm 0.2\,^{+0.6}_{-0.1}$	58.5 ± 16.3
150	70	2438	75	120	8.7	$4.4 \pm 0.4\,^{+1.3}_{-0.7}$	30.6 ± 7.3
150	80	2036	75	100	4.4	$5.8 \pm 0.5\,^{+1.7}_{-1.4}$	20.2 ± 5.8
150	90	2400	75	100	2.2	$8.5 \pm 0.5\,^{+1.3}_{-1.5}$	14.5 ± 2.5
150	100	2390	75	120	1.1	$8.8 \pm 0.5\,^{+1.1}_{-1.4}$	7.6 ± 1.1
150	110	2334	100	100	0.6	$10.2 \pm 0.6\,^{+0.9}_{-1.8}$	4.6 ± 0.7
200	50	2478	75	100	27.6	$1.5 \pm 0.2\,^{+0.5}_{-0.4}$	33.2 ± 11.7
200	60	2470	75	120	11.4	$2.5 \pm 0.3\,^{+0.9}_{-0.6}$	22.8 ± 7.0
200	70	2427	75	120	4.7	$4.8 \pm 0.4\,^{+0.8}_{-1.0}$	17.8 ± 3.6
200	80	2407	75	140	2.4	$5.8 \pm 0.4\,^{+1.0}_{-1.6}$	11.0 ± 2.6
200	90	2374	75	140	1.2	$8.8 \pm 0.5\,^{+1.1}_{-1.4}$	8.3 ± 1.3
200	110	2316	100	150	0.3	$9.2 \pm 0.5\,^{+0.6}_{-1.3}$	2.4 ± 0.3

Table 21: Signal information (intermediate M_0). Details of the errors are given in the text. The cross sections are calculated by `prospino`, also discussed in the text.

M_0 (GeV)	$M_{1/2}$ (GeV)	MC Events	$\not\!\!E_T >$ (GeV)	$H_T >$ (GeV)	σ_{NLO} (pb)	ϵ (%)	$< N >$
250	50	2475	75	120	19.7	$1.5 \pm 0.2\,^{+0.4}_{-0.4}$	22.9 ± 6.5
250	60	2461	75	150	7.1	$3.1 \pm 0.3\,^{+0.4}_{-0.9}$	17.3 ± 4.1
250	70	2443	75	160	3.1	$3.6 \pm 0.3\,^{+0.9}_{-0.5}$	8.6 ± 1.8
250	80	2370	75	150	1.3	$6.4 \pm 0.4\,^{+1.2}_{-1.1}$	6.6 ± 1.2
250	90	2332	75	150	0.6	$8.8 \pm 0.5\,^{+1.0}_{-1.6}$	4.3 ± 0.7
250	110	2228	75	160	0.2	$10.7 \pm 0.6\,^{+1.0}_{-0.9}$	1.4 ± 0.1
300	50	2488	75	120	15.7	$1.5 \pm 0.2\,^{+0.3}_{-0.2}$	18.5 ± 4.4
300	60	2444	75	120	5.3	$3.1 \pm 0.3\,^{+0.5}_{-0.4}$	13.1 ± 2.3
300	70	2406	75	160	2.0 2	$4.2 \pm 0.4\,^{+0.7}_{-0.8}$	6.7 ± 1.4
300	80	2362	75	160	0.9	$6.0 \pm 0.4\,^{+1.1}_{-1.2}$	4.0 ± 0.8
350	40	2491	75	100	48.3	$0.5 \pm 0.1\,^{+0.1}_{-0.2}$	20.6 ± 7.3
350	50	2479	75	120	14.1	$1.5 \pm 0.2\,^{+0.2}_{-0.4}$	16.5 ± 4.5
350	60	2468	75	120	4.6	$2.8 \pm 0.3\,^{+0.5}_{-0.8}$	10.0 ± 2.6
400	40	2494	75	100	46.3	$0.7 \pm 0.1\,^{+0.1}_{-0.4}$	25.8 ± 10.7
400	50	2480	75	120	13.4	$1.0 \pm 0.2\,^{+0.4}_{-0.2}$	10.7 ± 3.6
400	60	2461	75	120	4.4	$2.5 \pm 0.3\,^{+0.8}_{-0.5}$	8.7 ± 2.4

Table 22: Signal information (large M_0). Details of the errors are given in the text. The cross sections are calculated by `prospino`, also discussed in the text.

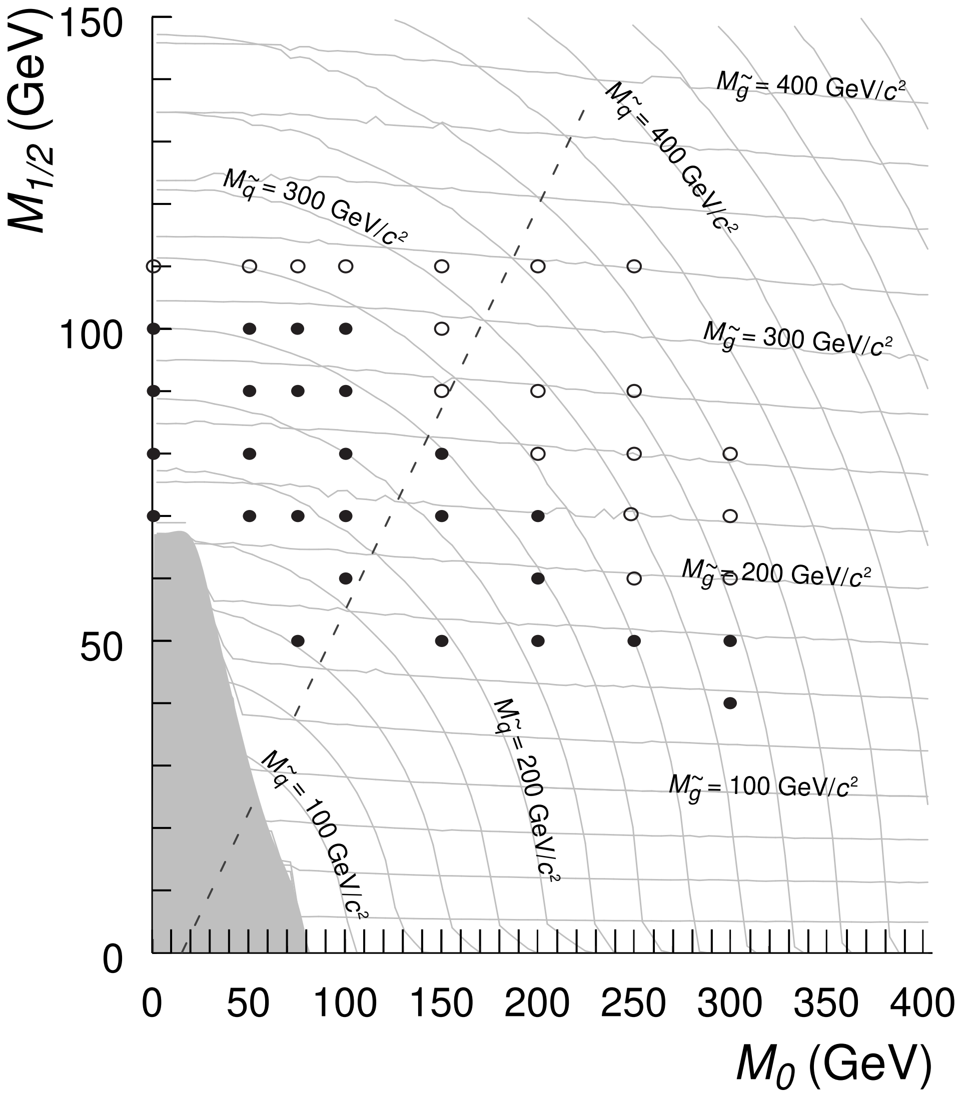

Figure 31: Excluded Monte Carlo signal points. Points excluded at 95% CL are filled. Points that cannot be ruled out are open. The other lines on the plot are described in the caption of Figure 27.

number of events seen and the luminosity. The limit calculator accounts for the correlated energy scale, luminosity, and cross section errors (the $t\bar{t}$ cross section error is uncorrelated with the others). Backgrounds where no events in the Monte Carlo pass the analysis requirements are not included in the limit calculation. The 95% CL upper limit on the total number of events that could contribute from those sources is 0.8 events.

The 95% CL upper cross section limits, σ_{95}, are shown in Tables 23 through 25. Figure 31 shows which SUGRA points are ruled out by this analysis when comparing σ_{95} to the NLO theoretical cross section. Theoretical and 95% CL cross sections for intermediate points are determined by interpolating [**?**].

An exclusion region in the $M_0 - M_{1/2}$ plane is determined by again comparing the theoretical next-to-leading order cross sections to σ_{95}. The exclusion contour is shown in Figure 32. For $M_0 < 100$ GeV, points with $M_{1/2} < \sim 103$ GeV are ruled out. Note that the dip in the dielectron limit (shown in grey in the figure) is not present in this analysis. The dip is due to sneutrinos becoming lighter than the second lightest neutralino as $M_{1/2}$ is decreased, spoiling the dielectron signature. Since this analysis is only concerned with jets, changes in the lepton branching fractions produces no effect.

Beyond M_0 of 100 GeV, the limit falls quickly. Figure 33 indicates why that happens. As seen in the figure, for small M_0 and large $M_{1/2}$ mostly squarks are being produced. Squarks tend to make larger E_T jets and $\not\!\!E_T$ than gluinos when they cascade decay, and so the efficiencies for the signals samples there are large. Accordingly, in that region the optimization tends to choose large $\not\!\!E_T$ and lower H_T, since while the jets have large E_T, there are fewer of them produced (compare the signal plots in Figure 11) than in gluino decays. As M_0 is increased, the squarks become heavier and so the gluinos processes start

M_0	$M_{1/2}$	$M_{\tilde{g}}$	$M_{\tilde{q}}$	$\not\!\!E_T >$	$H_T >$	σ_{NLO}	σ_{LO}	σ_{95}
0	70	209	182	75	100	30.1	20.0	**10.8**
0	80	240	207	100	100	11.7	7.6	**4.4**
0	90	262	228	100	100	5.8	3.7	**2.6**
0	100	288	250	100	100	2.8	1.8	**2.6**
0	110	314	272	100	100	1.3	0.8	1.8
50	70	211	188	75	100	25.6	17.0	**8.6**
50	80	237	210	100	100	11.3	7.3	**5.8**
50	90	263	232	100	100	5.1	3.3	**3.2**
50	100	288	254	100	100	2.5	1.6	**2.2**
50	110	315	276	100	100	1.2	0.7	1.8
75	50	161	153	75	100	121.5	81.4	**43.2**
75	70	212	195	100	100	21.2	13.9	**7.4**
75	90	266	239	75	120	4.3	2.7	**3.9**
75	100	289	259	100	100	2.2	1.4	**1.8**
75	110	315	281	100	100	1.1	0.7	2.0
100	60	190	185	75	100	36.1	23.6	**11.1**
100	70	214	205	75	100	16.7	10.8	**6.2**
100	80	240	225	100	100	7.7	4.9	**3.5**
100	90	266	246	90	100	3.7	2.3	**2.0**
100	100	290	266	90	100	1.8	1.1	**1.6**
100	110	316	287	100	100	0.9	0.6	1.3

Table 23: 95% CL cross section limits (small M_0). All cross sections are in pb. Masses and energies are GeV/c^2 and GeV respectively. Points that are ruled out ($\sigma_{95} < \sigma_{NLO}$) have the 95% CL cross section in bold.

M_0	$M_{1/2}$	$M_{\tilde{g}}$	$M_{\tilde{q}}$	$\not{E}_T >$	$H_T >$	σ_{NLO}	σ_{LO}	σ_{95}
150	50	165	196	75	100	48.6	30.0	**12.0**
150	70	221	231	75	120	8.7	5.4	**4.4**
150	80	243	249	75	100	4.4	2.7	**4.2**
150	90	269	268	75	100	2.2	1.3	2.5
150	100	294	287	75	120	1.1	0.7	2.2
150	110	319	305	100	100	0.6	0.3	1.2
200	50	169	234	75	100	27.6	16.0	**14.7**
200	60	195	247	75	120	11.4	6.7	**8.8**
200	70	224	263	75	120	4.7	2.8	**4.4**
200	80	246	278	75	140	2.4	1.4	4.8
200	90	272	295	75	140	1.2	0.7	2.3
200	110	322	330	100	150	0.3	0.2	0.9

Table 24: 95% CL cross section limits (intermediate M_0). All cross sections are in pb. Masses and energies are GeV/c^2 and GeV respectively. Points that are ruled out ($\sigma_{95} < \sigma_{NLO}$) have the 95% CL cross section in bold.

M_0	$M_{1/2}$	$M_{\tilde{g}}$	$M_{\tilde{q}}$	$\not{E}_T >$	$H_T >$	σ_{NLO}	σ_{LO}	σ_{95}
250	50	170	274	75	120	19.7	10.9	**14.6**
250	60	198	286	75	150	7.1	3.9	7.6
250	70	223	299	75	160	3.1	1.7	3.5
250	80	251	313	75	150	1.3	0.7	2.5
250	90	277	328	75	150	0.6	0.4	1.8
250	110	326	359	75	160	0.2	0.1	1.1
300	50	172	318	75	120	15.7	8.6	**14.2**
300	60	200	328	75	120	5.3	2.8	6.1
300	70	228	339	75	160	2.0	1.1	3.2

Table 25: 95% CL cross section limits (large M_0). All cross sections are in pb. Masses and energies are GeV/c^2 and GeV respectively. Points that are ruled out ($\sigma_{95} < \sigma_{NLO}$) have the 95% CL cross section in bold.

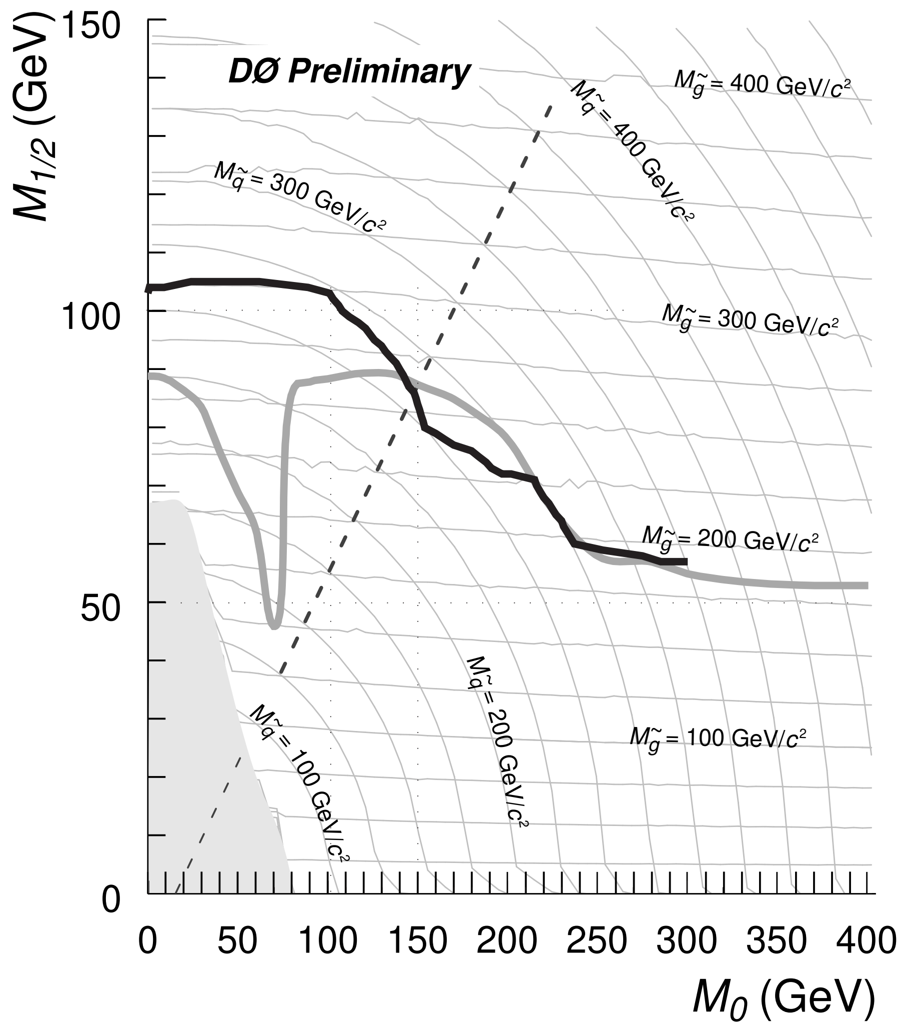

Figure 32: Exclusion contour in the M_0 – $M_{1/2}$ plane. This analysis rules out M_0 and $M_{1/2}$ points below the solid black line. The dielectron squark and gluino analysis contour [5] is shown in grey (note that analysis uses cross sections from `isajet`). The grey lines are contours of gluino and squark masses so marked. The shaded region is where SUGRA yields some unphysical condition (such as no electroweak symmetry breaking). The dashed line indicates where squarks and gluinos have equal mass.

to dominate the production. Gluino decays yield more jets, but they are softer and less $\not\!\!E_T$ is produced (compare the signal plots in Figure 10). The optimization tends to choose less $\not\!\!E_T$ and then larger H_T to gain advantage over the large backgrounds.

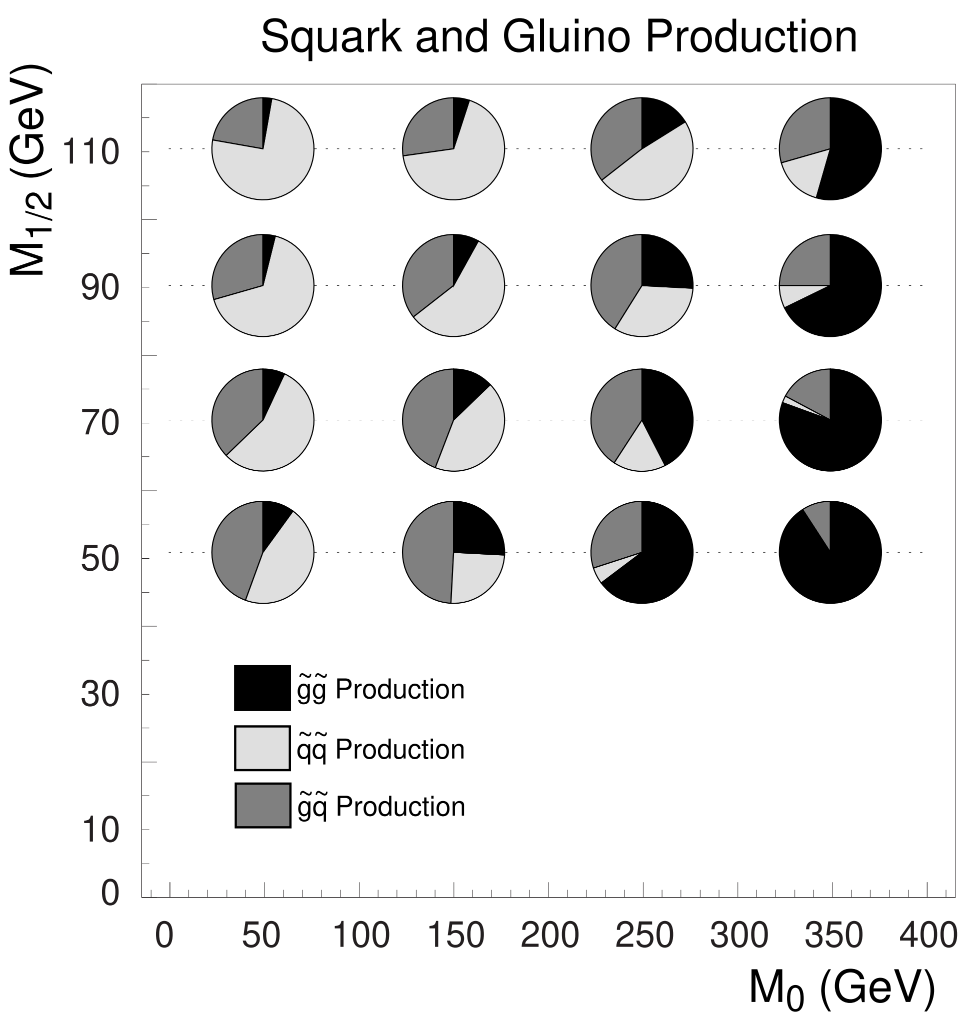

Figure 33: Fractions of the type of squark and gluino events produced shown in the M_0 – $M_{1/2}$ plane.

6 Conclusions

This analysis searches for squarks and gluinos within the minimal low energy Supergravity framework through their hadronic decays. The desired signal events are those with many jets and large missing energy. No significant excess over standard model backgrounds is observed, and so the results are in the form of cross section limits at 95% CL and corresponding limits on the SUGRA parameters of M_0 and $M_{1/2}$ which can be translated into masses of the squarks and gluinos.

Strong limits are set for low M_0. To set strong limits in the region of large M_0, it is necessary to dramatically increase the signal efficiency. In order to do so, the $\not\!\!E_T$ requirement must be lowered. To avoid the rapidly increasing backgrounds, one may consider raising the number of jets required. To drop $\not\!\!E_T$ low to gain enough efficiency, it may be necessary to use another trigger with a lower $\not\!\!E_T$ requirement. The lepton searches also win in that region, since though branching fractions to leptons are small, the backgrounds are also small and are more easily understood.

Appendices

A A Nonparametric Histogram Fitter

One frequently has a histogram of some distribution measured from data that is derived from signal (perhaps) and background sources. The problem is to determine the contribution to the data from each source. A program from Barlow and Beeston [24] exists for performing such a histogram fit within the framework of frequentist statistics using the maximum likelihood method. Unfortunately, if the contribution of a source to the data is expected to be at an extreme (minuscule or huge), the maximum likelihood method breaks down. If the maximum of the likelihood is at such an extremum, the log likelihood theorem does not apply and therefore no meaningful uncertainties can be extracted from the fit. A method [25, 26] similar to that of Bhat, Prosper, and Snyder [19] within the Bayesian statistics framework is not susceptible to such problems and is described here.

A.1 Derivation

The basic problem is depicted in Figure 34. The data histogram with N bins is of some distribution. There are D_i entries in bin i ($i = 1 \ldots N_{\text{bins}}$). The data correspond to a luminosity of $\mathcal{L}_{\text{data}}$. It is assumed that one or more physics or instrumental processes add up in some way to give the data observed. The expectation value of the number of events contributed to the data (with the data luminosity) from each source is the desired outcome of this calculation.

Histograms of the possible M sources of the data are made of the same distribution with the same binning. These define the shape of the signal and background sources. One may imagine that the source histograms come from separate experiments; some may be from

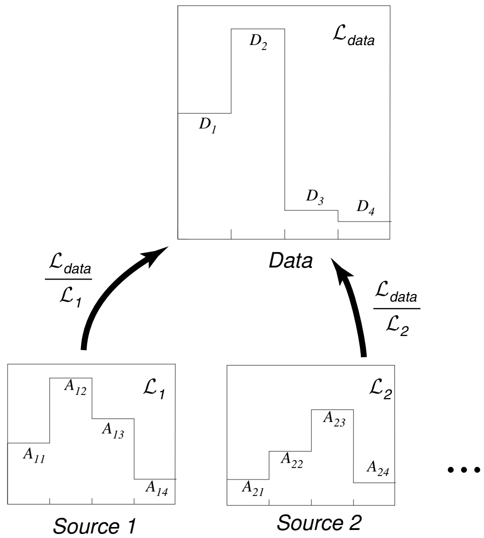

Figure 34: Bayesian Histogram Fitting. The data histogram is made up of some combination of the sources. One would like to know the contribution to the data for each source. The variables are defined in the text.

collider data and others from Monte Carlo experiments. The number of counts in bin i in the histogram of source j is given by A_{ji}. The data in source histogram j correspond to some luminosity $\mathcal{L}_j$ that may or may not be known.

The observations of counts in the histograms reflect some probability distribution for seeing those counts in those bins. For source histogram j, the true expectation value for the counts in bin i is given by a_{ji},

$$a_{ji} = \sigma_{ji}\mathcal{L}_j \tag{8}$$

where σ_{ji} is the cross section of the process for source j to produce an event in the i^{th} bin of its histogram, and $\mathcal{L}_j$ is the luminosity (Monte Carlo or collider) generated or observed.

The true expectation value (d_i) for the counts for a bin in the data distribution that is made up of the sources is then,

$$d_i = \sum_j^{M_{\text{sources}}} \mathcal{L}_{\text{data}}\, \sigma_{ji} = \sum_j^{M_{\text{sources}}} \frac{\mathcal{L}_{\text{data}}}{\mathcal{L}_j}\, a_{ji} \tag{9}$$

What one really wants to find, however, is the expectation value for the *total* number of events contributed to the data from each source. That quantity is given by μ_j; the expectation value of source j's total contribution to the data histogram,

$$\mu_j = \frac{\mathcal{L}_{\text{data}}}{\mathcal{L}_j} \sum_i^{N_{\text{bins}}} a_{ji} \tag{10}$$

The luminosities and the a_{ji} are generally not all known. Bayes' theorem allows their values to be inferred from the observations.

$$\mathcal{P}(\mathcal{L}_{\text{data}}\, \{\mathcal{L}_j\}\, \{a_{ji}\} \mid \{D_i\},\, I) = \frac{\mathcal{P}(\{D_i\} \mid \mathcal{L}_{\text{data}},\, \{\mathcal{L}_j\},\, \{a_{ji}\},\, I)\, \mathcal{P}(\mathcal{L}_{\text{data}}\, \{\mathcal{L}_j\}\, \{a_{ji}\} \mid I)}{\mathcal{Z}} \tag{11}$$

$\mathcal{P}(\mathcal{L}_{\text{data}}\, \{\mathcal{L}_j\}\, \{a_{ji}\} \mid \{D_i\},\, I)$ is the joint *posterior* probability, that is the probability distribution for the expectation values and luminosities given the observation of the data.[‡]

[‡]The notation for probabilities reflects the fact that all probabilities are conditional in the Bayesian framework; that is they must depend on some knowledge about the problem. For example, the probability that a tossed coin will come up heads would be written Prob(Heads | I) where I indicates the known information relevant to the problem, such as knowledge about the initial conditions of the flip and whether or not the coin is two headed. Assuming the coin is ordinary, the 50% probability of the coin coming up heads is derived from the fact that one does has little knowledge of the initial conditions (for if one knew the initial conditions *exactly*, the outcome of the flip could be predicted with certainty). $\mathcal{P}$ is a probability distribution. For example, the probability for observing N events *as a function of* N given that the true expectation value is μ would be written as $\mathcal{P}(N \mid \mu,\, I)$. I symbolizes relevant information about the problem (such as how the N events were obtained, whether the process is governed by Poisson statistics, etc.) that need not be shown explicitly. The expression is, in fact, the likelihood function for N given μ. $\mathcal{P}(A\, B \mid I)$ indicates a *joint*

I represents the other information pertinent to the problem, such as the observed source histogram counts, binning, and so on. $\mathcal{P}(\{D_i\} \mid \mathcal{L}_{\text{data}}, \{\mathcal{L}_j\}, \{a_{ji}\}, I)$ is the probability of observing the data D_i given the expectation values and luminosities. This expression is the likelihood function. $\mathcal{P}(\mathcal{L}_{\text{data}}\,\{\mathcal{L}_j\}\,\{a_{ji}\} \mid I)$ is the probability distribution of the expectations and luminosities given only the information in I. This distribution is the joint *prior* probability. $\mathcal{Z}$ is a constant that normalizes the posterior probability.

If the total count in each bin is assumed to be governed by Poisson statistics, then the likelihood function is familiar:

$$\mathcal{P}(\{D_i\} \mid \mathcal{L}_{\text{data}}, \{\mathcal{L}_j\}, \{a_{ji}\}, I) = \mathcal{P}(\{D_i\} \mid \{d_i\}, I) = \prod_{i}^{N_{\text{bins}}} \frac{e^{-d_i} d_i^{D_i}}{D_i!} \tag{12}$$

where d_i is given by Equation (9).

The joint prior probability can be split up with the product rule,

$$\mathcal{P}(\mathcal{L}_{\text{data}}\,\{\mathcal{L}_j\}\,\{a_{ji}\} \mid I) = \mathcal{P}(\mathcal{L}_{\text{data}}\,\{\mathcal{L}_j\} \mid \{a_{ji}\}, I)\ \mathcal{P}(\{a_{ji}\} \mid I) \tag{13}$$

The first term is the probability distribution of the luminosities given the true expectation values of the source histogram bins and the other information. Clearly, the values of the luminosities are logically independent of the bin expectation values, so $\mathcal{P}(\mathcal{L}_{\text{data}}\,\{\mathcal{L}_j\} \mid \{a_{ji}\}, I) = \mathcal{P}(\mathcal{L}_{\text{data}}\,\{\mathcal{L}_j\} \mid I)$. Although some of the luminosities may be known to within some errors, to make computation easier all of the luminosities are assumed to be completely unknown. Therefore, $\mathcal{P}(\mathcal{L}_{\text{data}}\,\{\mathcal{L}_j\} \mid I)$, their prior probability, is taken to be flat (equal to a constant).

probability distribution, or the probability for A and B given information I. $\mathcal{P}(\{N_i\} \mid \{\mu_i\}, I)$ is the joint probability distribution for observing the set of all N_i (N_1, N_2, ...), given the set of expectation values.

The second term of the joint prior in Equation (13) is the prior for the true expectation values of the counts in the source bins. Since A_{ji}, the observed counts in those bins, is known and is a part of I, an informative prior may be written using Bayes theorem again to infer the probability distribution for $\{a_{ji}\}$,

$$\mathcal{P}(\{a_{ji}\} \mid I) = \mathcal{P}(\{a_{ji}\} \mid \{A_{ji}\},\, I') = \frac{\mathcal{P}(\{A_{ji}\} \mid \{a_{ji}\},\, I')\,\mathcal{P}(\{a_{ji}\} \mid I')}{\mathcal{Z}'} \tag{14}$$

The first term in the numerator is the Poisson likelihood (the probability of observing the $\{A_{ji}\}$ given the true expectation values $\{a_{ji}\}$),

$$\mathcal{P}(\{A_{ji}\} \mid \{a_{ji}\},\, I') = \prod_{j}^{M_{\text{sources}}} \prod_{i}^{N_{\text{bins}}} \frac{e^{-a_{ji}}\, a_{ji}^{A_{ji}}}{A_{ji}!} \tag{15}$$

Since no special information is assumed to be known about the expectation values, the prior probability for $\{a_{ji}\}$ given the information in I', $\mathcal{P}(\{a_{ji}\}|I')$, is also assumed to be flat. Therefore, Equation (14) is just the likelihood multiplied by a constant flat prior.

Putting the constants into $\mathcal{Z}$, equation (11) now becomes,

$$\mathcal{P}(\mathcal{L}_{\text{data}}\, \{\mathcal{L}_j\}\, \{a_{ji}\} \mid \{D_i\},\, I) = \frac{1}{\mathcal{Z}} \left(\prod_{i}^{N_{\text{bins}}} \frac{e^{-d_i}\, d_i^{\,D_i}}{D_i!} \right) \left(\prod_{j}^{M_{\text{sources}}} \prod_{i}^{N_{\text{bins}}} \frac{e^{-a_{ji}}\, a_{ji}{}^{A_{ji}}}{A_{ji}!} \right) \tag{16}$$

The expression on the right side without the normalization constant is, in fact, the same expression that Barlow and Beeston use for the maximum likelihood method approach to this problem. The interpretation is very different in the Bayesian probability framework. Here, nothing is being sampled. The observed histograms are *the* observations, not one sample out of a hypothetical set of observations. The posterior probability distribution represents the degree of knowledge of the luminosities and the expectation values given the information provided in the observations of the histograms, *not* sampling distributions. Similarly, the prior probabilities for the luminosities and the expectation values, $\mathcal{P}(\mathcal{L}_{data}\,\{\mathcal{L}_j\} \mid I)$ and $\mathcal{P}(\{a_{ji}\}|I')$, represent the degree of knowledge of those parameters given information one knows about the problem other than that provided by the observations of the histograms. The flat priors that are used indicate one is completely uncertain about the values of those parameters, thus all values are given equal probability.

In order to obtain a more useful result, one would like to get information about μ_j, the total number of events source j contributes to the data. In principle, one would perform a change of variables to put Equation (16) in terms of μ_j. To determine the probability distribution for μ_k, the contribution from a particular source k to the data, Equation (16) is integrated over all values of the other μ_j, $(j \neq k)$,

$$\mathcal{P}(\mu_k \mid \{D_i\},\, I) = \int \cdots \int \mathcal{P}(\{\mu_j\} \mid \{D_i\},\, I)\, d\mu_j\,, \quad (j \neq k) \tag{17}$$

This integration *marginalizes* the posterior probability to eliminate the *nuisance* parameters. Nuisance parameters are parameters that are of no interest in the particular solution, which in this case are the μ_j other than $j = k$. It turns out that the change of variable to μ_j is very difficult to do, and so an approximation is made instead.

To make the problem tractable, one assumes that the expectation values for the contents of the source histograms, $\{a_{ji}\}$, are the nuisance parameters and the only interesting quantities are the luminosities. One marginalizes the posterior probability by integrating over all possible values of a_{ji},

$$\mathcal{P}(\mathcal{L}_{\text{data}}\,\{\mathcal{L}_j\}\mid\{D_i\},\,I) = \int\cdots\int \mathcal{P}(\mathcal{L}_{\text{data}}\,\{\mathcal{L}_j\}\,\{a_{ji}\}\mid\{D_i\},\,I)\,da_{ji}\,, \quad \text{for all } i \text{ and } j \tag{18}$$

In the expression for μ_j, one then makes an approximation of Equation (10),

$$\mu_j = \frac{\mathcal{L}_{\text{data}}}{\mathcal{L}_j}\sum_i^{N_{\text{bins}}} A_{ji} \tag{19}$$

Note that the a_{ji} have been replaced with A_{ji}. The observed counts in the bins of the source histograms is used as an approximation of the true expectation values for those counts. This approximation holds so long as the total number of counts in the source histograms is much larger than the number of bins, $\sum_i A_{ji} \gg N_{\text{bins}}$. The approximation is not dependent on the total counts in the data histogram. The probability distribution for the ratio of luminosities can then be determined from $\mathcal{P}(\mathcal{L}_{\text{data}}\,\{\mathcal{L}_j\}\mid\{D_i\},\,I)$.

Equation (18) can be solved analytically [19, 26]. Since flat priors are used for both the luminosities and the true expectation values of the contents in the source histograms, Equation (18) is essentially the likelihood function for observing the data and the source histograms given the expectation values (which is what Equation (16) turns out to be with the flat priors), integrated over all values of those expectation values. If more informative priors are used for the luminosities and expectation values, this solution will be different and may be difficult to obtain analytically or computationally impractical to solve numerically. The only extra piece is the normalization constant, which will be ignored (the desired probability distributions can always be normalized at the end or by integrating Equation (11) over all parameters and solving for $\mathcal{Z}$). The solution is

$$\mathcal{P}\left(\frac{\mathcal{L}_{\mathrm{data}}}{\{\mathcal{L}_j\}} \mid \{D_i\},\, I\right) = \prod_{i}^{N_{\mathrm{bins}}} \sum_{k_1,\ldots,k_M=0}^{D_i} \prod_{j}^{M_{\mathrm{sources}}} \binom{A_{ji}+k_j}{k_j} \frac{(\mathcal{L}_{\mathrm{data}}/\mathcal{L}_j)^{k_j}}{(1+\mathcal{L}_{\mathrm{data}}/\mathcal{L}_j)^{A_{ji}+k_j+1}} \tag{20}$$

The k_j are indices that satisfy the multinomial constraint $\sum_{j=1}^{N_{\mathrm{bins}}} k_j = D_i$. Since the luminosities always appear in the ratio $(\mathcal{L}_{\mathrm{data}}/\mathcal{L}_j)$, one obtains a probability for this ratio instead of the individual values Fortunately, the ratio is the desired quantity. For details on the derivation of this solution, see the appendix in Reference 19.

The solution is simple in the case of two source histograms [19]. Equation (20) can be written as

$$\mathcal{P}\left(\frac{\mathcal{L}_{\mathrm{data}}}{\mathcal{L}_1} \frac{\mathcal{L}_{\mathrm{data}}}{\mathcal{L}_2} \mid \{D_i\},\, I\right) = \prod_{i}^{N_{\mathrm{bins}}} \sum_{k=0}^{D_i} C_{k,1}\, C_{(D_i-k),2} \tag{21}$$

where constants C are defined by recursion relations,

$$C_{0,j} = \left(1 + \frac{\mathcal{L}_{\mathrm{data}}}{\mathcal{L}_j}\right)^{-(A_{ji}+1)}, \tag{22}$$

$$C_{r,j} = \left(\frac{(\mathcal{L}_{\mathrm{data}}/\mathcal{L}_j)}{1+(\mathcal{L}_{data}/\mathcal{L}_j)}\right)\left(\frac{A_{ji}+r}{r}\right) C_{r-1,j}\,, \quad (r = 1, \ldots, D_i,\ j = 1, 2) \tag{23}$$

The probability distribution for the contribution to the data from source 1 is obtained by integrating Equation (21) over all values of $\mathcal{L}_{\mathrm{data}}/\mathcal{L}_2$ (marginalization over the unwanted parameter). The resulting distribution is then multiplied by the number of events in source histogram 1 to get the probability distribution for the contribution to the data from source 1. The contribution from source 2 is obtained in a similar manner ($\mathcal{L}_{\mathrm{data}}/\mathcal{L}_1$ is the nuisance parameter). The "result" of the fitter, that is the actual number of events contributed from a source, is usually taken to be the mean of the final probability distribution with the square root of the variance as the error.

A.2 Test cases

The fitter for two source histograms is quite fast, so studies of the fitter performance can be made easily. One finds that so long as the approximation of Equation (19) holds, the fitter is very robust and gives good results. Several test cases are described below. In each test, there is some "signal" source and a "background" source that contribute in some way to the "data". Imagine that two experiments are performed. One to determine the shape of the signal and background distributions (Experiment #1), and another that obtains the shape of the distribution of the data (Experiment #2). This situation is not unlike a particle physics experiment where one runs Monte Carlo or analyzes a particular collider data set to determine the shape of the signal and background (Experiment #1), and then has data collected by the analysis trigger (Experiment #2). The data contains an unknown amount of signal and background, which are to be estimated by the fitter.

The signal and background each have some cross section. The degree to which the signal and background shapes are known in Experiment #1 (the number of events that go into the signal and background histograms) is determined by the amount of luminosity generated or collected multiplied by the cross section. For these tests, the signal and background are represented each by a Gaussian distribution of some parameter "x" with a fixed mean and width. The expectation value for the number of events in the signal or background histogram is the cross section for that process multiplied by the luminosity. The actual number of events in each histogram is a Poisson random number chosen from a distribution with the given expectation value. The signal and background histograms are then filled with Gaussian random numbers based on the signal's Gaussian mean and width and the background's Gaussian mean and width respectively.

The data histogram for Experiment #2 is built by determining the expectation value of the number of events contributed by the signal and background each (cross section of the source $\times$ luminosity of the *data* in Experiment #2). The actual number of events contributed by each source (N_{signal} and $N_{\text{background}}$) are again Poisson random numbers based on the expectation values. The data histogram is then filled with N_{signal} Gaussian random numbers based on the signal's Gaussian mean and width and $N_{\text{background}}$ Gaussian random numbers based on the background's Gaussian mean and width.

For these tests, the cross sections and luminosities of the signal and background in Experiment #1 and the luminosity of the data in Experiment #2 are fixed. In the real world, none of these values may be known. All that is input into the fitter are the signal and background histograms (the results of Experiment #1) and the data histogram (the result of Experiment #2). The goal of the fitter is to determine the *expected* number of events contributed from the signal and background sources.

The tests study the performance of the fitter under a variety of conditions, such as varying how well the signal and background shapes are known, varying how much data in Experiment #2 were collected, cases where the signal is overwhelmed by the background and so on. Each test is outlined below.

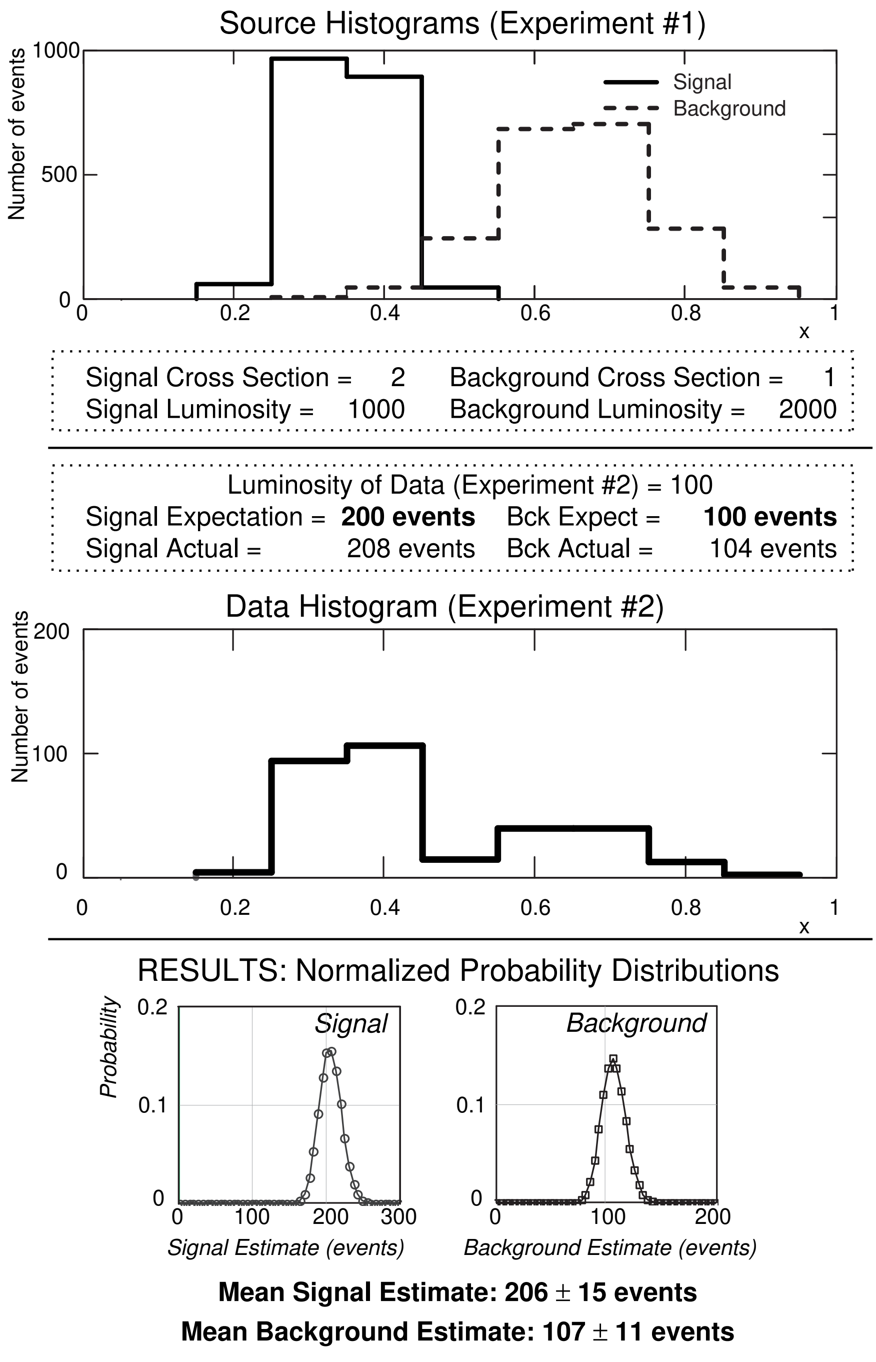

Figure 35: Case 1: Source shapes well known, large amount of data.

A.2.1 Case 1: Source shapes well known, large amount of data

Figure 35 illustrates this test. The top histogram shows the signal and background shapes and the degree to which they are known (here quite well – each source sample contains 2000 events). That histogram is the result of Experiment #1. The cross sections and luminosities used to generate the signal and background histograms are indicated below (in arbitrary units). These values may not be known in a realistic situation.

The middle histogram is the data of Experiment #2. The luminosity of the data is indicated along with the expected and actual contributions from signal and background. The sum of the actual contributions is the total number of events in the data histogram. The signal and background expectation values are the desired result of the fitter.

Only the histograms representing the signal, background, and data are input into the fitter. The results are shown at the bottom of Figure 35. The lower left plot is the probability distribution for the number of events contributed to the data from the signal. The lower right plot is the contribution from the background. The means of these distributions are shown below. The fitter tries to determine the expected number of events contributed, so the numbers to compare the answers to are the expected values shown in bold typeface in the middle section.

In this test, the signal, background, and data histograms are well populated with events. The probability distributions for the estimated number of events are sharply peaked, indicating the precision of the estimate. There are several factors that limit this precision and these will be explored in further tests. As seen, the true contribution from the sources are close to the fitter's estimate and well within errors.

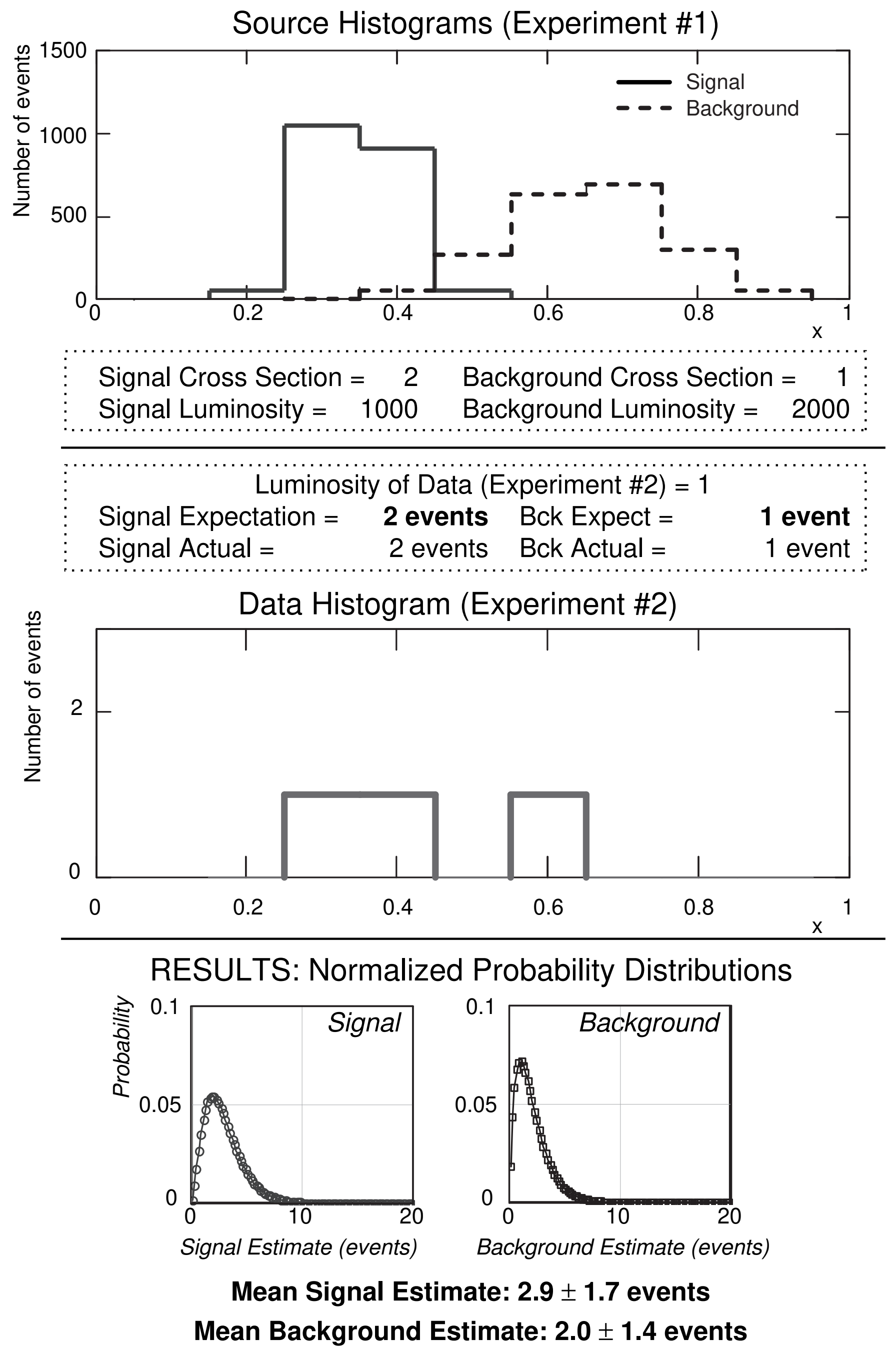

Figure 36: Case 2: Source shapes well known, small amount of data.

A.2.2 Case 2: Source shapes well known, small amount of data

Figure 36 tests the performance of the fitter when Experiment #2 yields a tiny amount of data. The signal and background shapes are well known (again, 2000 events for each). This in some ways reflects a common occurrence in real experiments. With enough Monte Carlo, the shapes of signal and background sources can be determined to good precision, but due to low cross sections, the number of these events in the data can be very small.

Of course with little data to work with, the fitter gives large errors. The probability distributions are still peaked away from zero, but have become wide and more asymmetric. In both cases, the probability for there being zero contribution is very small. Even with the small amount of data, the fitter still yields estimates close to the true values.

Figure 37 shows the effects of varying the luminosity of the data in Experiment #2 on the signal and background estimates. The data luminosity starts at 1/100th the luminosity of Experiment #1 and is increased to being equal to the Experiment #1 luminosity. The top plot is the estimate of the signal and the bottom is for the background. The dashed line is the expected amount of signal or background (luminosity of Experiment #2 $\times$ cross section). The solid line is the estimate from the fitter (mean of the probability distribution), and in grey is the error band (square root of the variance). Inset are plots of the fractional error of the signal or background estimate. As seen, the signal and background estimates track well with the expected values. Note how the fractional errors fall as the amount of data luminosity is increased. The fractional error eventually levels off, indicating that some other aspect of the problem (such as knowledge of the signal or background shapes) is limiting the precision.

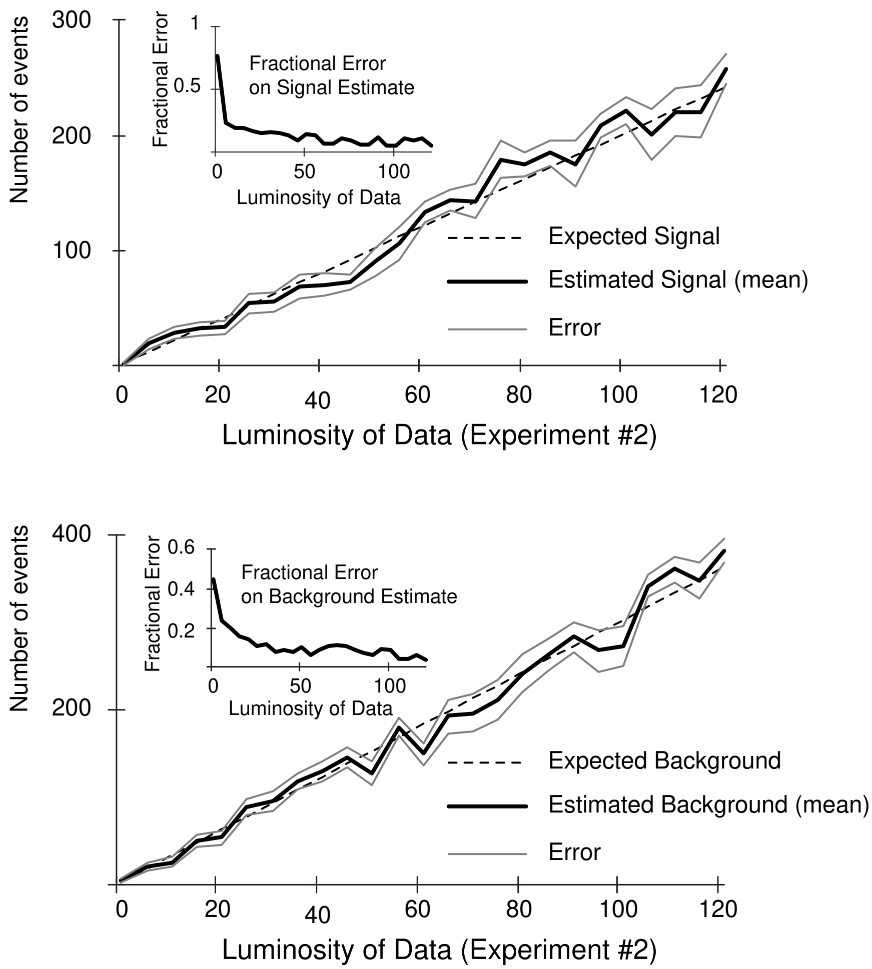

Figure 37: Varying the amount of data. The top plot shows the signal estimate while varying the luminosity of the data in Experiment #2. The bottom plot shows the background estimate.

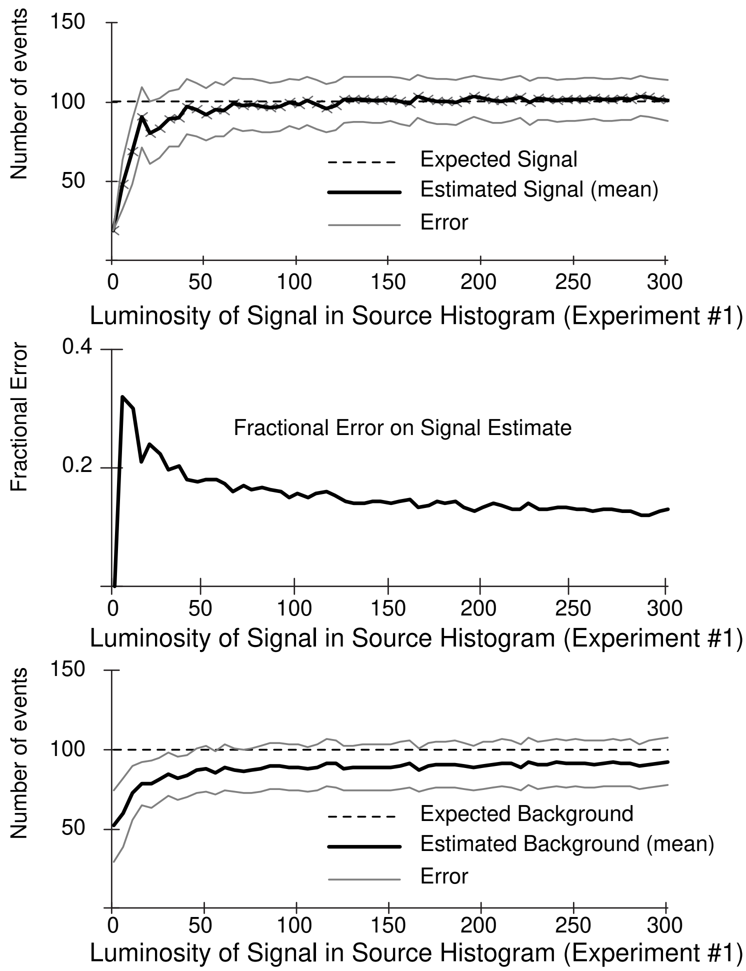

Figure 38: Case 3: Varying the knowledge of the signal.

A.2.3 Case 3: Varying the knowledge of the signal

Figure 38 shows what happens to the estimates when the knowledge of the signal is increased from very poor to very well known. The signal and background cross sections are equal (=1) and the background shape is alway known with 100 events in Experiment #1. In Experiment #2, the data always corresponds to a luminosity of 100, so the signal and data are expected to contribute 100 events each. The luminosity of the signal in Experiment #1 is varied from 1/100th that of the background (1 event in the Experiment #1 signal histogram) to three times the background. The top and bottom plots shows the estimate of the signal and background contributions respectively as the luminosity of the signal in Experiment #1 is increased. The middle plot shows the fractional error on the signal.

Note the first few bins of the top plot where the fitter severely underestimates the contribution of the signal. This effect is due to the approximation in Equation (19) breaking down. When the number of events in the signal histogram becomes larger than the number of bins, the fitter gives reasonable results.

A.2.4 Case 4: Source shapes well known, signal overwhelmed by background

It is unfortunate when the signal is buried under a very large background. Figure 39 depicts this case where the signal cross section is 1/100th that of the background. The signal and background shapes in Experiment #1 are known to the same precision (the luminosity of the signal in Experiment #1 is 100 times that of the background). In the data, the signal only contributes two events, while the background gives about 100. The probability distribution for the signal estimate is now peaked close zero, indicating that no contribution from the signal is quite probable. But there is still a long tail, so the probability that the signal

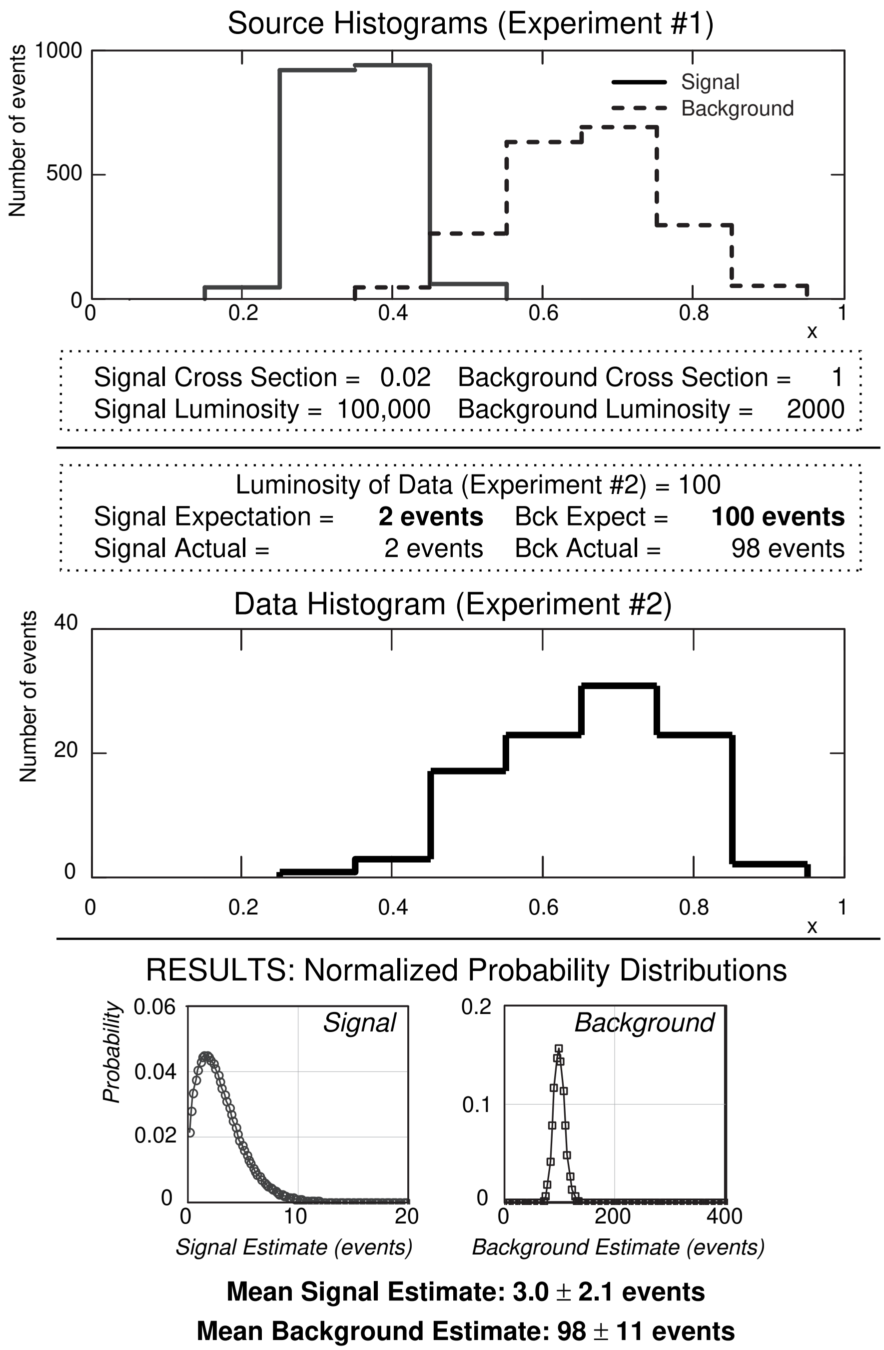

Figure 39: Case 4: Source shapes well known, signal overwhelmed by background.

contribution is nonzero is substantial. In fact, the mean of the distribution is close to the expected two events and well within the error.

A better look at this problem is shown in Figure 40. The signal and background estimates are shown while varying the signal cross section from 1/100th that of the data to equal the data. For this case, the background cross section is one and the data luminosity of Experiment #2 is 100. While the signal cross section varies, the luminosity of the signal in Experiment #1 is also varied so that the signal and background shapes are always known with 100 events each. The top plot shows the signal estimate against the expected number of events. Again, the estimate tracks well with the expected value, and the fractional drops as more signal is introduced to the data. The background estimate is largely unaffected by the increasing amount of signal.

A.2.5 Case 5: Signal known poorly, signal overwhelmed by background

Figure 41 shows the case where the signal is overwhelmed by the background in the data and the signal is known poorly (in this case at 1/10th the level of the background in Experiment #1). Even with the poor knowledge of the signal shape, the probability distribution of the signal contribution, while still with substantial probability for no contribution, is peaked slightly away from zero with a long tail. The mean of the distribution is not too far from the expected contribution and is within errors.

A.3 Conclusions

The nonparametric histogram fitter is a useful tool for determining signal and background contributions to data. As with any such tool, one must be sure that all of the approximations

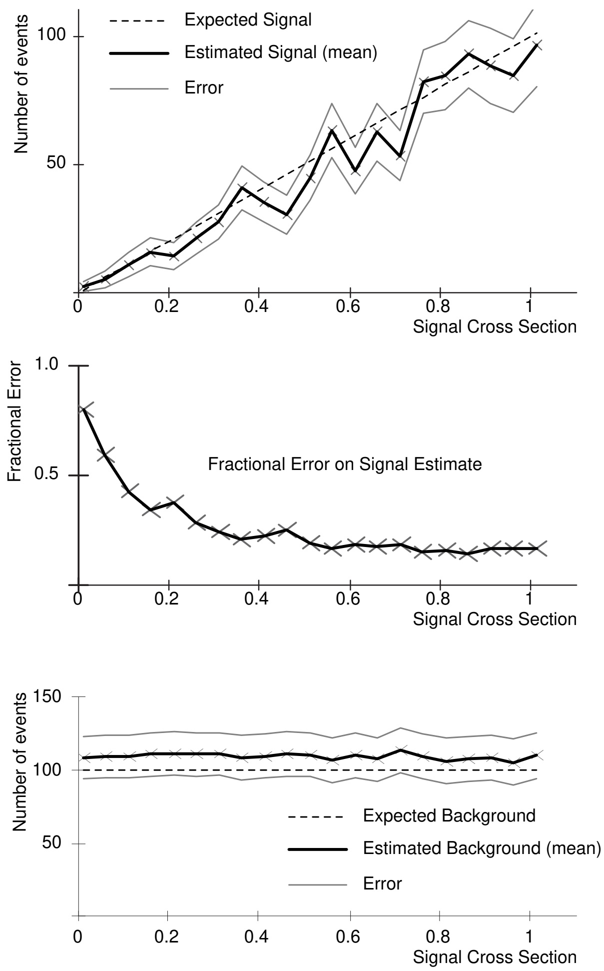

Figure 40: Varying the signal cross section

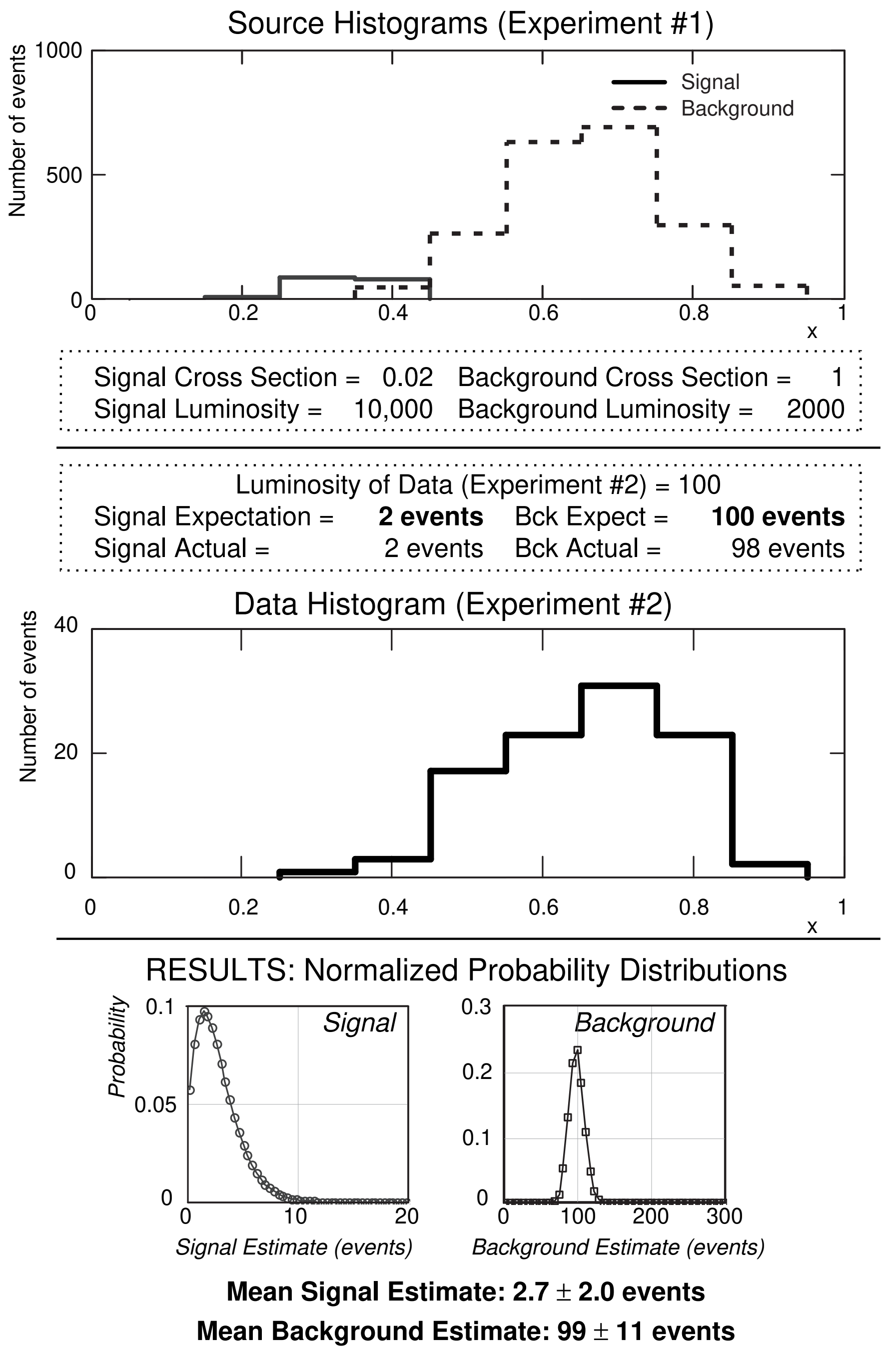

Figure 41: Case 5: Signal known poorly, signal overwhelmed by background.

made within the method hold before trusting any results.

References

[1] H. E. Haber and G. L. Kane, Phys. Rep. **117**, 75 (1985).

[2] H. P. Niles, Phys. Rep. **110**, 1 (1984).

[3] X. Tata, in *The Standard Model and Beyond*, edited by J. Kim (World Scientific, Singapore, 1991), p. 304.

[4] A. L. Lyon, "The Basics of Supersymmetry", DØ Internal Note 2523 (unpublished).

[5] N. K. Mondal, V. S. Narasimham, H. C. Shankar, and K. De, "Supergravity Inspired SUSY Search in the Dielectron Channel", DØ Internal Note 2763 (unpublished).

[6] M. Paterno, *A Search for Squarks and Gluinos in $p\bar{p}$ Collisions at $\sqrt{s}$ = 1.8 TeV with the DØ Detector*, Ph.D. Thesis, State University of New York at Stony Brook, 1994, (unpublished).

[7] DØ Collaboration, S. Abachi *et al.*, Phys. Rev. Lett. **75**, 618 (1995).

[8] I. Bertram *et al.*, "A Recipe for the Construction of Confidence Limits", DØ Internal Note 2775A (unpublished).

(URL: `http://www-d0.fnal.gov/d0notes/2775A.html`)

[9] G. Manning *et al.*, "DØ Software Documentation", in preparation (unpublished).

(URL: `http://d0sgi0.fnal.gov/software/offline_document.ps`)

[10] W. Cobau, J. Hobbs, P. Tamburello, and H. Zhu, "The Leptons Plus Jets Top Analysis", Dø internal note, 2000 (unpublished).

[11] J. Hobbs, Fermilab, private communication.

[12] T. Marshall and H. Haggerty, "Crud Removal from Muon Drift Chamber Wires Using *Zap* Cleaning", DØ Internal Note 2556 (unpublished).

[13] J. M. Butler, "EF Muon ID for b–Tagging in the Post-Zap Era", DØ Internal Note 2602 (unpublished).

[14] W. J. Thompson, *Search for the Top Quark in the Muon + Jets Channel at DØ*, Ph.D. Thesis, State University of New York at Stony Brook, 1994, (unpublished).

[15] E. Gallas, "The MTC Package (Muon Tracking in the Calorimeter)", DØ Internal Note 2066 (unpublished).

[16] G. Blazey *et al.*, DØ Internal Note 9999 (unpublished).

[17] B. Abbot, DØ Internal Note 1990 (unpublished).

[18] A. Bohnlein and G. Wang, Fermilab, Florida State University, private communication.

[19] P. C. Bhat, H. B. Prosper, and S. S. Snyder, "Bayesian Analysis of Multi-Source Data", FERMILAB–Pub 96/397 (unpublished).

[20] F. Hseih, R. Partridge, and S. Snyder, "Jet Energy Scale Uncertainty for Top Cross Section PRL", DØ Internal Note xxxx (unpublished).

[21] H. Baer, F. E. Paige, S. Protopopescu, and X. Tata, Technical Report No. FSU-HEP-930329, UH-511-764-93 (unpublished).

[22] W. Beenakker, R. Höpker, M. Spira, and P. M. Zerwas, "Squark and Gluino Production at Hadron Colliders", Preprint hep-ph/9610490, DESY 96-150, CERN-TH/96-215 (unpublished).

[23] W. Beenakker, R. Höpker, and M. Spira, "PROSPINO: A Program for the Production of Supersymmetric Particles in Next to Leading Order QCD", Preprint hep-ph/9611232 (unpublished).

[24] R. Barlow and C. Beeston, Comp. Phys. Comm. **77**, 219 (1993).

[25] M. Paterno, Unversity of Rochester, private communication.

[26] H. Prosper, Florida State University, private communication.